MODELING OF INTERNAL COMBUSTION ENGINE THERMODYNAMICS, VALVE DYNAMICS AND VALVE FLOW

By

Paul Ngcebo Tudor Williams

Supervisors
Dr. A. B. Taylor.
Dr. G. D. Thiart.

Department of Mechanical Engineering
University of Stellenbosch

Thesis presented in partial fulfilment of the requirements for the degree of Master Science of Engineering at the University of Stellenbosch.

November, 2002

DECLARATION

I, the undersigned, declare that the work contained in this thesis is my own original work which has previously not been submitted to any other university, partially or fully, in order to obtain a degree.

SUMMARY

In the design or modification of internal combustion (IC) engine components, the South African Automotive industry has always relied on either design by mother companies or quasi-empirical design methods. These methods have restricted the performance and reliability of local designs.

A personal computer based model of four stroke engine operation has been developed as a rapid and cost-effective aid to users who wish to determine the performance of an engine with reasonable accuracy before dynamometer testing is possible. This model consists of a thermodynamic model of combustion and gas exchange linked to a manifold flow model. Accompanying this is a simulation of valve flow and a cam dynamic model, enabling full assessment of the optimum cam profiles and valve angles for various automotive engine configurations.

The accuracy of these models has been verified by comparison with a set of engine dynamometer tests. The models have also been used with great success in local and international development projects in conjunction with local automotive manufacturers. In particular, two engine upgrade projects have been successfully completed, in which the program was used to aid the design of inlet manifolds, the selection of camshafts, and the selection of compression ratios.

OPSOMMING

In die ontwerp of modifikasie van binnebrandenjin-komponente het die Suid-Afrikaanse Motorbedryf gewoonlik staatgemaak op óf die ontwerpe van die moedermaatskappy óf is van quasi-empiriese ontwerp metodes gebruik gemaak. Hierdie metodes het die werkverrigting en uithouvermoë van plaaslike ontwerpe beperk.

'n Rekenaar model wat die werking van 'n vierslagenjin moduleer, is ontwikkel as 'n vinnige en koste effektiewe hulpmiddel vir ontwerpers om 'n redelike akkurate voorspelling van enjin werkverrigting te verkry, voordat dynamomotor toetswerk moontlik is. Die model bestaan uit 'n termodinamise model vir ontbranding en die gas uitruilproses, gekoppel aan 'n spruitstuk vloeimodel. Die model word saam met 'n simulasie van klepvloei en 'n nok dinamiese model gebruik, wat toelaat dat 'n goeie raming van die optimum nokprofiele en klephoeke gemaak kan word vir verskeie automobielenjin konfigurasies.

Die akuraatheid van hierdie modelle is bevestig deur die vergelyking van simulasie resultate met 'n omvangreike stel enjin dynamomotor toetse. Die modelle is ook met groot sukses in verskeie plaaslike en internasionale ontwikkelingsprojekte, in samewerking met die plaaslike motorbedryf, gebruik. In besonder is twee enjinontwikkelingsprojekte suksesvol voltooi, waarin die simulasie program gebruik is om die ontwerp van die inlaat spruitstuk, die keuse van nokasse en die keuse van drukverhouding te vergemaklik.

ACKNOWLEDGEMENTS

The author would like to express his gratitude to the following people

- Dr Andrew Taylor, my supervisor for his guidance and support.
- Christie van Vuuren, for his development of the CFD code and help in constructing the engine model.
- Arthur Bell for his development and contribution of the Two-Zone and Chemical Equilibrium models.
- Everyone at the Centre for Automotive Engineering at the University of Stellenbosch for their assistance with laboratory testing.
- The product development teams at Nissan South Africa and Volkswagen South Africa for their support in the joint projects.

This work is dedicated to my wife, Debi.

Her support strengthens me.

TABLE OF CONTENTS

LIST OF FIGURES

The standard symbols, as used in this document are given. Where the text deviates from this, special comment and re-definition will be given.

A.....area

A, B…P .....(non italics) matrix coefficients for solution of thermodynamic system

A_f.....valve flow area

$AMEP$ .....auxiliary mean effective pressure

A_p .....minimum port area

A_t.....valve curtain area

$ATDC$.....after top dead center

b.....cylinder bore

$BMEP$ .....brake mean effective pressure

$BTDC$.....before top dead center

c .....damping coefficient

$\mathbf{C}$ .....matrix of damping coefficients

C_1, C_2.....calibration constants for Woschni's equation

C_d .....valve discharge coefficient

CFD.....computational fluid dynamics

c_m .....mean piston speed

C_P.....constant pressure specific heat

C_V.....constant volume specific heat

d.....characteristic length for Woschni's equation

d.....distance from center of oscillation to center of gravity of a rocker

d_{si} .....lash distance of valve train component i

D_{is}.....valve seat inner diameter

D_{os} .....valve seat outer diameter

EGR.....exhaust gas recirculation

EVC.....exhaust valve closes (crankshaft angle)

EVO.....exhaust valve opens (crankshaft angle)

F.....applied force

$\mathbf{F}$.....matrix of applied forces

$FMEP$ .....friction mean effective pressure

g.....gravitational acceleration

h.....enthalpy (usually of gas in the cylinder)

h.....follower displacement (cam dynamics section)

h_0.....valve lash

h_b.....enthalpy of burnt gas portion in the cylinder

HLA .....hydraulic lash adjuster

h_u.....enthalpy of unburned gas portion in the cylinder

h_w .....heat transfer coefficient

h_Θ .....distance from piston to top of stroke at crank angle θ

i.....transmission ratio of rocker

i.....distance from valve stem to rocker shaft centre

I_0 .....moment of inertia of rocker around oscillation point

I_C.....moment of inertia of rocker around rocker shaft

IC .....internal combustion (engine)

I_G.....moment of inertia of rocker around center of gravity

$IMEP$ .....indicated mean effective pressure

IVC.....inlet valve closes (crankshaft angle)

IVO.....inlet valve opens (crankshaft angle)

j.....distance from oscillation point to center of gravity of rocker

k.....spring rate

$k_{i,x}$.....k values for Runge-Kutte-Fehlberg integration

$\mathbf{K}$.....matrix of spring rates

$KLSA$ .....knock limited spark advance

l.....conrod length

L.....valve lift

L_1, L_2.....lengths of valve train rocker arms

L_k.....lift ratio of valve

L_{lim}.....valve lift limit for flow area calculation

m .....mass of gas in the cylinder (thermodynamics section)

m .....effective mass of valve (cam dynamics section)

m .....mass of rocker

m_b.....mass of burnt gas in cylinder

m_{eff}.....effective mass of valve spring

m_{re} .....effective mass of rocker

m_s .....mass of spring

$\mathbf{M}$ .....mass matrix

MBT .....most beneficial torque

MEP .....mean effective pressure

m_f .....mass of fuel consumed

m_{in} .....mass of gas into cylinder through intake valve/s (during one time / crank angle step)

m_{in} .....mass of gas into cylinder through intake valve/s calculated using isentropic flow theory

m_l .....mass loss from the cylinder (primarily blow-by)

m_{out} .....mass of gas out of cylinder through exhaust valve/s (during one time / crank angle step)

m_u .....mass of unburned gas in cylinder

N .....engine speed (rpm)

N_{cyl}.....number of cylinders

P.....pressure (usually in cylinder)

$\mathbf{P}$.....engine power

P_0 .....cylinder pressure under motored conditions

$\boldsymbol{P}_1$ .....matrix of coefficients for thermodynamic system

P_{0c} .....stagnation pressure in the cylinder

P_{atm} .....atmospheric pressure

P_p .....pressure in intake pipe

PC .....personal computer

$PMEP$ .....pumping mean effective pressure

q .....valve displacement (indicates that derivatives are with respect to cam angle not time)

Q .....heat loss or addition

$\boldsymbol{Q}_1$ .....matrix of coefficients for thermodynamic system

Q, R, S, T .....(non italics) matrix coefficients for solution of thermodynamic system

Q_b .....heat loss from burnt gas portion

Q_{in} .....heat addition due to combustion (energy of fuel)

Q_l .....heat loss from cylinder

Q_u .....heat loss from unburned gas portion

r .....cam eccentricity radius

r_b .....radius of burnt zone

R.....gas constant

R_{atm}.....gas constant for atmospheric gas

R_b.....gas constant (burnt zone)

R_c.....compression ratio

RON.....rated octane number

R_p.....pressure ratio (cylinder to pipe)

R_s.....ratio of conrod length to crank radius

R_u.....gas constant (unburned zone)

s.....entropy

s.....crankshaft stroke

SFC.....specific fuel consumption

t.....time

T.....temperature (chapter 2)

T.....kinetic energy (chapter 4)

T.....torque (chapter 5)

T_{atm}.....atmospheric temperature

T_b.....temperature of burnt gas in cylinder

T_{0c}.....stagnation temperature in the cylinder

T_{piston}.....average temperature of piston crown

T_{head}.....average temperature of cylinder head combustion chamber surface

T_{Uliner}.....temperature at the lower end of the cylinder liner (lowest point of piston crown travel)

T_{Lliner}.....temperature at the upper end of the cylinder liner

T_{liner}.....average temperature of exposed portion of the cylinder liner

$T_{lineratpiston}$.....temperature of the cylinder liner at the point of the piston crown

T_u.....temperature of unburned gas in cylinder

u.....specific internal energy (usually of gas in cylinder)

u_b.....internal energy of burnt gas in cylinder

u_u.....internal energy of burnt gas in cylinder

V.....volume (usually of cylinder)

V_b.....volume of burnt gas in cylinder

V_d.....volume displaced by engine or one cylinder (see text)

V_u.....volume of unburned gas in cylinder

VVT.....variable valve timing

w, x, y, z.....(non italics) matrix values: solution of thermodynamic system

W.....work done

x.....combustion fraction (fraction of total heat to be added)

x.....valve lift perpendicular to valve seat (valve flow calculations)

x.....valve displacement (cam dynamics calculations)

$x_1..x_n$.....mole fractions of chemical species

$\boldsymbol{X}$.....matrix containing solution for thermodynamic system

$y_{i,n}$.....timestep results for Runge-Kutte-Fehlberg integration

β.....rocker angle

β.....parameter for Newmark method

β_0.....rocker start angle (zero position)

ϕ.....equivalence ratio – the inverse of lambda

ϕ.....valve seat angle

γ.....ratio of specific heats : C_P/C_V

γ.....parameter for Newmark method

η_{vol}.....volumetric efficiency

η_{mech}.....mechanical efficiency

$\eta_{thermal}$.....thermal efficiency

φ.....angle of point of contact on camshaft

λ.....lambda (Air / Fuel ratio relative to stoichiometric)

θ.....crankshaft

θ.....crankshaft rotational angle (thermodynamics sections)

θ.....camshaft rotational angle (cam dynamics sections)

θ_b.....burn angle

θ_s.....spark angle (start of combustion)

τ.....period of oscillation of a rocker

ω, ω_θ.....coefficients for standard form of cam dynamic equation

ξ.....variable for convolution interval

ψ.....constant for convolution interval

ζ, ζ_θ.....coefficients for standard form of cam dynamic equation

1. INTRODUCTION

1.1 Background

The competitiveness of the international automotive industry has provided a great stimulus for development in the design of internal combustion engines in the past century. As South Africa has opened to world markets, local vehicles have had to compete with, and match up to many different imported models. Although the larger global automotive manufacturers provide the primary development, the uniqueness of the South African market has provided great scope for development of local derivatives of these designs. In recent years, however, there has been a swing towards global products designed to be sold in many countries across the world without the need for local adaptation or development. This has placed a large strain on the engineering sections of the local automotive industry but has also created new opportunities for involvement in international design and development projects, especially those aimed at other emerging markets.

In order to be competitive, the local industry must stay abreast of the developments in modern technology in the design of engines and be prepared to use this knowledge in an innovative way so as to produce cheap, reliable and efficient engines. One of the ways in which to meet these requirements is in the upgrading and modernisation of older engine designs, the tooling for which is easily and cheaply available internationally. Often, small modifications can be made to these designs, increasing the competitiveness of these engines enough to compete in emerging markets in developing countries. In most cases, most of these modifications are to the exhausts, manifolds, valves, cams and ports of the engines in order to increase the breathing capacity, and thus the performance of the engines.

This research attempts to provide a tool for developers to reduce or eliminate both the guesswork and iterations needed for such a design upgrade. This tool is in the form of a computer program for simulation of the engine operation process. The program utilises geometrical properties and operating

conditions to model the performance of a proposed design. The theoretical development and computer programs provide not only for an educated design process but also for the ability to analyse various designs before the manufacture of prototypes.

Experience has shown that the design variable that often has the greatest effect on engine performance with the smallest change in parts is the valve lift profile, changes to which can be easily implemented by a camshaft change. The modelling of the dynamic response of the valve train to the cam profile, the resulting gas flow through the valves, and the thermodynamic processes that then take place in the cylinder, allow for design or selection of cam profiles that will produce the optimum compromise between performance and reliability.

1.2 Engine Modelling

The development of computer based internal combustion engine models has been the subject of much research (Benson, 1982; Blair, 1998; Charlton, 1990 and others), particularly with the recent increases in memory capacity and computing power of both mainframe and personal computers (PC). The IC engine can be viewed as a thermodynamic system into which a fuel and air mixture is introduced, compressed and burnt to release energy, which is used for the expansion of a cylinder volume. This is mechanically converted to torque at the crankshaft. Modelling of this system thus requires development of thermodynamic and gas flow models for compression, combustion, expansion, heat transfer, friction and transfer of gasses through the valves and induction and exhaust systems of the engine.

Software codes for engines therefore make use of various models, from extremely simple empirical based theory, through single dimensional models to full three- dimensional computational fluid dynamic calculations. Each step in this progression requires vast increases in processing power, the full computational fluid dynamics (CFD) codes requiring extremely large

mainframe computers for realistic processing time on even the simplest cases.

One-dimensional thermodynamic models for in-cylinder pressure, and temperature calculations are reasonably simple and have been used in PC based models such as *SPICE* (Simulation Program for Internal Combustion Engines) by the University of Bath (Charlton, 1990), for many years now. Only recently, have developments in personal computer capacity lead to the possibility of codes for the PC that can simulate the complex, unsteady, pulsed flows in manifolds. An example of such a code is the commercial *Dynomation* code (Audie Technology, 1994) that makes use of very simple in-cylinder and wave action codes to predict engine performance given a simple set of engine dimensions and operating conditions.

1.3 Objectives

The objective of this project was to design, develop and verify a system of PC based models allowing a user to determine with reasonable accuracy the effect of cam profiles and valve angles on engine performance for various engine configurations. This would then aid the determination of optimum valve timing and cam profiles.

This development consisted of a full engine simulation model containing the following linked models, from which the engine performance can be calculated:

- An in-cylinder thermodynamic model providing pressures and temperatures during the entire engine cycle.

- A dynamic model of valve train response to an input cam profile providing valve lift profiles at various speeds.

- A valve and port flow model.

- A CFD inlet and exhaust manifold flow model using the method of characteristics. This model allows calculation of the amount of gas and fuel mixture transferred in and out of the cylinder during induction, exhaust and crossover. (van Vuuren, 2001).

It was also a stated objective of this development that the interfaces of the computer models must be user friendly so as to provide an easily useable tool for engine development by all types of users. Such models would then be commercially attractive to the local motor industry.

1.4 Overview

The following sections are presented:

- An introduction covering the scope of the research in general terms.

- Three chapters (2, 3 and 4) containing the background, theory, and development of the equations used in the, in-cylinder, valve train dynamic and valve flow models. Details and flow charts of coding technique are provided where deemed necessary. A description of the testing and verification of each model is given.

- A chapter (5) describing the integration of these various models and the manifold flow models into a working model of the full engine process.

- A chapter (6) describing the testing and verification of the program using comparisons of simulated results and measurement on the engine test bed.

- Conclusions and recommendations for future research (Chapter 7).

- Where appropriate, detailed derivations and user instructions for the various computer programs are given in the Appendices.

2. IN-CYLINDER THERMODYNAMICS

2.1 Introduction

At the heart of any engine simulation is the calculation of the energy released by the expanding combustion gasses. The thermodynamic modelling of the combustion process enables the cylinder pressure at each crank angle to be calculated. This pressure can then be integrated over the two revolutions that form the cycle of a four-stroke engine, to give energy. Finally an energy balance can be made, from which an output can be calculated. The thermodynamic system can be viewed as a control volume into which a fuel and air mixture is introduced and then compressed, burnt and expanded to provide energy in the form of pressure on the piston. This energy is transferred to the moving piston and becomes available, after subtraction of losses, as torque.

The solution of the thermodynamic system can take many forms, two of which are chosen for this modelling and are described here. Both of these forms can be termed quasi-one-dimensional since they do not take into account the variations in mixture or velocity of the gasses in the cylinder.

The first model described is termed the “one-zone” model. This model assumes a uniform distribution of all gasses, burnt and unburned, through the cylinder and uses simple thermodynamic relationships to calculate the bulk pressure and temperature. This model, although remarkably simple, provides sufficient accuracy for initial estimates. Its primary use, however, is as a “kick start” to provide more accurate initial conditions for the two zone model. If one or two iterations of the one-zone model are run before the two-zone model is started, convergence of the more complex and slower two-zone model is achieved very quickly.

The “two-zone” model has a number of added complexities that improve the accuracy considerably. The most important of these is that the combusting gasses are split into two zones, one of which is burnt and the other still

unburned. As combustion takes place, the burnt zone increases and the unburned zone decreases in mass until the unburned zone mass reaches zero. At the same time, a chemical equilibrium calculation is performed for each zone allowing more accurate calculation of gas properties, as well as the energy released during the transfer of mass from the one zone to the other. The fundamental equations of the two-zone model have been expanded to include the periods of gas transfer through the valves, enabling simulation of the entire engine cycle.

The initial and boundary conditions of this model are obtained from the model of valve flow discussed in chapter 3, which links this model to the model of gas flow in the inlet and exhaust tracts.

2.2 Overview

The model description is divided into the following sections:

- A list of definitions and assumptions used in defining the model.
- The fundamental equations of the single-zone thermodynamic model.
- The development of the two-zone thermodynamic model.
- The equations of the two-zone thermodynamic model, modified and expanded to include the gas exchange process.
- Descriptive equations of the various sub models used by the one- and two-zone models, such as heat loss and gas properties.
- Numerical methods used for solution of the mathematical systems of equations describing these models.

The integration of these models into the computer program is described in chapter 5.

2.3 Definitions and Assumptions

The following definitions and assumptions are made:

- The fixed geometric properties of the engine are known while the variable geometric properties are defined relative to the crankshaft rotation angle, θ.

- The engine rotates at constant speed so that $\frac{d\theta}{dt}$ is constant.

- The cycle begins when the inlet valve closes and ends when the exhaust valve opens, so that no mass is gained or lost (the cycle is later extended to include the gas exchange processes). The initial conditions for the model are the conditions at inlet valve closure.

- The start and rate of heat release are known and defined relative to crank angle.

- Apart from heat loss, all energy losses (i.e. friction) do not vary with crank angle. These are subtracted separately from the total work done thermodynamically.

- The output of the model is the pressure and temperature at each division of crank angle.

- The pressure is uniform throughout the cylinder.

- The work done can then be calculated using the relationship

$$\frac{dW}{d\theta} = P \cdot \frac{dV}{d\theta}. \qquad (2.1)$$

2.4 One-Zone Thermodynamic Model

The one-zone model assumes a uniform distribution of all gasses, burnt and unburned, through the cylinder. The fundamentals of the one-zone model are

based on the idealised development of the arbitrary heat release cycle by Ferguson (1986), which is repeated briefly here as some of the equations are also used in the two-zone model

The equation of state for an ideal gas is

$$PV = mRT\,. \tag{2.2}$$

The first law of thermodynamics for the ideal gas in differential form can be written as

$$m \cdot C_V \cdot \frac{dT}{d\theta} = \frac{dQ}{d\theta} - P \cdot \frac{dV}{d\theta}\,. \tag{2.3}$$

Considering equation 2.2, the left side is divided by mRT and the right side by PV, giving

$$\frac{1}{T} \cdot \frac{dT}{d\theta} = (\gamma - 1) \cdot \left(\frac{1}{P \cdot V} \cdot \frac{dQ}{d\theta} - \frac{1}{V} \cdot \frac{dV}{d\theta} \right). \tag{2.4}$$

Looking again at equation 2.1, taking the logarithm of both sides, and differentiating with respect to crank angle gives

$$\frac{1}{P} \cdot \frac{dP}{d\theta} + \frac{1}{V} \cdot \frac{dV}{d\theta} = \frac{1}{T} \cdot \frac{dT}{d\theta} \tag{2.5}$$

which can be combined with equation 2.3 to give

$$\frac{dP}{d\theta} = -\gamma \cdot \frac{P}{V} \cdot \frac{dV}{d\theta} + (\gamma - 1)\left(\frac{1}{V} \cdot \frac{dQ}{d\theta} \right). \tag{2.6}$$

The rate of heat addition is defined as a function of crank angle, so that

$$x = x(\theta) \tag{2.7}$$

and

$$dQ = Q_{in} \cdot dx - dQ_l \ . \tag{2.8}$$

where Q_{in} is the heat of combustion of the fuel and Q_l is the heat loss due to heat transfer.

Equation 2.2 then becomes

$$\frac{dP}{d\theta} = -\gamma \cdot \frac{P}{V} \cdot \frac{dV}{d\theta} + (\gamma - 1)\left(\frac{Q_{in}}{V} \cdot \frac{dx}{d\theta} - \frac{1}{V} \cdot \frac{dQ_l}{d\theta} \right). \tag{2.9}$$

This equation is a linear first order differential equation. It can be solved numerically for pressure, as described in section 2.8. The temperature at each time step is calculated from the pressure using the ideal gas law.

2.5 Two-Zone Thermodynamic Model

Consider the gas in the cylinder using a control volume encasing the cylinder contents. The inlet and exhaust valves as well as the ring pack are parts of the boundary where gas may pass through to add or reduce the mass of fuel / air mixture trapped. The properties of the unburned and burnt zones of gas are considered separately with the burnt zone increasing and the unburned zone decreasing in mass according to a predefined burn function.

This analysis is performed for the case where fuel and air are inducted through the inlet valve and have evaporated to exist as a homogeneous mixture. The development of Bell (1998), which follows that of Krieger and Borman (1966), is presented in Appendix E, since the work of Bell has not been published. Certain elements of this derivation are repeated for clarity. Similar but separate developments will be considered for events without gas exchange (compression, combustion, expansion) and events with gas exchange (intake, overlap, exhaust). This will allow simulation of the entire engine cycle.

The deduction of the governing equations from the appropriate thermodynamic theory is followed in the next sections by a discussion of the calculation of the various terms required by these equations. Separate sets of equations are determined for the different phases of engine operation, termed compression, combustion and expansion. Note that in most cases, the combustion phase incorporates a portion of the compression and expansion phases, but that these terms are used only for easy reference.

Figure 2.1 is a schematic (similar to that of Bell, 1998) showing an engine cylinder while combustion is occurring in an infinitely thin flame separating the burnt zone from the unburned zone.

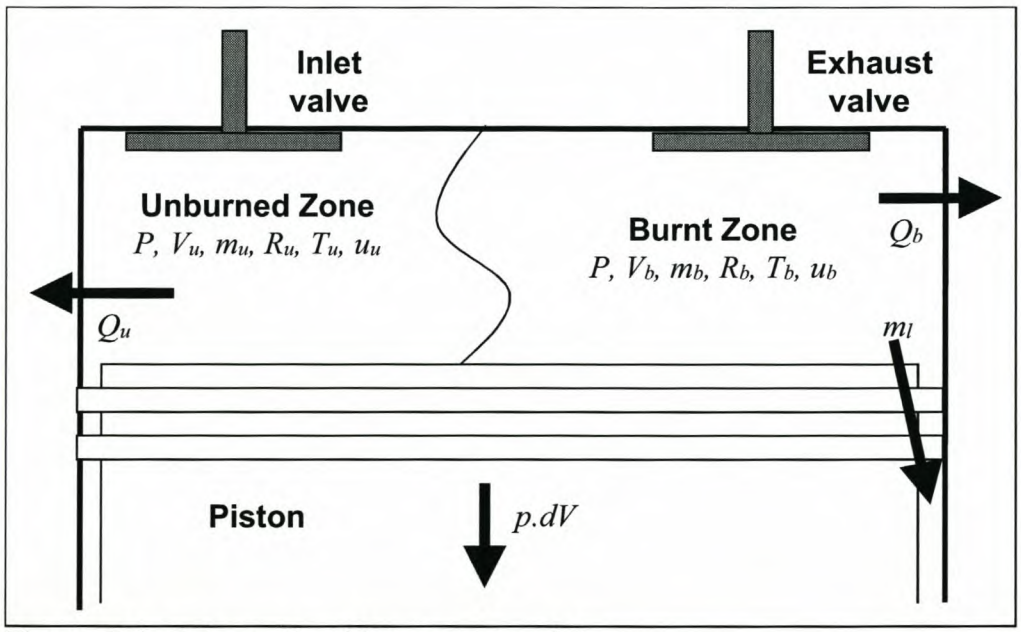

Figure 2.1. Schematic of two zone model.

The following assumptions are unique to the two-zone model:

- Pressure, P, in the burnt and unburned zones is equal
- The individual zones are in thermal equilibrium (no temperature gradients within the zones); this assumption leads to a "fully mixed model"
- There is no heat transfer between the burnt and unburned zones

- No chemical reactions take place in the unburned zone (zone is said to be frozen). The following relationships can then be used for the unburned zone

  i.e. $$\frac{\partial x}{\partial T_u} = \frac{\partial x}{\partial P} = 0 \Rightarrow \frac{\partial m_u}{\partial T_u} = \frac{\partial R_u}{\partial T_u} = \frac{\partial m_u}{\partial P} = \frac{\partial R_u}{\partial P} = \frac{\partial u_u}{\partial P} = 0 \qquad (2.10)$$

- The flame has zero volume or mass, i.e. the total cylinder volume and mass is taken up by the burnt and unburned volumes and masses only

  $$\therefore\ V = V_u + V_b \text{ and } m = m_u + m_b \qquad (2.11)$$

The unknowns are P, T_u, T_b and V_b. Four equations relating these, or their derivatives with respect to crank angle, must be found.

For mass transfer between the zones, the conservation of mass must be observed and can be written as

$$\dot{m}_b = -\dot{m}_u \qquad (2.12)$$

Differentiating the ideal gas equation (2.2) and dividing by PV gives

$$\frac{dV}{V} + \frac{dP}{P} = \frac{mR}{PV}dT + \frac{mT}{PV}dR + \frac{RT}{PV}dm \qquad (2.13)$$

Using equation 2.10 this gives

$$\frac{dV}{V} + \frac{dP}{P} = \frac{dT}{T} + \frac{dR}{R} + \frac{dm}{m} \qquad (2.14)$$

The ideal gas law (equation 2.2) can be written for the burnt and unburned zones as

$$P = \frac{m_b R_b T_b}{V_b} = \frac{m_u R_u T_u}{V_u} \qquad (2.15)$$

Writing equation 2.14 in reduced notation (derivatives with respect to crank angle are denoted with a point above the symbol) and applying to unburned and burnt zones provides

$$\frac{\dot{P}}{P} = \frac{\dot{m}_b}{m_b} + \frac{\dot{R}_b}{R_b} + \frac{\dot{T}_b}{T_b} - \frac{\dot{V}_b}{V_b} = \frac{\dot{m}_u + \dot{m}_l}{m_u} + \frac{\dot{R}_u}{R_u} + \frac{\dot{T}_u}{T_u} - \frac{\dot{V}_u}{V_u} \tag{2.16}$$

A further required equation is the definition of Enthalpy

$$h = u + RT \Rightarrow u - h = -RT \tag{2.17}$$

The energy equation for the unburned zone is written between two fictitious time points (denoted 1 and 2). The change of internal energy is equated to mass lost past the rings (blow-by), heat transfer across the cylinder walls, and work done through forced motion of the piston ($p.dV$). Although the volume of the zone changes due to combustion, no direct term is provided for the energy added by combustion or the mass transfer across the flame front as this energy transfer is incorporated into the change of internal energy term. Between two time steps (while combustion occurs), the mass of the unburned zone decreases ($m_{u2} < m_{u1}$) and that of the burnt zone increases by the same amount. Because the internal chemical energy of the burnt zone (calculated from chemical properties) is much lower than that of the unburned zone, the resulting energy balance forces an increase of the work term, thereby providing the work done. The equation can therefore be written as follows:

$$m_{u2}u_{u2} - m_{u1}u_{u1} = -\Delta m h_u + Q_u - \int_1^2 P dV_u \tag{2.18}$$

where h_u is the enthalpy of the unburned gas. This becomes, in differential form:

$$\dot{\overline{m_u u_u}} = \dot{m}_u h_u + \dot{m}_l h_u + \dot{Q}_u - P dV_u \tag{2.19}$$

For the sake of this development, the mass loss (m_l) due to blow-by is assumed to be zero. We can therefore expand the terms to obtain

$$\dot{m}_u u_u + m_u \dot{u}_u = \dot{m}_u h_u + \dot{Q}_u - P\dot{V}_u \tag{2.20}$$

Similarly, writing the energy equation for the burnt zone between two time steps (denoted 1 and 2) gives

$$m_{b2}u_{b2} = m_{b1}u_{b1} + \Delta m h_u + Q_b - \int_1^2 P dV_b \tag{2.21}$$

Again, this can be written in differential form and expanded

$$\dot{\overline{m_b u_b}} = \dot{m}_b h_u + \dot{Q}_b - P dV_b \tag{2.22}$$

$$\dot{m}_b u_b + m_b \dot{u}_b = \dot{m}_b h_u + \dot{Q}_b - P\dot{V}_b \tag{2.23}$$

The integration method used by Bell (1998) requires solving for T_u. In this application, however, this is unnecessary and the simplest form can be found. From equation 2.20, and expanding the terms:

$$\dot{m}_u(u_u - h_u) + m_u\left(\frac{\partial u_u}{\partial T_u}\dot{T}_u + \frac{\partial u_u}{\partial P}\dot{P}\right) = \dot{Q}_u - P\dot{V}_u \tag{2.24}$$

Neglecting the rate of change of internal energy with respect to pressure, as discussed, and including the definition of enthalpy (equation 2.17), this becomes

$$\dot{m}_u R_u T_u - m_u \frac{\partial u_u}{\partial T_u}\dot{T}_u = P\dot{V}_u - \dot{Q}_u \tag{2.25}$$

The second equation is obtained from equation 2.23. The development of Bell can be followed here and provides

$$\dot{m}_b\left((u_b-u_u)+\left(\frac{R_uT_u}{R_b}-T_b\right)\frac{\partial u_b}{\partial T_b}\right)=\dot{Q}_b+\left(m_uR_u\dot{T}_u-P\dot{V}\right)\left(1+\frac{\partial u_b}{\partial T_b}\frac{1}{R_b}\right) - \dot{P}V\left(\frac{\partial u_b}{\partial T_b}\frac{1}{R_b}+\frac{\partial u_b}{\partial P}\frac{m_b}{V}+\frac{V_u}{V}\right) \tag{2.26}$$

The third equation is obtained from equation 2.16, and the mass and volume definitions of the burnt and unburned zones (equations 2.11 and 2.12.)

$$\frac{\dot{P}}{P}=\frac{\dot{m}_u}{m_u}+\frac{\dot{T}_u}{T_u}-\frac{\dot{V}_u}{V_u} \tag{2.27}$$

$$\therefore\quad \frac{\dot{V}_u}{V_u}=\frac{\dot{m}_u}{m_u}+\frac{\dot{T}_u}{T_u}-\frac{\dot{P}}{P} \tag{2.28}$$

$$\therefore\quad \dot{V}_u=V_u\left(\frac{-\dot{m}_b}{m_u}+\frac{\dot{T}_u}{T_u}-\frac{\dot{P}}{P}\right) \tag{2.29}$$

$$\therefore\quad \dot{V}-\dot{V}_b=V_u\left(\frac{-\dot{m}_b}{m_u}+\frac{\dot{T}_u}{T_u}-\frac{\dot{P}}{P}\right) \tag{2.30}$$

$$\therefore\quad \dot{V}_b=V_u\left(\frac{\dot{m}_b}{m_u}-\frac{\dot{T}_u}{T_u}+\frac{\dot{P}}{P}\right)+\dot{V} \tag{2.31}$$

For the fourth equation, again, starting with the energy equation for the burnt zone (equation 2.23) and rearranging

$$\dot{m}_b u_b+m_b\left(\frac{\partial u_b}{\partial T_b}\dot{T}_b+\frac{\partial u_b}{\partial P}\dot{P}\right)=\dot{m}_b h_u+\dot{Q}_b-P\dot{V}_b \tag{2.32}$$

$$\therefore\quad m_b\frac{\partial u_b}{\partial T_b}\dot{T}_b=\dot{m}_b(h_u-u_b)+\dot{Q}_b-P\dot{V}_b-m_b\frac{\partial u_b}{\partial P}\dot{P} \tag{2.33}$$

The result is four equations of the form

$$f\left(\theta, \frac{dP}{d\theta}, \frac{dT_b}{d\theta}, \frac{dT_u}{d\theta}, P, T_b, T_u\right) = 0 \tag{2.34}$$

In order to integrate these equations, they are rearranged into the standard form

$$\frac{dP}{d\theta} = f_1(\theta, P, T_b, T_u, V_b) \tag{2.35}$$

$$\frac{dT_b}{d\theta} = f_2(\theta, P, T_b, T_u, V_b) \tag{2.36}$$

$$\frac{dT_u}{d\theta} = f_3(\theta, P, T_b, T_u, V_b) \tag{2.37}$$

$$\frac{dV_b}{d\theta} = f_4(\theta, P, T_b, T_u, V_b) \tag{2.38}$$

These equations form a system of the following form:

$$\begin{bmatrix} A & B & C & D \\ E & F & G & H \\ I & J & K & L \\ M & N & O & P \end{bmatrix} \begin{bmatrix} w \\ x \\ y \\ z \end{bmatrix} = \begin{bmatrix} Q \\ R \\ S \\ T \end{bmatrix} \tag{2.39}$$

where

$$w = \frac{dV_b}{d\theta}, x = \frac{dP}{d\theta}, y = \frac{dT_b}{d\theta}, z = \frac{dT_u}{d\theta} \tag{2.40}$$

Note that values A...T and w...z form array place holders only and are not related to any defined symbols. The constants A to T are functions of V_b, P, T_b, T_u and θ.

The system can be solved to obtain w, x, y and z in terms of the defined constants. The solution of the system, which leads to the definition of the constants, is given in Appendix A. For each time step, the constants are calculated, and then substituted into the solution formulas.

A reduced form of the same equations is used to model compression and expansion. For compression, as the burnt zone does not exist,

$$\dot{m}_b = -\dot{m}_u = 0 \tag{2.41}$$

Also, two of the unknowns are zero.

$$\dot{V}_b = 0 \ , \ \dot{T}_b = 0 \tag{2.42}$$

We therefore need only two equations to solve for the two unknowns. The energy equation in the unburned zone is written as

$$m_u \dot{u}_u = \dot{Q}_u - P\dot{V}_u \tag{2.43}$$

$$\therefore \quad m_u \frac{\partial u_u}{\partial T_u} \dot{T}_u = +\dot{Q}_u - P\dot{V}_u \tag{2.44}$$

$$\therefore \ \dot{T}_u = \frac{\dot{Q}_u - P\dot{V}_u}{m_u \dfrac{\partial u_u}{\partial T_u}} \tag{2.45}$$

The second equation also uses equation 2.16 as before and is modified to provide

$$\frac{\dot{P}}{P} = \frac{\dot{T}_u}{T_u} - \frac{\dot{V}_u}{V_u} \tag{2.46}$$

$$\therefore \dot{P} = \frac{P\dot{T}_u}{T_u} - \frac{P\dot{V}_u}{V_u} \tag{2.47}$$

Including equation 2.45:

$$\dot{P} = \frac{P}{T_u}\left(\frac{\dot{Q}_u - P\dot{V}_u}{m_u \frac{\partial u_u}{\partial T_u}}\right) - \frac{P\dot{V}_u}{V_u} \tag{2.48}$$

For the expansion stroke, the equations can be derived in the same manner; the primary difference being that $\frac{\partial u_b}{\partial P}$ can no longer be assumed to be zero. The energy equation is written as

$$m_b\left(\frac{\partial u_b}{\partial T_b}\dot{T}_b + \frac{\partial u_b}{\partial P}\dot{P}\right) = \dot{Q}_b - P\dot{V}_b \tag{2.49}$$

and equation 2.16 becomes

$$\frac{\dot{P}}{P} = \frac{\dot{T}_b}{T_b} - \frac{\dot{V}_b}{V_b} \tag{2.50}$$

Solving these simultaneously for $\dot{T}_b$:

$$m_b \frac{\partial u_b}{\partial T_b}\dot{T}_b = \dot{Q}_b - P\dot{V}_b - m_b \frac{\partial u_b}{\partial P}\dot{P} \tag{2.51}$$

$$\therefore \quad m_b \frac{\partial u_b}{\partial T_b}\dot{T}_b = \dot{Q}_b - P\dot{V}_b - m_b \frac{\partial u_b}{\partial P} P\left(\frac{\dot{T}_b}{T_b} - \frac{\dot{V}_b}{V_b}\right) \tag{2.52}$$

$$\therefore \quad \left(m_b \frac{\partial u_b}{\partial T_b} + m_b \frac{\partial u_b}{\partial P}\frac{P}{T_b}\right)\dot{T}_b = \dot{Q}_b - P\dot{V}_b + m_b \frac{\partial u_b}{\partial P} P\frac{\dot{V}_b}{V_b} \tag{2.53}$$

$$\therefore \quad \dot{T}_b = \frac{\dot{Q}_b - P\dot{V}_b + m_b \frac{\partial u_b}{\partial P} P \frac{\dot{V}_b}{V_b}}{m_b \frac{\partial u_b}{\partial T_b} + m_b \frac{\partial u_b}{\partial P} \frac{P}{T_b}} \tag{2.54}$$

Equation 2.50 can be rearranged to solve for $\dot{P}$

$$\dot{P} = P\frac{\dot{T}_b}{T_b} - P\frac{\dot{V}_b}{V_b} \tag{2.55}$$

$$\therefore \quad \dot{P} = \frac{P}{T_b}\left(\frac{\dot{Q}_b - P\dot{V}_b + m_b \frac{\partial u_b}{\partial P} P \frac{\dot{V}_b}{V_b}}{m_b \frac{\partial u_b}{\partial T_b} + m_b \frac{\partial u_b}{\partial P} \frac{P}{T_b}} \right) - P\frac{\dot{V}_b}{V_b} \tag{2.56}$$

We then have the full system of 4 equations for each of the conditions compression, combustion and expansion. The remaining conditions for which equations are required are those of intake, exhaust and overlap, in which gas exchange takes place.

2.6 Two-Zone Thermodynamic Model with Gas Exchange

The development of section 2.5 has been expanded to include the gas exchange process. Figure 2.2 shows these additions relative to figure 2.1.

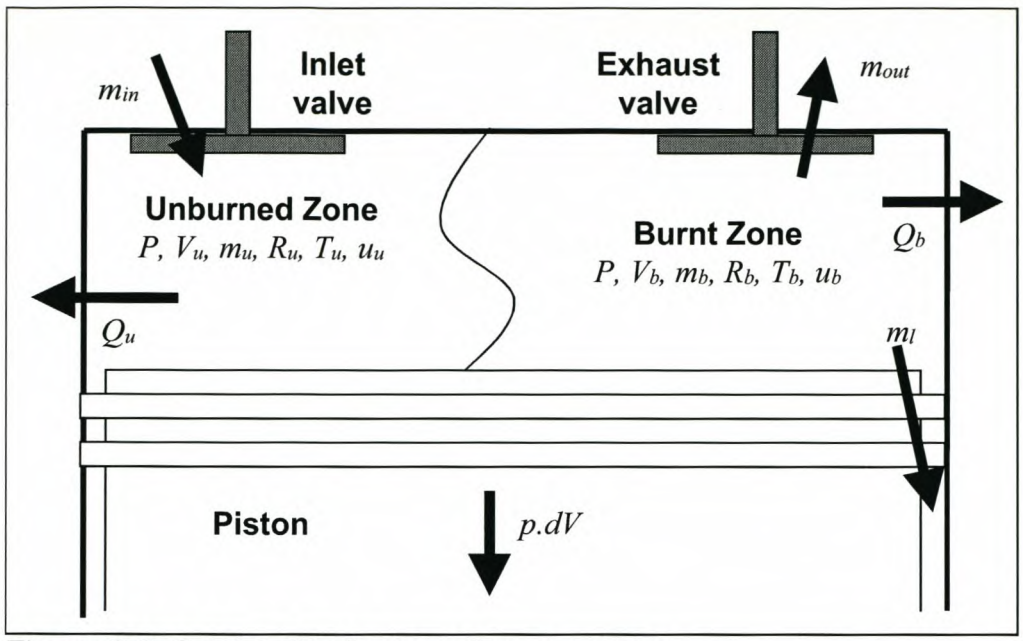

Figure 2.2. Schematic of gas exchange process

The unknowns are again P, T_u, T_b and V_b. As in section 2.5, four equations relating these are found. Changes are made to the derivation where necessary to include the mass transfer.

The energy equation for the unburned zone is derived in the same way as before. We start again with the energy balance

$$m_{u2}u_{u2} - m_{u1}u_{u1} = -\Delta m h_u + Q_u - \int_1^2 P dV_u \tag{2.57}$$

In this case we must note the addition of a term for the mass flow in through the valve. Neglecting blow-by, and also noting that

$$\dot{m}_u = 0 \tag{2.58}$$

as there is no combustion in the gas exchange phase, we can write

$$\dot{m}_{in}(u_u - h_u) + m_u \dot{u}_u = \dot{Q}_u - P\dot{V}_u \tag{2.59}$$

$$\therefore \quad -\dot{m}_{in} R_u T_u + m_u \dot{u}_u = \dot{Q}_u - P\dot{V}_u \tag{2.60}$$

$$\therefore \quad -\dot{m}_{in} R_u T_u + m_u \frac{\partial u_u}{\partial T_u} \dot{T}_u = \dot{Q}_u - P\dot{V}_u \tag{2.61}$$

Substituting equation 2.11

$$-\dot{m}_{in} R_u T_u + m_u \frac{\partial u_u}{\partial T_u} \dot{T}_u = \dot{Q}_u - P\left(\dot{V} - \dot{V}_b\right) \tag{2.62}$$

$$\therefore \quad -\dot{m}_{in} R_u T_u + m_u \frac{\partial u_u}{\partial T_u} \dot{T}_u = \dot{Q}_u - P\dot{V} + P\dot{V}_b \tag{2.63}$$

Similarly, writing the energy equation for the burnt zone gives

$$\dot{m}_{out}\left(h_b - u_b\right) + m_b \dot{u}_b = \dot{Q}_b - P\dot{V}_b \tag{2.64}$$

With the direction of $\dot{m}_{out}$ defined as positive when flowing into the cylinder,

$$\dot{m}_{out}\left(u_b - h_b\right) + m_b\left(\frac{\partial u_b}{\partial T_b}\dot{T}_b + \frac{\partial u_b}{\partial P}\dot{P}\right) = \dot{Q}_b - P\dot{V}_b \tag{2.65}$$

Simplifying as before, and assuming that $\frac{\partial u_b}{\partial P} = 0$ since the reactions "freeze" at low temperature

$$-\dot{m}_{out} R_b T_b = \dot{Q}_b - P\dot{V}_b - m_b \frac{\partial u_b}{\partial T_b}\dot{T}_b \tag{2.66}$$

Then, from equation 2.16 the third and fourth equations are found. For the burnt zone

$$\frac{\dot{P}}{P} = \frac{\dot{m}_{out}}{m_b} + \frac{\dot{R}_b}{R_b} + \frac{\dot{T}_b}{T_b} - \frac{\dot{V}_b}{V_b} \tag{2.67}$$

If, however, the assumption is made that $\frac{\partial u_b}{\partial T_b} = \frac{\partial u_b}{\partial P} = 0$ (this is supported by the numerical investigation of Olikara and Borman, 1975), then $\dot{R}_b = 0$ and therefore

$$\frac{\dot{P}}{P} = \frac{\dot{m}_{out}}{m_b} + \frac{\dot{T}_b}{T_b} - \frac{\dot{V}_b}{V_b} \tag{2.68}$$

The fourth equation is obtained for the unburned zone in the same way.

$$\frac{\dot{P}}{P} = \frac{\dot{m}_{in}}{m_u} + \frac{\dot{T}_u}{T_u} - \frac{\dot{V}_u}{V_u} \tag{2.69}$$

From the definition of the zone volumes (equation 2.11) and substituting:

$$\frac{\dot{P}}{P} = \frac{\dot{m}_{in}}{m_u} + \frac{\dot{T}_u}{T_u} - \frac{\dot{V} - \dot{V}_b}{V_u} \tag{2.70}$$

$$\therefore \quad \frac{\dot{P}}{P} = \frac{\dot{m}_{in}}{m_u} + \frac{\dot{T}_u}{T_u} - \frac{\dot{V}}{V_u} + \frac{\dot{V}_b}{V_u} \tag{2.71}$$

These equations (2.63, 2.66, 2.68 and 2.71) are again in the standard form and can be solved in an identical manner.

2.7 Sub models

Various sub models are used to describe processes within the larger model:

2.7.1 Gas Properties

The one-zone model considers only the gas property, γ, the ratio of specific heats. Ferguson (1986) shows that for hydrocarbon fuels with a stoichiometric mixture,

$$\gamma \approx 1.3 \tag{2.72}$$

If the fuel/air mixture deviates from stoichiometric, then we can use the lambda value to calculate

$$\gamma \approx 1.4 - \frac{0.16}{\lambda} \tag{2.73}$$

where lambda is the ratio between the air/fuel ratio and the stoichiometric air/fuel ratio.

For the two-zone model, the fuel/air mixture inside the cylinder is divided into a burnt zone and an unburned zone. The instantaneous gas properties of each of these zones are calculated and stored separately. Equilibrium gas properties are assumed as the reactions take place on a time scale far smaller than that present in the engine combustion process.

The models for these calculations are a development of the models of Bell (1998) who based his work on the paper of Olikara and Borman (1975). Olikara and Borman show the development of the equations to calculate the equilibrium mole fractions and their derivatives with respect to temperature, pressure and equivalence ratio for the products of combustion of any hydrocarbon fuel and air. The hydrocarbon fuels are defined according to their ratios of Carbon, Hydrogen, Oxygen and Nitrogen atoms: $C_nH_mO_lN_k$. The fuel and air at equivalence ratio, ϕ (the inverse of lambda) are assumed to react to equilibrium according to the equation

$$\left[C_n H_m O_l N_k + \frac{n + \frac{m}{4} - \frac{l}{2}}{\phi} \left(O_2 + 3.7274 \cdot N_2 + 0.0444 \cdot Ar \right) \right] \longrightarrow$$
$$x_1 H + x_2 O + x_3 N + x_4 H_2 + x_5 OH + x_6 CO + x_7 NO + x_8 O_2 +$$
$$x_9 H_2 O + x_{10} CO_2 + x_{11} N_2 + x_{12} AR \tag{2.74}$$

where x_1 through x_{12} are mole fractions of the product species. To balance this chemical equation, the atom balances together with the equilibrium constants from the JANAF Thermo-chemical Tables (Ferguson, 1986) are used.

Using these results, the enthalpy and other thermodynamic properties of the burnt and unburned zones can be calculated by summing the relative contributions of the products (Gordon and McBride, 1971). The properties calculated are Constant pressure specific heat *(C_p)*, Gas constant *(R)*, internal energy *(u)*, enthalpy *(h)* and entropy *(s)*.

2.7.2 Cylinder Volume

The cylinder volume, V, and rate of change of cylinder volume, $dV/d\theta$ are calculated from the geometry of the standard piston, conrod, and crankshaft. Heywood (1988) shows that

$$\frac{V}{V_c} = 1 + \frac{1}{2}(R_c - 1)\left[R_s + 1 - Cos\theta - \left(R_s^{\,2} - \sin^2\theta\right)^{\frac{1}{2}} \right] \qquad (2.75)$$

where

$$R_s = \frac{2 \times l}{s} \qquad (2.76)$$

is the ratio of conrod length, l, to crank radius (stroke / 2). The cylinder clearance volume can be calculated from the compression ratio and the swept volume as

$$V_c = \frac{R_c}{R_c + 1}\left(\frac{\pi b^2 s}{4}\right). \qquad (2.77)$$

The cylinder volume at a given crank angle can then be shown to be

$$V(\theta)=\left(\frac{R_c}{R_c+1}\left(\frac{\pi b^2 s}{4}\right)\right)\cdot\left\{1+\frac{1}{2}(R_c-1)\left[\frac{2l}{s}+1-Cos\theta-\left(\left(\frac{2l}{s}\right)^2-\sin^2\theta\right)^{\frac{1}{2}}\right]\right\} \tag{2.78}$$

The term $dV/d\theta$ is then obtained by taking the derivative of this equation with respect to crank angle and reduces to

$$\frac{\mathrm{dV}}{\mathrm{d}\theta}=\frac{\pi b^2 s}{8}\sin\theta\cdot\left(1+\frac{\frac{s}{2l}\cos\theta}{\sqrt{1-\left(\frac{\mathrm{s}}{2\cdot l}\sin\theta\right)^2}}\right) \tag{2.79}$$

2.7.3 Rate of Combustion

The mass fraction of the cylinder contents that have been burnt at any point of combustion can be modelled using various bell shaped curves. Starting with a burnt fraction of

$$x=\frac{1}{2}\left[1-\cos\left(\frac{\pi(\theta-\theta_s)}{\theta_b}\right)\right], \tag{2.80}$$

we obtain the sinusoidal distribution

$$\frac{dx}{d\theta}=\frac{1}{2}\cdot\frac{\pi}{\theta_b}\times\sin\left(\frac{\pi(\theta-\theta_s)}{\theta_b}\right) \tag{2.81}$$

where x is the fraction of mass burnt, θ the crank angle, θ_b the burn angle and θ_s the spark angle (start of combustion) (Ferguson, 1986). One must be careful when using data from literature in these equations since the definitions of spark and burn angle vary. Here the burn angle is the crank angle period from 0 to 100% of combustion. The spark angle is the crankshaft angle at which combustion commences.

2.7.4 Heat Loss

The terms $\dot{Q}_u$ and $\dot{Q}_b$ indicate the heat lost by the unburned and burnt zones of in-cylinder gas respectively due to heat transfer to the walls of the cylinder, piston and head of the engine. This heat in turn is transferred to the cooling water of the engine, or, in the case of an air-cooled engine, to the air passing over the cooling fins of the cylinder head and sleeve.

Models for this heat transfer vary from complex multiple resistances to simple, empirical based models. As data on the structure of the head and cylinder liner, the coolant passages and the nature of the coolant varies a great deal from engine to engine, and this model is intended to cover as many engines as simply as possible, heat flux in this study is modelled by making use of the simple heat transfer equation

$$\frac{dQ_l}{dt} = h \cdot A \cdot \left(T_{gas} - T_{wall}\right) \tag{2.82}$$

In order to make use of this equation, the temperatures of the gasses, the temperature of the walls, the areas of contact and the heat transfer coefficient must be known or calculated. The heat transfer coefficient must be calculated in such a way that the changing pressure, velocity and temperature conditions in the engine are taken into consideration.

2.7.4.1 Gas Temperature

For the one zone model, the gas has a uniform temperature: T. For the two-zone model, two different gas temperatures, T_b and T_u, the temperatures of the unburned and burnt regions of gas present in the cylinder, are defined. These temperatures are the products of the integration of the system equations and are therefore available for heat transfer calculation at any time step.

2.7.4.2 Wall Temperature

Four different temperatures for the cylinder were defined. T_{piston}, T_{head}, T_{Uliner} and T_{Lliner} are the temperatures of the piston and the head, and the temperatures of the top (upper) and the bottom (lower) of the cylinder liner wall. Assuming a linear distribution between the top and bottom of the liner, an average temperature to be used for the liner heat transfer is

$$T_{liner} = \frac{1}{2}\left(T_{Uliner} + T_{lineratpiston}\right) \tag{2.83}$$

where

$$T_{lineratpiston} = T_{Uliner} - \frac{h_\theta}{s}\left(T_{Uliner} - T_{Lliner}\right) \tag{2.84}$$

and h_Θ is the distance travelled by the piston from the top of the stroke, s. Estimates for T_{piston}, T_{head}, T_{Uliner} and T_{Lliner} must either be measured, estimated from empirical data, or calculated from a measurement of heat rejection of a test engine.

2.7.4.3 Wall Area

As most of combustion takes place as the piston is near top dead centre, and assuming a simple cylindrical cylinder / head / piston shape, the areas of each of the three temperature zones as affected by each of the two gas regions can be calculated as follows:

The region of burnt gas is assumed to be cylindrical, with radius of r_b. At crank angle θ the distance between the top of the cylinder and the head is assumed equal to the distance travelled by the piston from TDC (h_θ). The volume of the burnt region is therefore

$$V_b = \pi r_b^2 h_\theta \tag{2.85}$$

so that the radius of that region is

$$r_b = \sqrt{\frac{V_b}{\pi h_\theta}} \tag{2.86}$$

The various calculated areas are shown in table 2.1.

Area	$r_t < b/2$	$r_b <= b/2$
Burnt gas on Head / Piston	πr_b^2	$\frac{\pi b^2}{4}$
Unburned gas on Head / Piston	$\pi\left(\left(\frac{b}{2}\right)^2 - r_b^2\right)$	0
Burnt Gas on Walls (Liner)	0	$\pi \cdot b \cdot h_\theta$
Unburned Gas on Walls (Liner)	$\pi \cdot b \cdot h_\theta$	0

Table 2. 1: Heat Transfer Areas for Burnt and Unburned Zones

The head areas are approximate and modifications to this should be made for engines with complex combustion chambers, or large valve areas.

2.7.4.4 Heat Transfer Coefficient

Various empirical and theoretically based semi-empirical models are available for the heat transfer coefficient in internal combustion engines. As the conditions in different types and sizes of I.C. engines vary enormously, each of these has been subjected to much criticism in its ability to predict a "general" heat transfer coefficient.

The heat transfer coefficient model chosen for this model is Woschni's Equation. Woschni (1967) performed experiments on both a spherical

combustion "bomb" as well as on a modified test engine and various standard engines. He evaluated the theoretical conduction, convection and radiation under engine type conditions and determined the driving terms of an equation for the heat transfer coefficient. The trends and coefficients of this equation were evaluated by numerous engine tests providing his final equation

$$h = 110 \cdot d^{-0.2} \cdot P^{0.8} \cdot T^{-0.53} \cdot \left[C_1 c_m + C_2 \frac{V_c T_1}{p_1 V_1} (P - P_0) \right]^{0.8} \qquad (2.87)$$

where h is the heat transfer coefficient, d is a characteristic length (the bore is used), P_0 is the cylinder pressure for motored conditions, C_1 and C_2 are calibration constants and c_m is the mean piston speed. The subscript 1 refers to the conditions at a known reference condition (usually inlet valve closure)

In this equation, $C_1=6.18$ must be applied to the scavenging period, $C_1=2.28$ to the compression and expansion strokes, and $C_2=3.24E\text{-}3$. These constants can be modified to suit a particular case if combustion and heat transfer data is available for the engine to be simulated.

2.7.5 Mass Loss and Blow-by

Mass loss or blow-by is the term used to describe the loss of fuel/air mixture and combustion gasses past the ring pack due to the pressure differential. This can be accounted for by the use of a pressure dependant mass loss term. Due to the lack of data on this for the test cases, as well as the very small effects that such losses have on an engine of good condition, blow-by effects have not been included in the current simulation but may be added later with relative ease.

2.7.6 Exhaust Gas Recirculation (EGR)

Exhaust gas re-circulation occurs in two ways. The first portion of this re-circulation is allowed for in the program interface, which accommodates a "forced" EGR in which a fixed percentage of the exhaust gas is fed into the intake, as in the case of many modern engines, in an effort to reduce emissions. The second is the "natural" EGR in which a portion of the burnt gas is left in the cylinder due to less than ideal flow. This is calculated at each engine cycle by taking the known mass of burnt gas in the cylinder at exhaust valve closure and subtracting the total mass that flowed out of the cylinder into the exhaust. This "remaining" mass is added to the total mass that flowed into the cylinder during intake (which already has a portion of "forced" EGR) and the gas composition routines calculate the composition and initial gas temperature based on this.

2.7.7 Friction

The Friction Mean Effective Pressure is calculated using a simplistic speed based model (Heywood, 1988). The FMEP is given by the equation

$$FMEP = 0.97 + 0.15\frac{N}{1000} + 0.05\left(\frac{N}{1000}\right)^2 \qquad (2.88)$$

where N is engine speed in rpm. As this definition of FMEP includes the pumping work, the PMEP is subtracted from this to obtain FMEP as the current author defines it. This is also a simplistic approach, and in the case of a detailed development, the user should measure the engine friction and modify this equation accordingly.

3. FLOW THROUGH POPPET VALVES

3.1 Introduction

The traditional mechanism controlling the exchange of air between the cylinder and the inlet and exhaust systems of four stroke internal combustion engines is the camshaft-controlled poppet valve. Although this system is far from ideal, designers over the years have failed to develop an alternative that is as reliable and cost effective for production vehicles. As an overwhelming proportion of modern engines make use of overhead poppet valves, these are the focus of this study.

Even in the simplest of engines, the timing of the valve events plays an exceedingly vital role in the performance. This role becomes even more important with the increasing use of ram and pressure pulse supercharging to obtain high volumetric efficiencies. In engines with "tuned" manifolds, the valve geometry and valve events must be carefully designed to provide the least resistance to flow in the periods when the pressure in the manifolds is favourable for gas exchange.

The development of any engine simulation model would be incomplete and thus inaccurate without some modelling of the effects of the flow losses through the valves. In addition, the model must have the ability to simulate the dynamic pressure effects as waves are reflected from the closed or partially opened valves.

The valve flow model presented here forms the coupling between the in-cylinder model presented earlier and the CFD code for manifold flow developed by van Vuuren (2001). These three models together form a complete simulation of the intake, combustion and exhaust process. The mass flow between the cylinder and manifolds is calculated at the last grid point (boundary point) of the CFD model and forms part of the iteration process of the method of characteristics. This section describes the methodology required to determine the model inputs for a specific case.

3.2 Poppet Valve Flow Mechanisms

As the intake or exhaust gasses flow between the cylinder and a duct, there is a reduction of the flow area as they pass through the valve. This reduction of area causes changes in the pressure, velocity and other thermodynamic conditions of the gas, including a full or partial reflection of the pressure waves from the valve. Apart from these effects, the sudden area changes and intricate geometry can cause the flow to become detached or separated from the walls of the pipe and the valve surfaces, causing a *vena-contracta* where the actual flow area of the gas stream is smaller than the geometrical area of the flow orifice.

Study of the flow field through a poppet valve (Heisler, 1995) shows that there are a number of different flow patterns that occur at different values of valve lift.

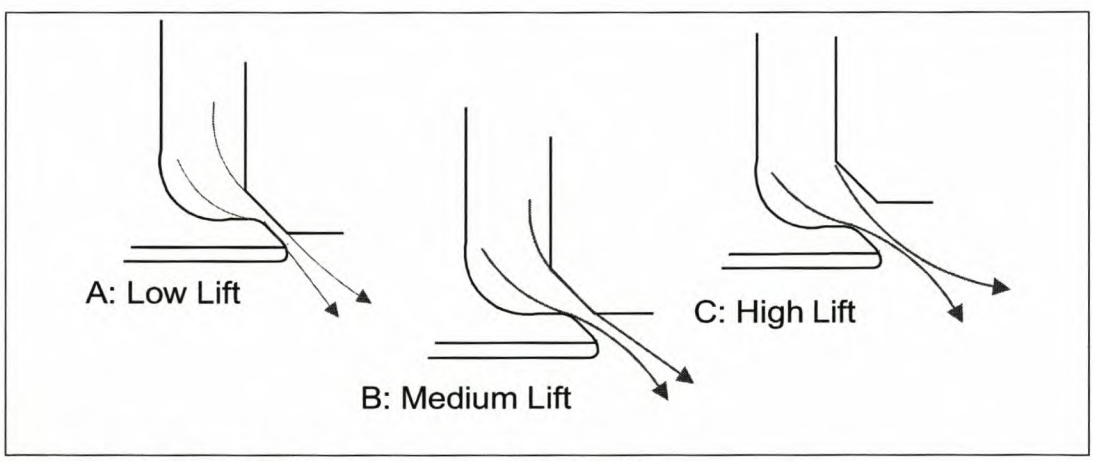

Figure 3.1. Flow patterns at various valve lifts

Figure 3.1 shows the separation that occurs between the flow and the valve seat and head as the valve lift and thus the flow rate increases. At low lift the flow is attached to the seat and valve head and a high flow relative to the valve area is measured. At medium lift the flow separates from the valve head and the relative flow decreases but increases with lift as the separated region remains constant but the area increases. At high lift the flow separates from inner edge of seat and the relative mass flow decreases once again. The flow patterns for reverse flow are of a similar nature.

3.3 Model Requirements

The flow effects must be captured as accurately as possible by the model. Since the method of characteristics used by Van Vuuren (2001) is quasi-one dimensional (flow is one dimensional but variations in area along the pipe are accounted for), the method used to describe these effects must be compatible with this method. A careful study of the literature provided the following solution:

The valve forms the boundary of the flow model for a particular manifold pipe and is therefore the last point of the calculation grid of the method of characteristics. Geometrical reduction in flow area from the manifold through the port up to the valve is taken into account by the model of van Vuuren (2001), which includes area changes.

The model described here must provide the geometrical flow area through the valve at any point of the engine cycle. The reduction in flow area and other flow losses at the valve are included using a discharge coefficient, symbolised as C_d.

The model must take into account the following flow conditions: forward flow from the inlet manifold through the inlet valve into the cylinder, reverse flow out of the inlet valve into the inlet manifold, forward flow from the cylinder out of the exhaust valve and reverse flow into the cylinder through exhaust valve.

The following sections describe the methods used to obtain the flow area and the discharge coefficient in the engine model.

3.4 Valve Discharge Coefficient, C_d

The coefficient of discharge has traditionally been defined as

$$C_d = \frac{\dot{m}_{in}}{\dot{m}_{is}} \qquad (3.1)$$

where $\dot{m}_{in}$ is the mass flow rate measured and $\dot{m}_{is}$ is the mass flow rate determined using isentropic nozzle theory between the cylinder and the throat for outflow and the pipe and throat for inflow. The subscript *is* denotes the relationship based on isentropic theory. The derivation of the ideal mass flow has been documented by Winterbourne et al. (1999), who showed that the ideal mass from the cylinder through a valve be written as

$$\dot{m}_{is} = \frac{P_{0c} A_v}{\sqrt{RT_{0c}}} \left[\frac{2\gamma}{\gamma - 1} \left(\frac{P_p}{P_{0c}} \right)^{\frac{2}{\gamma}} \left\{ 1 - \left(\frac{P_p}{P_{0c}} \right)^{\frac{\gamma - 1}{\gamma}} \right\} \right]^{\frac{1}{2}} \qquad (3.2)$$

where P_{0c} and T_{0c} denote the stagnation pressure and temperature in the cylinder and P_p denotes the pressure in the pipe. The gas dynamic theory on which this derivation is based can be found in more detail in Zucrow and Hoffmann (1976). Ramos (1989) gives a similar equation to 3.2, but extends this to the case where the flow is choked. In this case

$$\frac{P_p}{P_{0c}} \leq \left(\frac{2}{\gamma + 1} \right)^{\frac{\gamma}{\gamma - 1}} \qquad (3.3)$$

$$\dot{m}_{is} = \frac{P_{0c} A_v \gamma^{\frac{1}{2}}}{\sqrt{RT_{0c}}} \left(\frac{2}{\gamma + 1} \right)^{\frac{\gamma + 1}{2(\gamma - 1)}} \qquad (3.4)$$

An identical derivation provides the idealised flow through the inlet valve.

In most cases, flow loss data is based on measurements taken on a flow bench, a device where the head of the vehicle in question is attached to a pipe simulating the cylinder and the flow of air at various pressures and valve lifts is measured. Figure 3.2 shows such a device. It has been shown that the discharge coefficient varies primarily with changes in valve lift and pressure drop across the valve.

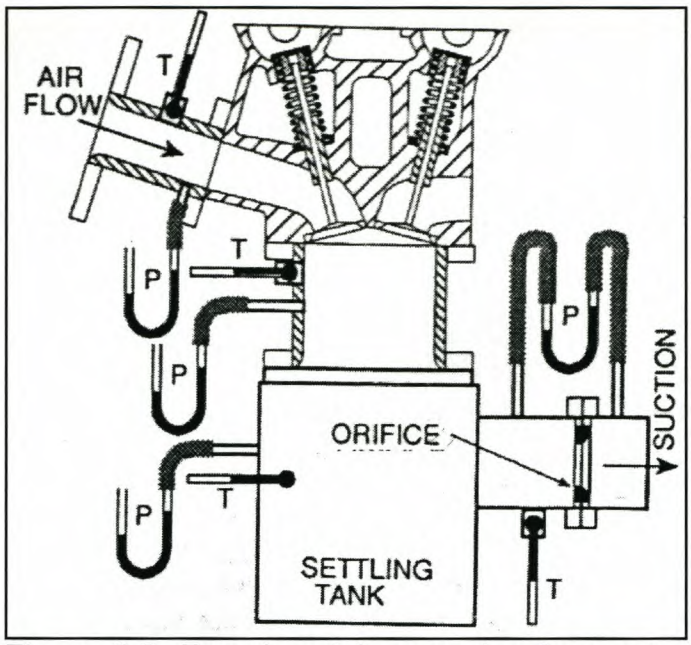

Figure 3.2. Experimental apparatus for measurement of C_d of flow into the cylinder through the intake valve (Winterbourne et al., 1999).

The following definitions are useful in the calculation of C_d. The pressure ratio, R_p, is defined as

$$R_P = \frac{P_{cylinder}}{P_{pipe}} \qquad (3.5)$$

and the lift ratio, L_k, as

$$L_k = \frac{valve\ lift}{maximum\ lift} \qquad (3.6)$$

The pressure ratio, R_P, is inverted for flow out of the valve so that the ratio remains greater than unity. The discharge coefficient must thus be presented to the simulation software in the form of a three dimensional map of C_d vs R_p vs L_k. Many of the earlier researchers found it sufficient to measure C_d vs R_p only and a large proportion of the literature provides only this relation. This has, however, been found to be insufficient for modelling purposes but is often the only data available to the engineer.

The paper of Blair and Drouin (1996) shows that the approximation in the form of equation 3.2 can be greatly in error (up to 20%) under certain circumstances when used in computer engine simulation. Ensuring that the method of calculation of Cd follows the same theory and iterative procedure as that used for the calculations within the computer simulation can solve this inaccuracy. The value of C_d derived in this way is known as the 'actual' coefficient of discharge.

The discharge coefficient is traditionally measured in a steady flow experiment and applied to an unsteady flow simulation in a quasi-steady fashion so as to enhance the reality and accuracy of the predictions it provides. (Blair and Drouin, 1996) A valid point of concern is the difference between the coefficients for steady state and pulsed flow, but there are no research results in this area available to the author.

3.5 Valve Flow Area, A_f

For the calculation of the actual C_d value, it is important that the flow area through the valve is calculated accurately. The physical geometry of a poppet valve and the valve flow area are shown in figure 3.3.

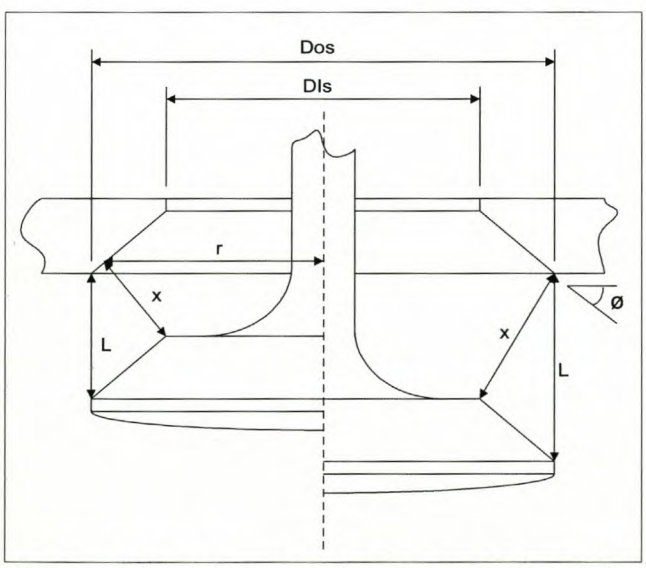

Figure 3.3. Valve curtain areas at two lift positions (After Blair and Drouin, 1996).

Traditionally, for small valve lifts the flow area has been calculated as the curtain area. The curtain area is the area formed by a "curtain" hanging between the seat and the valve.

$$A_t = CurtainArea = \pi D_{is} L\,, \tag{3.7}$$

For larger valve lifts, the flow area is defined as the smallest of the minimum port area and the curtain area.

$$\begin{aligned} A_t < A_p \quad A_f = A_t \\ A_t \geq A_p \quad A_f = A_p \end{aligned}\,, \tag{3.8}$$

The minimum port area is the smallest area formed by the valve port in the region of the valve. Due to poor design, and interference of the valve stem, this area is often less than the area formed by the valve lift and therefore forms the primary restriction in the system. More careful examination of the geometry shows that the valve curtain area is not a simple cylinder but can be represented by the frustrum of a cone defined by x, ϕ, and the seat diameters. Furthermore, the nature of this cone changes when the dimension x can no longer be measured perpendicular to the valve seat as on the left half of figure 3.3. It can be shown by simple geometry (Blair and Drouin, 1996) that this limit is

$$L_{\lim} = \frac{D_{os} - D_{is}}{\sin 2\phi}\,, \tag{3.9}$$

and that the true curtain area is

$$A_t = \pi L \cos\phi \left(D_{is} + L \sin\phi \cos\phi\right)\,, \quad L \leq L_{\lim} \tag{3.10}$$

$$A_t = \pi \left(\frac{D_{is} + D_{os}}{2}\right) \sqrt{\left(L - \left(\frac{D_{os} - D_{is}}{2}\right)\tan\phi\right)^2 + \left(\frac{D_{os} - D_{is}}{2}\right)^2}\,, \; L > L_{\lim} \tag{3.11}$$

For each time step in each valve event (inlet or exhaust), this area is then multiplied by the appropriate number of intake or exhaust valves respectively to obtain the total flow area.

3.6 Theory of Measurement and Calculation of C_d

In section 3.4, the differences between the various methods of calculation of C_d from measurements taken on a flow rig have been described. Figure 3.2 shows the position of measurement of the various pressures and temperatures required for this calculation.

For correct calculation of C_d for use with the Method of Characteristics routines of Van Vuuren (2001), the same flow theory as used in the simulation routines must be used. The thesis of van Vuuren provides ample description of the derivation of the flow equations and the modification of these for use in the method of characteristics, so these will not be repeated here. The computer code for the routines has been donated by van Vuuren and re-applied by the present author for the case of flow to or from a constant pressure cylinder through a restriction. The resulting Microsoft Windows application combines this simulation with the valve flow area and isentropic theory for calculation of C_d values from test data. These values are then valid for use in the simulation application.

The accuracy of the computer program was verified using the paper of Dent and Chen (1994), who provide C_d values for a test case, with full details of the flow case studied. These details were entered into the program, which then provided similar results to those measured by Dent et al.

3.7 Computer Program for the Calculation of C_d

The computer program can be found in the directory *Cd_calc* on the accompanying compact disk. The application is compatible with Microsoft Windows 95, 98, NT, Me and 2000.

The screen shot in figure 3.4 shows the application after a calculation. The values obtained in the measurement are entered into the given spaces and the calculate button is then used to initiate the routines. The results are displayed in the table in the lower half of the screen.

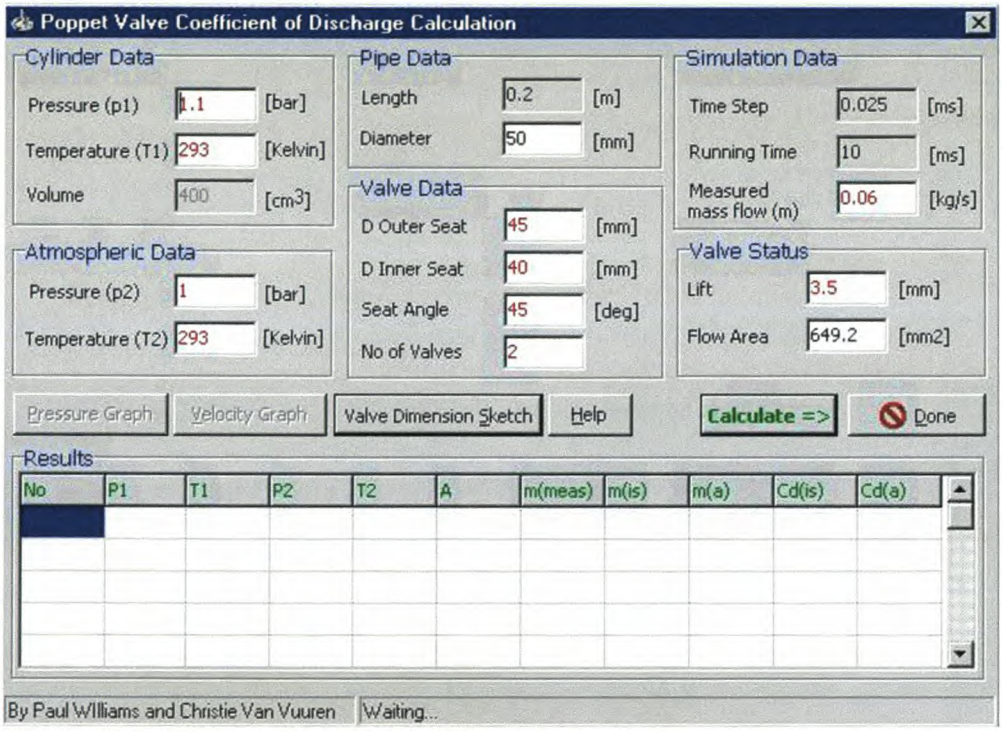

Figure 3.4. Screen shot of the *Cd_calc* program.

Full details of the program operation can be obtained by clicking the help button.

3.8 Other methods for Determination of C_d

The method of application of the discharge coefficient requires that it be determined as function of both pressure and area ratio. Measurement of this coefficient and calculation using the program described in section 3.7 has been shown to be the most accurate means of determination but this is often not possible due to availability of the engine or flow measurement equipment. Other options available to the engineer are listed below.

3.8.1 3D Flow Simulation

Simulation of the flow using a full three-dimensional flow simulation code such as STAR-CD has shown to provide good correlation with measured data (Dent and Chen, 1994). The primary restriction of this type of analysis is the necessity for multiple simulations in order to cover the full range of valve lift and pressure ratio conditions. These results can then be utilised in the computer program described in section 3.7 to obtain the required discharge coefficients.

3.8.2 Other Authors

Data can also be approximated by adaptation of existing empirical data from cases of similar geometry. This provides a problem in that the data cannot be used without careful study of the methods used in the determination of the coefficients, as well as a full understanding of the differences between the two configurations. In most cases, the coefficients must be recalculated using the flow measurement data, where supplied. The literature provides many test cases that can be used as a source of initial estimates.

3.9 Application in the Engine Simulation Program, ESA

Application in the computer program was achieved by allowing the user to enter the following variables for both the inlet and exhaust sides

- No of valves
- Valve outer and inner diameter (D_{is} and D_{os})
- Valve seat angle, ϕ
- Lookup tables for the discharge coefficient vs pressure and lift ratios for in and out flow through the valves. (calculated using the program in section 3.7)

The lookup table file is in the format of a text file where the first line is the axis of pressure ratios and the first column is the axis of lift ratios. The program is also able to interpolate between the values to obtain a more correct answer but will show an error message if the pressure ratio should fall outside the given values. It should also be noted that, theoretically, it is impossible to measure a C_d at zero lift ratio but a value must be defined here for interpolation reasons. The table can also be visualised by means of a three dimensional surface as in figure 3.5.

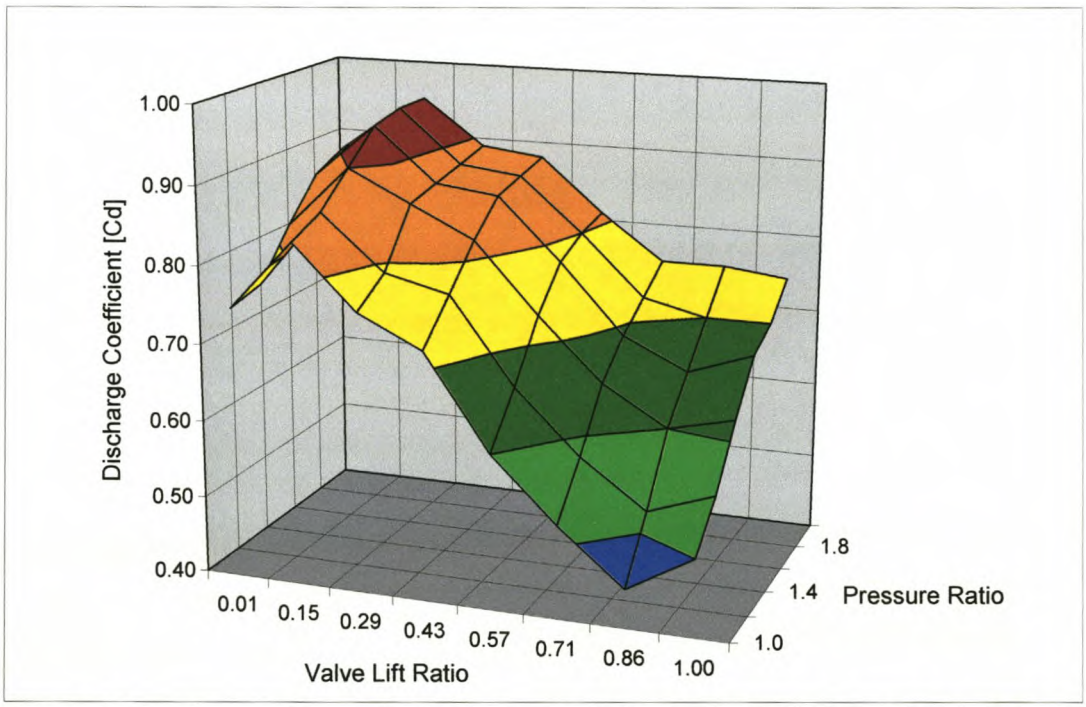

Figure 3.5. Discharge coefficient vs. pressure and lift ratios. (data reworked from Blair and Drouin (1996)).

4. CAMS AND VALVE TRAIN DYNAMICS

4.1 Introduction

4.1.1 General

In the previous chapter, the theory and practice of the modelling of the flow through poppet valves has been developed. This flow modelling requires knowledge of the motion of the valves throughout the engine operating cycle.

Because of the high forces generated in cam follower systems operating at high engine speeds, and the flexibility of valve trains, this motion can only be calculated from the cam profile if an accurate definition of this profile as well as the dynamics of the valve train can be found.

This chapter contains the theoretical developments necessary for the calculation of the dynamic valve lift response as required by the engine simulation model.

4.1.2 Overview

The chapter starts with a discussion of the theory of automotive valve train dynamics, including a development of a form of the governing equations of various dynamic models, as well as solution methods for these models. The next section discusses the issues surrounding the nature of cam and valve lift profile data, including the measurement of such data and the numerical treatment of the resulting data sets. The theory and numerical models are then implemented in a computer programs for numerical analysis of cam profiles. A short discussion on the verification of the model is given.

4.2 Theory of Automotive Valve Train Dynamics

4.2.1 Automotive Valve Train Types

Various types of valve train are in use in modern engines. Increasing use of multi-valve engines has led to the double overhead camshaft (DOHC) being the standard for passenger car engines. In these systems, the cam lobe acts directly onto a hydraulic tappet, which in turn acts on the valve stem. There are, however, still many applications, especially in larger diesel engines, where rockers and sometimes pushrods are also used. For this reason, consideration is given to all of these valve train types.

4.2.2 Automotive Cam Profiles

A short general discussion of cam profiles is given here in order to define and explain certain terms used in this section. Figure 4.1 provides definition of the various points. Figure 4.2 shows this same the cam profile, which when drawn as a radial plot on top of the base circle, forms a scale drawing of the cam as it is manufactured.

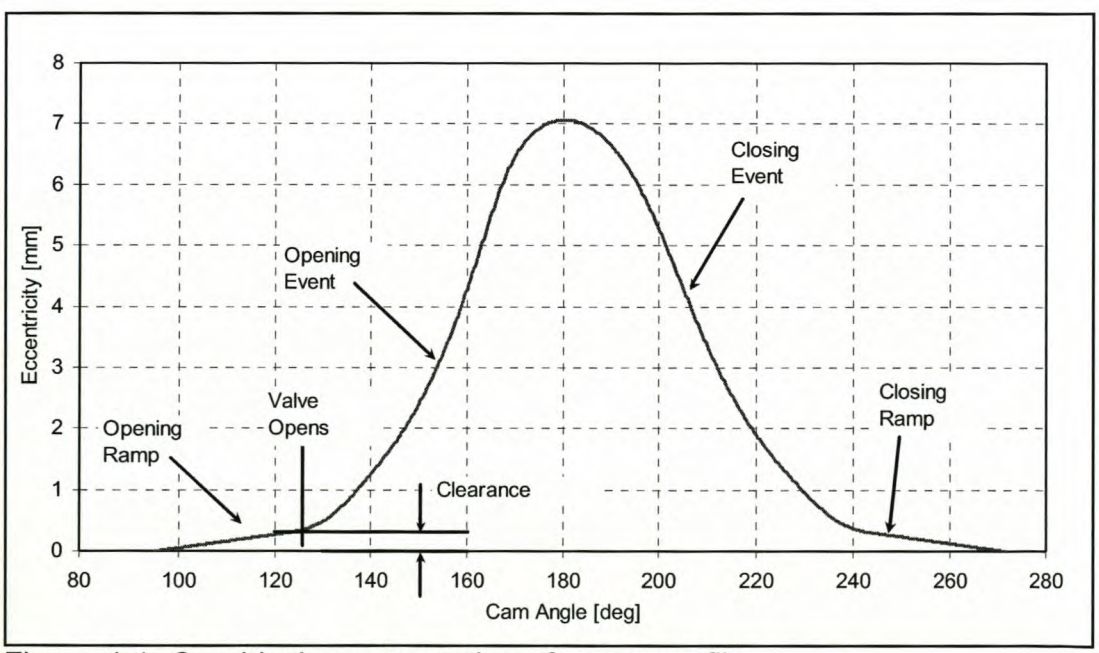

Figure 4.1. Graphical representation of a cam profile

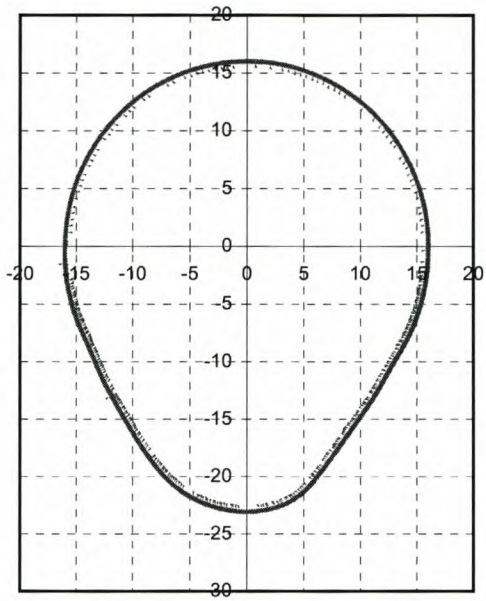

Figure 4.2. A cam profile.

Cam profiles can be defined relative to the rotation of the camshaft or the crankshaft angle, with the camshaft running at half engine speed.

Most cam profiles have a pre-event ramp that is used to take up the clearance between the cam and follower (on a system without hydraulic lifters) as well as valve train pre-load. A post-event ramp ensures that the valve seats at the correct velocity. An excessive velocity can cause damage to the valve or seat while an insufficient velocity can cause particles to remain between the valve and seat, causing a slight air-gap, which can lead to valve burn.

Valve opening and closing angles are defined in various ways, usually as the angle of a specified valve lift such as the 1 mm point. This definition varies between automotive manufacturers. In this work they will be defined as the points at which the static clearance is taken up.

The shape of the cam profile can be symmetrical if the motion of the follower is in a straight line away from the cam, and the opening and closing rams are identical. In the case of the profile of figure 4.2, the use of

an oscillating roller follower causes the profile to have an unsymmetrical shape.

The plot of cam eccentricity vs. cam angle can be differentiated to provide cam velocity and acceleration. It is very important to note that these do not necessarily have a physical meaning as the contact point of the follower on the cam profile will move according to the nature of the follower. The derivatives of the eccentricity, namely velocity, acceleration, jerk, quirk, and so on, can therefore only be used as a quick comparison with other profiles using the same follower system. The true valve motion and its derivatives will be of the same approximate form as that of the cam profiles.

Figure 4.3 shows a computer output of a differentiated cam profile. The blue and grey lines are acceleration of the follower and valve respectively while the magenta lines show the cam profile and valve motion. The positive accelerations at the start and end of the events can be clearly seen. The first provides the opening acceleration and the second slows the valve just before it closes. In between there is a period of negative acceleration where the valve slows and starts to close.

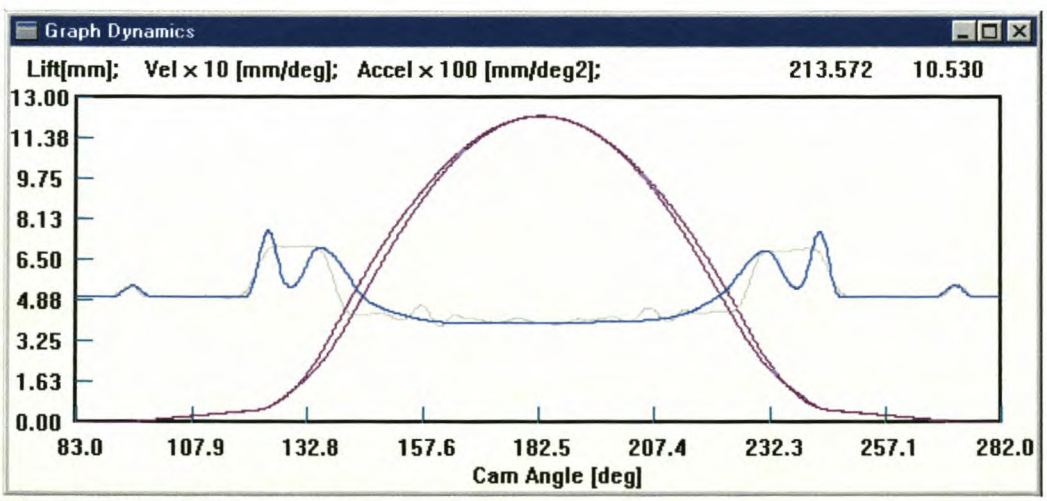

Figure 4.3. Differentiated cam profiles

4.2.3 Dynamic Models

4.2.3.1 Introduction

The moving valve train elements are subject to accelerations as the valve opens and closes. These accelerations consist of a nominal and a vibrating component. The nominal acceleration is that that would arise in a follower moving in conformity with the cam curve, the camshaft rotating at constant angular velocity. The cam mechanism is, however, a flexible system subject to inertial forces and is thus prone to deflection. This deflection consists of a component directly proportional to the nominal acceleration, and a component of the vibratory type, which remains after the cam event. The study of these deviations is important to the designer, not only to ensure that the correct valve lift profile is obtained from the designed cam profile and valve train, but also to reduce noise, wear and damage to the valve train and valve seats. The residual vibrations in the valve train can also lead to valve bounce (or slap) if these are not carefully regulated. It should be noted that all these deflections are proportional to acceleration and thus vary with engine speed. Valve train dynamic response will thus vary across the engine speed range.

4.2.3.2 Overview

Dynamic models can be divided into continuous and lumped mass models. In the case of continuous models, the equations of motion of each of the components of the system are written by considering the dynamic behaviour of a differential element of the component. This behaviour is then associated, in the limit, to an infinite number of nodes in each element, resulting in the differential equations of motion for that element. As the equations for even the simplest of such models rapidly become complex, these methods are restricted to simple systems or adapted to finite element type models. For standard analysis of the lowest natural frequencies, simple lumped mass models are utilised and

are normally characterised by the numbers of degrees of freedom that they contain.

4.2.3.3 Simple One Degree of Freedom Model

The most basic model of cam systems is the single degree of freedom (1-DOF) model. (figure 4.4) This consists of a single lumped mass, m, held in place by a retaining spring and driven through the valve train by the cam lift function $h(t)$ or $h(\theta)$ where t denotes time and θ denotes camshaft rotational angle. The spring constant, k, and the damping constants, c, have the subscripts f and s for the follower and the spring respectively.

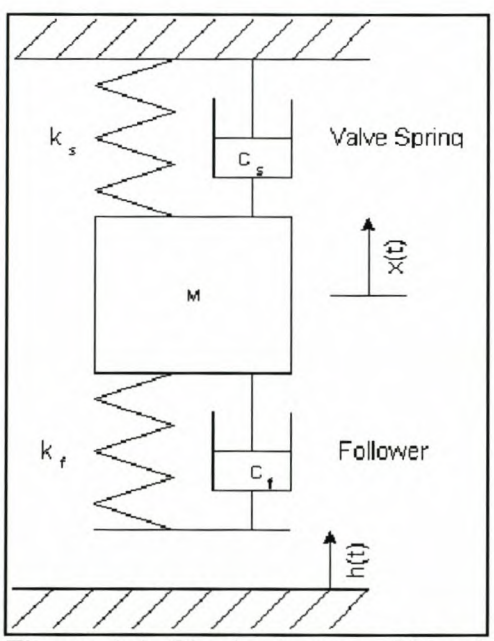

Figure 4.4. Single degree of freedom model

Using Newton's second law operating on the mass, m, we can write

$$m\ddot{x} + (c_f + c_s)\cdot \dot{x} + (k_f + k_s)\cdot x = k_f h + c_f \dot{h}. \qquad (4.1)$$

where x is the displacement of the mass and $\dot{x}$ and $\ddot{x}$ the first and second derivatives of this displacement with respect to time. (i.e. velocity and acceleration of the mass).

4.2.3.4 One Degree of Freedom Model with Rocker

This model is easily extended to include the rocker ratio as in figure 4.5.

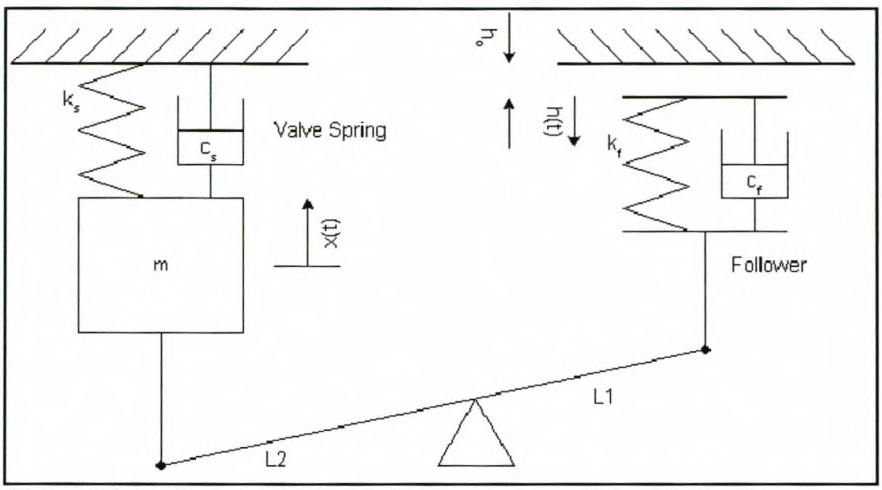

Figure 4.5. Single degree of freedom model with rocker

The equation describing this system is in the same form as equation 4.1

$$m\ddot{x} + \left(c_f \left(\frac{L_1}{L_2} \right)^2 + c_s \right) \cdot \dot{x} + \left(k_f \left(\frac{L_1}{L_2} \right)^2 + k_s \right) \cdot x = k_f (h - h_0) \left(\frac{L_1}{L_2} \right) + c_f \dot{h} \left(\frac{L_1}{L_2} \right) - k_s x_0 \tag{4.2}$$

or, including the transmission ratio $i = L_1/L_2$

$$m\ddot{x} + \left(c_f i^2 + c_s \right) \cdot \dot{x} + \left(k_f i^2 + k_s \right) \cdot x = k_f (h - h_0) \cdot i + c_f \dot{h} i - k_s x_0 \tag{4.3}$$

This can be written in the standard form for such dynamic equations

$$\ddot{x} + 2\omega\zeta\dot{x} + \omega^2 x = r \tag{4.4}$$

by setting

$$\omega = \sqrt{\frac{k_f i^2 + k_s}{m}}, \tag{4.5}$$

$$\zeta = \frac{c_f i^2 + c_s}{2\omega m} \tag{4.6}$$

$$r = \frac{k_f (h - h_0) i + c_f \dot{h} i - k_s x_0}{m} \tag{4.7}$$

For use in cam analysis, it is often easier to work on a cam angle basis so that

$$\dot{x} = \frac{dx}{dt} = \frac{dx}{d\theta} \cdot \frac{d\theta}{dt} \tag{4.8}$$

and

$$\frac{d\theta}{dt}\left[\frac{\text{deg}}{\text{sec}}\right] = N\left[\frac{rev}{\text{min}}\right] \cdot \frac{1}{60}\left[\frac{\text{min}}{\text{sec}}\right] \cdot 360\left[\frac{\text{deg}}{rev}\right] = 6N\left[\frac{\text{deg}}{\text{sec}}\right] \tag{4.9}$$

so that we can substitute q for the displacement with

$$\dot{q} = \frac{dq}{d\theta} \quad and \quad \ddot{q} = \frac{d^2 q}{d\theta^2} \tag{4.10}$$

Consequently,

$$\dot{x} = \frac{dx}{d\theta} \cdot \frac{d\theta}{dt} = 6N \cdot \frac{dx}{d\theta} = 6N\dot{q} \tag{4.11}$$

$$\therefore \quad \ddot{x} = \left(\frac{d\theta}{dt}\right)^2 \cdot \frac{d^2 x}{dt^2} = (6N)^2 \cdot \frac{d^2 x}{d\theta^2} = (6N)^2 \ddot{q} \tag{4.12}$$

The standard form (equation 4.4) can now be written as

$$(6N)^2 \ddot{q} + (6N) \cdot 2\omega\zeta\dot{q} + \omega^2 q = r \tag{4.13}$$

So that our standard form becomes

$$\ddot{q} + 2\omega_\theta \zeta_\theta \dot{q} + \omega^2 q = r \,. \tag{4.14}$$

with redefined substitutions

$$\omega_\theta = \frac{1}{6N}\sqrt{\frac{k_f i^2 + k_s}{m}} \tag{4.15}$$

$$\zeta = \frac{1}{6N}\frac{c_f i^2 + c_s}{2\omega_\theta m} \tag{4.16}$$

The solution of the resulting equation is discussed in section 4.2.4.

4.2.3.5 Multiple Degree of Freedom Models

Many authors have investigated the result of extending these models to more degrees of freedom as in the model of figure 4.6.

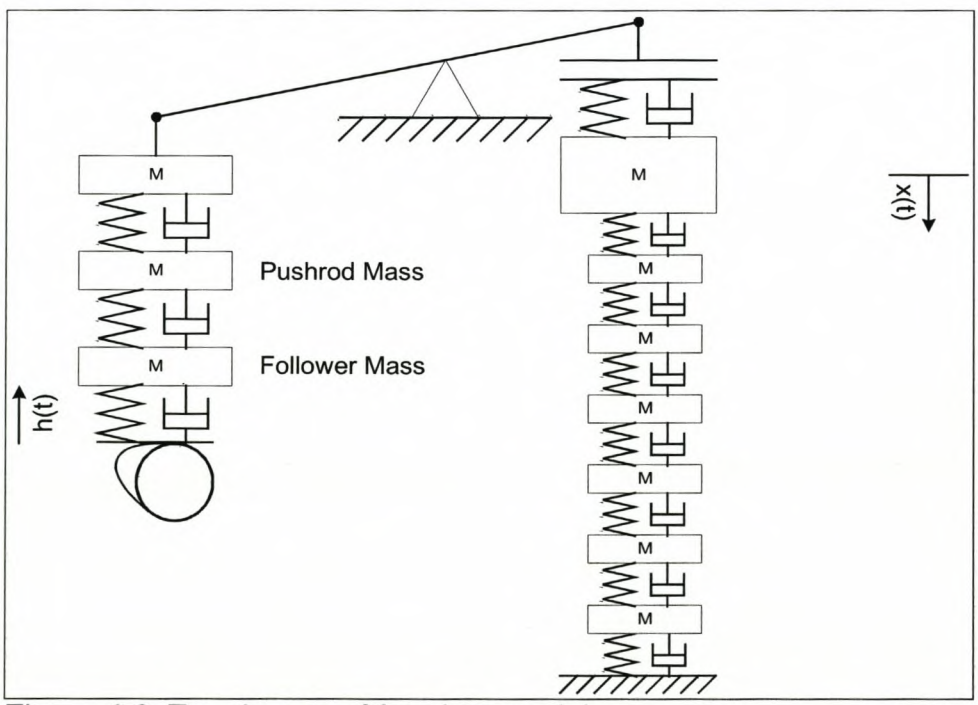

Figure 4.6. Ten degree of freedom model

Koster (1974) investigated the responses of complex models with one, two and four degrees of freedom. He concluded that the replacement of a multi degree of freedom model by a single degree of freedom model

with the same lowest natural frequency produces errors in the response of only a few percent. He notes, however, that the accelerational response at impact requires some care.

Wagstaff (1968) compared the response of a single DOF and a ten-mass system as in figure 4.6. From the comparison of these models to experimental data he concluded that the simulation of the valve spring was the most important factor in obtaining agreement with experimental response. He found a marked lack of agreement between the single DOF model and measured data in both the vibrational frequency and amplitude during the central period of the cam event. The model with multiple masses representing the valve spring was able to simulate valve spring surge and thus provided a more accurate response and was especially useful in determining the point at which valve bounce occurred. He also concluded that a cam design based on the one degree of freedom model would therefore be unlikely to control the valve motion adequately in this negative acceleration period.

The equations of motion for this system can be written by combining the equations of motion for each individual mass into a matrix system so that

$$\mathbf{M}\underline{\ddot{x}} + \mathbf{C}\underline{\dot{x}} + \mathbf{K}\underline{x} = \underline{f}(t)\,. \qquad (4.17)$$

The matrices $\mathbf{M}$, $\mathbf{C}$, and $\mathbf{K}$ are the mass, dampening and stiffness matrices respectively.

The development of the equations of motion for the multiple degree of freedom model is lengthy and is therefore presented separately in Appendix B.

4.2.3.6 Valve Spring Modelling

There have been many studies of the dynamic response of valve springs in high-speed engines. Philips et al. (1989) showed that an over-simplified model neglected the spring surge effects that were shown to

play a large part in the dynamic response of the system. This is due firstly to the valve spring being a very elastic medium compared with the rest of the valve train and secondly to the fact that, unlike the rest of the valve train, which becomes detached and inactive during the cam dwell period, the spring remains fastened at both ends and oscillates. This oscillation lasts through the dwell period of the cam and provides non-zero initial conditions for the valve motion. The valve spring model must therefore take at least the first few modes of oscillation into account and simulate these through the entire cam rotation. Two different approaches can be taken here, modelling in the frequency domain with the summation of the natural modes of the spring, and a discrete model with a number of masses. An iterative procedure should be used to obtain the steady state response of the system through the entire cycle.

Philips et al. (1989), and later Schamel et al. (1993) developed a simple modal approach for linear valve springs which they extended to an approach to handle a modal model of progressive springs in the frequency domain. When extended to include progressive effects (such as coil clash), this model was shown to provide accurate simulation of valve spring surge. They compared the results of this model with a discrete model including coil clash conditions and found that the discrete model was more accurate for most conditions, although the modal model predicted behaviour of the valve spring well for the period that the valve was closed. The best results were obtained by using the modal model to predict the initial conditions of the discrete model, thereby reducing the number of iterations necessary to obtain convergence.

4.2.3.7 Hydraulic Lash Adjusters.

Hydraulic tappets or lash adjusters (HLAs) have become globally accepted as the best method of eliminating follower lash and thus valve train noise and are present in almost all modern valve train designs. The effects of hydraulic tappets on the dynamic response of the valve train are therefore of great importance to the cam design, especially in the

case of the overhead cam (OHC) where the HLA forms the only link between the cam lobe and the valve and therefore dictates the response.

If the response of the HLA is judged to be of importance, the designer is forced to make a detailed study of the design of the adjuster so that an accurate model can be constructed.

Models of lash adjusters take the following into account:

- Geometry and mass of the adjuster.
- Compressibility of the oil in the central chamber.
- Compressibility of the air entrapped in the oil.
- Leak down rate of the oil (oil viscosity).
- Properties of internal adjustment spring.
- Physical properties of the adjuster (material spring rate etc.)

The development of such a model is not given here as the HLA components are normally purchased 'off the shelf' or developed together with companies specialising in these components (e.g. INA bearings, Germany). These companies are able to supply a reduced dynamic model of any of their standard adjusters for development purposes. The reader is also referred to the paper of Zou and McCormick (1996).

4.2.3.8 Follower Lift Functions

The follower is defined as the object or surface that is in direct contact with the cam lobe while the camshaft is rotating. This surface can have various forms, some of which are highly complex. These complex shapes are unusual and are used to either simplify the form of the cam lobe, or to provide variable cam timing, when linked to a moving mechanism. The most common form of follower used in the past has been the flat face of a hydraulic tappet. This is increasingly being replaced by a circular roller, mounted on bearings, that reduces the friction inherent in these systems while at the same time allowing a

negative cam profile flank radius, increasing the scope of accelerations available to the profile designer. The following sections describe the geometrical theory necessary to be able to model the movements of such follower types when in contact with a cam lobe

4.2.3.8.1 Point follower.

The point follower is the simplest of the follower systems to model, even when a possible offset of the follower line of action from the camshaft centre is included.

At this point it is necessary to differentiate between the camshaft rotational angle, θ, which is the angle through which the camshaft has rotated from a defined zero position, and the camshaft angle, φ, which is the angle used to locate a point on a camshaft profile when the camshaft is in position θ. These developments are based on a discrete (φ, r) definition of the cam profile. For each camshaft rotational angle, θ, the discrete profile points can be transferred into points on an appropriate x, y axis system using the following relations.

$$x = r \cdot \sin(\varphi + \theta); \quad y = r \cdot \cos(\varphi + \theta) \tag{4.18}$$

Generally the axis system is chosen through the rotational centre of the camshaft with the y-axis along the plane of motion of the follower. The location of the follower along the x-axis is known. It is then simple to mathematically identify the cam surface y value for each θ at this given x value. Because the cam data is given as discrete values, a cam data point will seldom exist at exactly the given follower x location and so the point identification routine must allow for interpolation values.

4.2.3.8.2 Flat Foot Follower.

This development is also easily implemented in a computer model. With the y-axis chosen perpendicular to the face of the follower, for

each camshaft angle, the cam lobe point that has the greatest y value is the point of contact. The difference between this y value and the base circle y value then gives the follower lift.

4.2.3.8.3 Roller Follower.

The calculation of the follower lift for each angle progresses as in section 4.2.3.8.2, except that the contact point must be obtained by an iterative method.

As the camshaft is rotated, the positions of each of the lobe points in the x,y plane can be calculated. The iterative process centres on the height of the roller follower base circle centre point. For each follower centre position, the distance between the centre of the roller and each lobe profile point can be calculated. The target of the iteration is then a roller height at which the smallest distance between a lobe point and the roller centre is the diameter of the roller. The roller position giving this smallest distance is then used to calculate the lifter displacement.

4.2.3.8.4 Rocker With Curved Contact Face

This development is similar to the Roller follower development and is based on the nomenclature of figure 4.7. The complexity of this development arises from the fact that the contact point between the rocker face and the cam surface moves in both the horizontal (x) and the vertical (y) direction as the rocker is pushed upwards by the lobe of the cam. This causes a change in the geometry of the relationship between cam and follower centre positions.

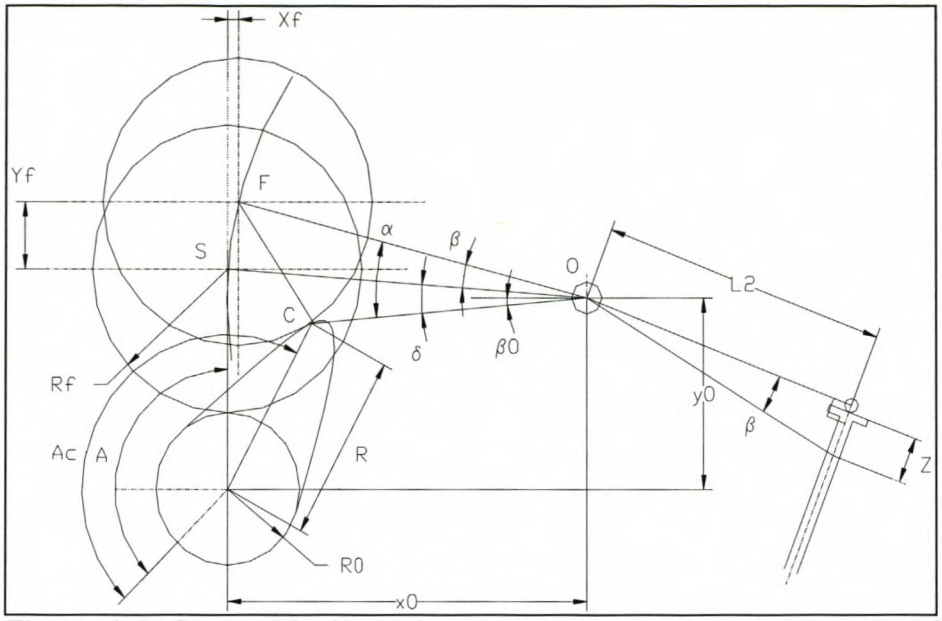

Figure 4.7. Geometrical development: rocker with curved contact face.

The iteration varies the angle β from which the follower centre point can be calculated as follows.

Referring to figure 4.7, with the origin located at the camshaft centre,

F = Follower centre , (x_f, y_f)

O = Rocker centre, (x_o, y_o)

C = Contact Point, (x_c, y_c)

S = Original Follower centre, (x_s, y_s)

With the rocker in the lowest position, the angle β is

$$\beta_0 = \arctan\left(\frac{y_s - y_o}{x_o}\right) \quad \text{with} \quad x_s = 0. \tag{4.19}$$

The following distances are needed to find the new angle β

$$CO = \sqrt{(x_c - x_o)^2 + (y_c - y_o)^2} \tag{4.20}$$

$$CF = R_f \tag{4.21}$$

$$FO = L_1 \tag{4.22}$$

$$OS = \sqrt{(x_s - x_o)^2 + (y_s - y_o)^2} \tag{4.23}$$

$$SC = \sqrt{(x_s - x_c)^2 + (y_s - y_c)^2} \tag{4.24}$$

Using known geometrical relations in ΔFOC:

$$\alpha = \frac{\arccos\left(FO^2 + CO^2 - CF^2\right)}{2.FO.CO} \tag{4.25}$$

and in ΔSOC

$$\delta = \frac{\arccos\left(OS^2 + CO^2 - SC^2\right)}{2.OS.CO} \tag{4.26}$$

giving

$$\beta = \alpha - \delta\,. \tag{4.27}$$

The new point F can then be calculated from

$$x_f = L_1 \cos(\beta + \beta_0) \quad y_f = L_1 \sin(\beta + \beta_0) \tag{4.28}$$

The contact point is then calculated iteratively as for the roller follower in section 4.2.3.8.3, and the angle β determined. The rocker drive arm length rotated through this angle then provides the output lift on the valve side of the rocker.

4.2.3.9 Other Considerations

There are other considerations that can be taken into account in the analysis of the valve train response. These include:

- Oil film dynamic effects
- Camshaft torsional dynamics
- Variable tappet stiffness
- Spring coil clash
- Spring end non-linearities
- Hysteresis of valve train elasticity

Analyses of all of these types of effects can be found in the literature, but have effects that are so small as to be negligible in the current study.

4.2.3.10 Model Extent

The developments in section 4.1 and 4.2 have shown the different options available with respect to the degrees of freedom and the extent of the features that can be included in a dynamic model. However, it is important to remember that excessive detail and accuracy in this section of the modelling will be wasted if the same accuracy is not achieved in the valve flow and engine models.

A study in the literature of the relative accuracy of the single and multiple degree of freedom models shows that the difference in calculated valve lift between the two models is in the order of 1%, except for cases where the valve train becomes disconnected at high speed and valve bounce or severe spring surge takes over from the normal tightly controlled operation. Since the overwhelming proportion of production engines have valve trains designed to operate without bounce within their speed range, it is unnecessary for us to consider these options and we are free to use a vastly simplified model to calculate the valve lift.

The user who finds, using the simplified model, that the valve train dynamics are not tightly controlled (i.e. bounce occurs), can use the

developments of the multi degree of freedom model to construct a simulation that can reveal these deviations in more detail.

4.2.4 Solution of Dynamic Models

Once a dynamic model has been constructed, and model input data has been determined, an attempt can be made to extract information on the dynamic movement of the valve head over the duration of camshaft rotation. In many cases, this solution will be in the form of a discrete lift values for each crankshaft angle. In other cases, an analysis of the model can provide information regarding the expected resonance frequencies of the existing components and so aid with the design of new components.

Solution of such models can be performed in various ways, the two most important being the use of a commercially available dynamics computer package, and the writing of purpose-designed code for the solution of a specific problem. In this case, the development of such solutions is discussed.

In order to obtain a valve lift profile solution for a certain cam profile input, a numerical solution of the defining equations is required. A common method chosen for the numerical solution of one degree-of-freedom models is the Newmark Method (Theron, 1996). The Multi-DOF model can be solved by use of the Generalised Alpha method. (Chung, 1993).

These methods are described briefly here but complete details of the solution methods and the numerical convergence and accuracy of the solutions can be found in the given references.

For each solution method, numerical values for the mass, elasticity and damping values of each component in the model should be available. The model is solved for a non-steady vibration with the cam-profile providing the input function. At each time-step, the derived equations are solved for the motion at that point, before the solver passes on to the next time step.

Since vibration of the valve train can continue through the rest-period of the cam providing non-zero initial conditions for the various components, the numerical approximation should be run through a number of rotations of the camshaft so that convergence of the initial conditions can be obtained.

4.2.4.1 The Newmark Method

The Newmark method is a two step method based on the solution of the differential equation shown in equation 4.15. The method solves the equation of motion at time-step i+1 where.

$$\ddot{q}_{i+1} + 2\omega\zeta\dot{q}_{i+1} + \omega^2 q_{i+1} = r_{i+1} \quad ,i = 1,2,3...n \tag{4.29}$$

The Newmark method accepts that the displacement and velocity at t_{i+1} is given as

$$q_{i+1} = q_i + \Delta\theta\dot{q}_i + \frac{\Delta\theta^2}{2}\left[(1-2\beta)\ddot{q}_i + 2\beta\ddot{q}_{i+1}\right] \tag{4.30}$$

$$\dot{q}_{i+1} = \dot{q}_i + \Delta\theta\left[(1-\gamma)\ddot{q}_i + \gamma\ddot{q}_{i+1}\right] \tag{4.31}$$

By substituting equations (4.30) and (4.31) into (4.29), it follows that

$$\ddot{q}_{i+1} = \frac{r_{i+1} - \omega^2 q_i - \left(2\zeta\omega + \omega^2\Delta\theta\right)\dot{q}_i - \left[2(1-\gamma)\zeta\omega\Delta\theta + (1-2\beta)\frac{\omega^2\Delta\theta^2}{2}\right]\ddot{q}_i}{1 + 2\gamma\zeta\omega\Delta\theta + \beta\omega^2\Delta\theta^2} \tag{4.32}$$

where β and γ are two parameters that can be changed to change the behaviour of the integration method. These are left as variables in the model and computer simulation but are usually chosen to be $\beta=1/4$ and $\gamma=1/2$, which is known as the Constant Average Acceleration Method. (Theron, 1996)

4.2.4.2 The Generalised-Alpha Method for Multi-DOF Models

The multiple degree of freedom model results in a set of equations of the form

$$\mathbf{M}\underline{\ddot{x}} + \mathbf{C}\underline{\dot{x}} + \mathbf{K}\underline{x} = \underline{f}(t) \tag{4.33}$$

This equation is a simplification of a set of coupled equations of motion, which can be reduced to a set of single degree-of-freedom models. A weighted approximation of the differentials can be incorporated and the resulting sets of equations solved for each time step, providing the dynamic response of each point in the system over time.

4.3 Dynamic Model Input Data

The accuracy of the results of an analysis of valve train dynamics can only be as good as the data used in the model. In many cases, the lumped mass models make use of assumptions of combined masses, spring rates and damping values that prevent the direct measurement of these values from existing components, or the calculation of these values from the design specifications. The accuracy of the cam profile data used is also of great importance since errors of only one or two microns of deflection can cause large errors in the derivatives of this motion. Many approximations have to be used in obtaining this data. This section describes the methods of measurement and derivation of the necessary values, as well as the probable effects of necessary approximations.

4.3.1 Valve Train Data

4.3.1.1 Lumped Masses

Lumped mass values can be directly measured by weighing components, or derived from design drawings. In some cases, however, the form of the parts is such that an approximation as a lumped mass would be inaccurate.

4.3.1.2 Valve Spring Rates

Valve spring rates for use in the design and analysis models can be measured by the simple method of noting the deflection at various loads. Measurement at close intervals can serve as an indication of the linearity of the spring within the region of operation. Where two or more springs are used in parallel or in series, these can be measured separately and the results combined.

For use in a multi DOF simulation, the valve spring is modelled as a number of individual masses and springs. The spring element between each mass will have the same spring rate as the entire coil. Further accuracy can be obtained by a static analysis of the relative movement of each coil under pre-determined loads.

4.3.1.3 Valve Train Spring Rates and Histeresis

An important input into the model is the spring rate of the follower system. Unless a detailed finite element analysis has been performed on the system, this data is best obtained by experimentation. This experiment requires compression loading of the static valve train with measurement of the deflection of the train under this load. The spring value of the valve train is then a linearisation of the measurements of the applied force divided by the deflection under that force, within the range of operation of the component.

The paper of Kanesaka et al. (1977) raises an issue that can contribute to a slight inaccuracy of this analysis. It is shown that there is a certain amount of friction in any valve train that causes a slight hysteresis in the elasticity value. This analysis can also be used to incorporate the stiffness of the camshaft and camshaft bearing system itself, if the measurement is done in such a way that these deflections are also incorporated.

4.3.1.4 Damping Coefficients

Obtaining valid values for the damping coefficients of the various elements of the valve train is a difficult task and, because of the small effects of these values, it is often not worth the time required. The most common methods of obtaining these values are

- Literature: using a value from a similar system.
- Measurement of the decay of a vibration created in the system.
- Detailed physical analysis.

4.3.1.5 Effective Masses

Many parts of the valve train either do not have a centre of gravity that coincides with that of the lumped mass, or that rotates around a pivot, so that the effect of the mass in the model can only be encompassed by the use of an effective mass.

There are two main masses that must be approximated by effective masses. The first is the effective mass of rotating parts such as rockers and the second is the mass of the coils of the valve spring.

The effective mass of a rotational part such as a rocker can be calculated using the moment of inertia of the rocker. This can be found by measuring the period of oscillation of the rocker, τ, when suspended from an axis close to the valve train side of the rocker. The moment of inertia around that point is then

$$I_0 = \frac{mdg\tau^2}{4\pi} \tag{4.34}$$

where m is the mass of the component and d is the distance from the point of oscillation to the centre of gravity of the part. This moment of

inertia can then be translated to the normal centre of rotation (i.e. the rocker shaft centre) using the following relationships:

$$I_G = I_0 - md^2 \tag{4.35}$$

$$I_C = I_G + mj^2 \tag{4.36}$$

$$I_C = m_{re} i^2 \tag{4.37}$$

The subscripts C, G and O indicate the moment of inertia around the rocker rotational point, centre of gravity and oscillation measurement point respectively. The three distances d, j and i are, respectively, the distance from the centre of gravity to the measurement point, the distance from the rotational point to the centre of gravity, and the distance from valve stem to the rocker shaft centre. The result is then

$$m_{re} = \frac{m}{i^2}\left(\frac{dg\tau^2}{4\pi} - d^2 + j^2\right) \tag{4.38}$$

The effective mass of the valve spring can be found by calculating the kinetic energy of an element of the spring element located a distance, y from the end of a spring of length l. The velocity of this element is

$$\dot{x}\frac{y}{l} \tag{4.39}$$

Integrating over the spring length,

$$T = \frac{1}{2}\int_0^l \left(\dot{x}\frac{y}{l}\right)^2 \frac{m_s}{l} dy \quad = \quad \frac{1}{2}\frac{m_s}{3}\dot{x}^2 \tag{4.40}$$

Since the kinetic energy can also be written as

$$T = \frac{1}{2} m_{eff} \dot{x}^2 \tag{4.41}$$

it follows that the effective mass of the spring is

$$m_{eff} = \frac{m_s}{3} \tag{4.42}$$

4.3.2 Cam Profile Measurement

The accurate measurement of cam lobe profiles is the most important part of the dynamic modelling. In many cases the manufacturer's data is available as an input in tabulated form, but often this must be measured from existing components. There are many commercial systems available consisting of a measurement bench with an angle measurement device, a point follower and a displacement transducer, together with a software package for processing the data. Experience shows that the best results can be obtained by averaging over a large number of measurement cycles. It is also important that values of cam eccentricity be measured at very small increments of angle (i.e. 0.25 deg) for greatest accuracy.

Perhaps even more important than the measurement of the profile is the processing of the measured data. The raw data from such a measurement, although smooth to the eye, often contains large fluctuations in the second and third derivatives of the eccentricity with respect to the cam angle. Because these derivatives are used in the dynamic calculations, it is important that the best representation of the cam profile with smooth derivatives is obtained. Various methods of smoothing have been investigated, including Fourier analysis and various types of curve fitting. The best results have been obtained using a least squares fit to a third order polynomial function. The reader is referred to the detailed analysis of these methods by Gerald and Wheatley (1989).

4.4 Application in a Computer Program: ESACam

The target of this development was a computer program with the ability to produce a table of valve lift vs. crankshaft angle. This could then be used, as described in chapter 3, to calculate the valve flow area for each stage of the engine cycle, which is an input to the ESA engine simulation program.

A computer program, ESACam was written to accompany the ESA engine simulation. This has a simple Microsoft Windows interface and allows the calculation of the valve motion from a tabulated cam profile and follower physical properties.

4.4.1 Model Type

The single degree of freedom model has been used for analysis. This can be combined with a flat, point, roller or rocker roller follower model. The resulting equations are solved using the Newmark method.

4.4.2 Use of the Computer Program

A computer program, ESACam has been written for cam profile analysis. The user is able to input a table of measured cam data, as well as the physical and dynamic properties of the valve train, and a resulting valve lift is calculated. This is in the form of a table of valve lift vs. crankshaft angle, which can be used directly in the ESA engine simulation program.

The computer program as well as the Borland Delphi Windows code can be found on the accompanying compact disc. A user manual for the program is presented in Appendix F.

4.5 Verification of the Computer Program

Although the results obtained from the ESAcam program followed the expected trends, it was deemed important that a test case be applied for which an analytical solution exists so that confidence in the program could be increased.

The test case used was the analysis of a "theoretical" cam profile consisting of a step from 0 mm to 1mm follower lift at cam angle=0.

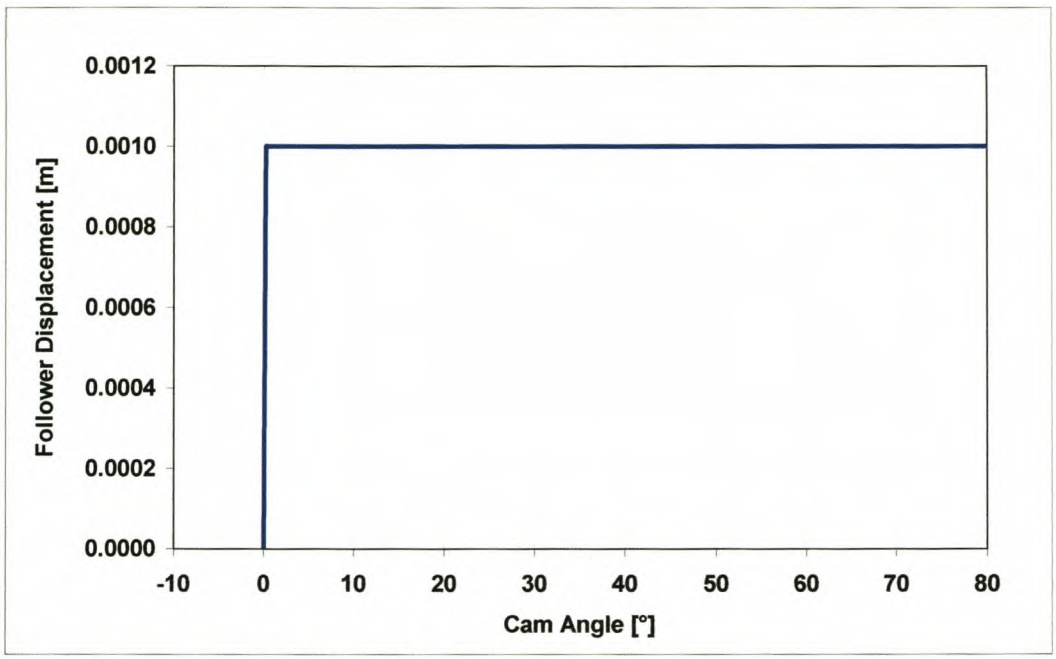

Figure 4.8. "Step" cam function.

The follower variables used in the program are shown in the screen capture from the program input dialog:

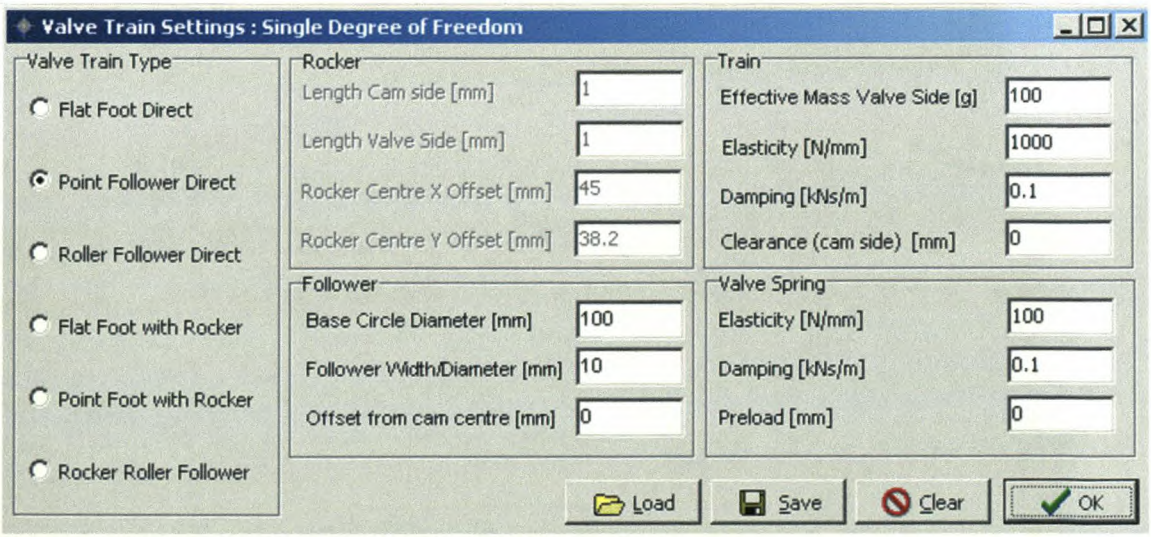

Figure 4.9. Input variables for the ESACam test case.

The analytical solution for this test case was obtained using the method described by Thomson (1993). In his example, a simple mass-spring-damper

system is excited by a force, F_0, at time $t=0$. The system is described by the equation

$$\ddot{x} + 2\omega\zeta\dot{x} + \omega^2 x = \frac{F}{m} \tag{4.43}$$

Thomson shows that the application of the convolution integral

$$x(t) = \int_0^t f(\xi)h(t-\xi)d\xi \tag{4.44}$$

with the step function

$$f(\xi) = F_0, \quad t > 0 \tag{4.45}$$

gives the solution

$$x(t) = \frac{F_0}{k}\left[1 - \frac{e^{-\zeta\omega_n t}}{\sqrt{1-\zeta^2}} \cdot \cos\left(\sqrt{1-\zeta^2}\,\omega_n t - \psi\right)\right] \tag{4.46}$$

where

$$\tan(\psi) = \frac{\zeta}{\sqrt{1-\zeta^2}} \tag{4.47}$$

This solution was applied to the governing equations developed in section 4.2.3.4, with an engine speed of 4000 rpm. The analytical solution was calculated for each cam angle in a simple spreadsheet. The result is shown in Figure 4.10.

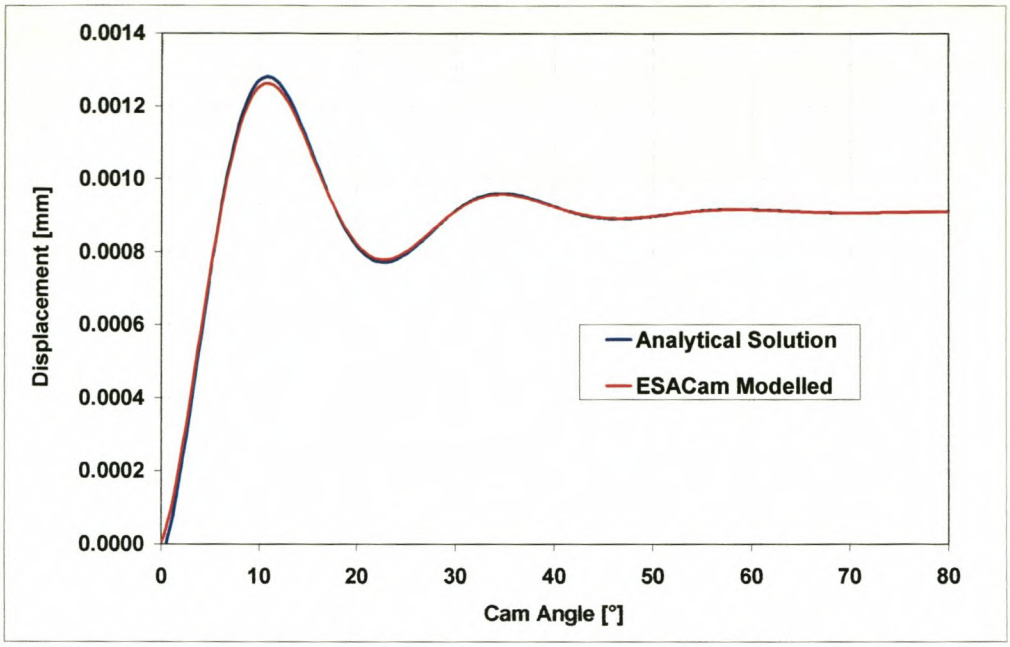

Figure 4.10. Comparison of analytical and ESACam simulated results.

The similarity of the results makes it difficult to differentiate between the lines, which are almost totally identical. The spreadsheet containing this analysis can be found on the accompanying compact disk.

This result has given great confidence in the use of the program.

5. ENGINE SIMULATION MODEL

5.1 Introduction

A simple study of the operation of the internal combustion engine reveals that the performance of the engine is primarily a function of the ability of the engine to ingest, combust and expel a fuel/air mixture. Chapters 2, 3 and 4 present the theory of modeling of internal combustion engine thermodynamics and valve flow. In parallel with this study, van Vuuren (2001) has derived the equations necessary for simulation of the pulsed flow in the inlet and exhaust manifolds. The operation of each of these elements has been described theoretically by sets of governing equations, for which a numerical solution may be found, given the correct initial and boundary conditions.

Although each of these models can be described relatively simply, the demands for accuracy quickly lead to complex sets of equations. The simultaneous solution of these as a system adds complexity. Solution is further hampered by the fact that the flow through the engine is non-steady so that boundary conditions between the models are a function of time as well as engine operating condition. Such a system lends itself to simulation by means of computer code.

The idea of a computer based engine simulation model is by no means unique and has been the focus of much study since that advent of computers. Software models for engines vary from extremely simple empirical based theory, through single dimensional models to full three-dimensional computational fluid dynamic calculations. Each step in this progression requires vast increases in processing power. At the time of publication of this thesis, a full three-dimensional CFD analysis of engine flow required processing time in the order of days for even the simplest cases.

This chapter describes the implementation of the derived theory into a computer code for the PC that can be used to simulate the performance of an engine within a short time frame (less than 8 hours).

5.2 Overview

The first section outlines in broad terms the structure of the computer implementation of the models described and defines the method of interaction between the different models on a thermodynamic level.

A section describing the theory whereby the output of the engine may be calculated from the thermodynamic results follows this.

Finally, there is a section describing the code implementation in more detail, as well as describing the structure and use of the resulting Windows application.

5.3 Structural Overview

This development is based on a quasi-one-dimensional pipe flow model linked to a thermodynamic modeling of one cylinder only, with no interaction between cylinders. The pipe flow model is termed quasi-one dimensional as the pipes have a variable flow area. This model includes compression, combustion, expansion, heat transfer, friction and transfer of gasses through the induction and exhaust systems of the engine.

Similar developments have been used in PC based models such as Dynomation (Audie Technology, 1994) and SPICE (Charlton, 1990). Often these models make use of very simple in-cylinder and wave action codes to predict engine performance, given a simple set of engine dimensions and operating conditions. These simplifications are made in order to reduce processing time.

Only recently have developments in personal computer capacity lead to the possibility of developing codes for the PC that can simulate the complex, unsteady, pulsed flows in manifolds, as well as the combustion of the resulting cylinder charge. It was the aim of this development to generate such a program that could be used to reduce engine development time and prototype manufacturing cost within the framework of the South African motor industry.

Chapters 2, 3 and 4 have described some of the models required in the full simulation of engine operation. These models are required to interact with each other so that an accurate simulation may be obtained. The system has a domain that stretches from the plenum end of the inlet tract, through the tract, inlet valves, cylinder, exhaust valves, and exhaust tract up to the first expansion of the exhaust at a silencer box. The boundaries thus described contain the elements with the greatest influence on engine performance.

The model consists of the defining equations of many sub-models at small time steps throughout the 720 crankshaft degrees of the engine operation (four stroke operation is assumed). These time steps are chosen as crankshaft degree increments for ease of calculation and data input. The thermodynamic and flow conditions at the end of each time step are calculated from the values at the previous time step as well as the boundary conditions of the system, by use of an integration method.

At the start of the calculation, the initial conditions of the pressure and velocity inside the manifold pipes and cylinder are assumed, and integration commences at the point of inlet valve closure (IVC).

For each time step the following calculations occur.

- Solution of equations of state to obtain the gas properties inside the cylinder (the one-zone model is used for the first 2 iterations and thereafter the two-zone equations are applied).

- Solution of the pressure and velocities present inside the inlet and exhaust tracts.

- Calculation of the mass flow through the valves, based on the pressure difference across the valve and the valve lift.

- A mass and energy balance inside the cylinder, with heat addition where there is combustion, and losses where appropriate.

The output of the engine can then be summed across the engine cycle (2 revolutions for 4-stroke engines).

5.4 Indicated Output

The thermodynamic model of an engine is based on an energy balance within the cylinder, which is a control volume with a moving wall. At completion of this balance, the energy produced by the engine can be calculated from an integration of the energy transferred to the pistons as work. After deduction of losses, this can then be used to calculate engine torque and thus power.

The pressure vs. specific volume diagram of an engine is known as the indicator diagram. The area within this cycle is a measure of the work done by the gas and can be shown to be

$$W_{ab} = \int_{a}^{b} P.dV \tag{5.1}$$

where a and b are the start and end points of the calculation, usually defined in terms of engine crankshaft angle. In comparing the performance of internal combustion engines it is also useful if the terms used to express this performance are independent of the size of the engine. For these reasons, the performance can be given in terms of mean effective pressures where

$$MEP = \frac{W}{V_d} \tag{5.2}$$

W and V_d are the work done by, and the displaced volume of one cylinder. indicated mean effective pressure ($IMEP$), for each cylinder, is therefore defined as

$$IMEP = \frac{\int_{IVC}^{EVO} P.dV}{V_d} \tag{5.3}$$

which is determined directly from the indicator diagram of the engine. We define brake mean effective pressure ($BMEP$) as the mean effective pressure calculated from dynamometer measured brake torque (T) as follows

$$BMEP = \frac{Work\ per\ rev}{Displ\ per\ rev} = \frac{2\pi T}{V_d / 2} \tag{5.4}$$

for a 4 stroke engine.

We then also define three other forms of mean effective pressure: friction mean effective pressure ($FMEP$), pumping mean effective pressure ($PMEP$) and auxillary mean effective pressure ($AMEP$), which are the power losses to engine friction, gas pumping and engine auxiliaries respectively. We can then write

$$IMEP = BMEP + PMEP + FMEP + AMEP \tag{5.5}$$

and define mechanical efficiency as

$$\eta_{mech} = \frac{BMEP}{IMEP} \tag{5.6}$$

These performance indicators provide the framework for determination of the results of the model (Taylor, 1996).

The performance calculations are performed at the end of the simulation for comparison of different engine configurations. Note that a mass balance for the cycle (total mass in = total mass out) is the measure of convergence of the solution. During the engine cycle the following values are calculated:

$$IMEP = \frac{\int_{IVC}^{EVO} P.dV}{V_d} \tag{5.7}$$

$$PMEP = \frac{\int_{EVO}^{IVC} P.dV}{V_d} \tag{5.8}$$

$$MassFlow = \int_{IVO}^{IVC} \dot{m}_{in}.d\theta = \int_{EVO}^{EVC} \dot{m}_{out}.d\theta \tag{5.9}$$

$$HeatLoss = \int_{EVC}^{IVO} \left(\dot{Q}_b + \dot{Q}_u\right) d\theta \tag{5.10}$$

The above equations allow us to calculate the BMEP using

$$BMEP=IMEP-PMEP-FMEP \tag{5.11}$$

From the definitions of $BMEP$, Torque and Power for a 4-stroke engine are

$$T = \frac{BMEP \times V_d \times N_{Cyl}}{4\pi} \tag{5.12}$$

$$\mathrm{P} = \frac{2 \times T \times N \times \pi}{60} \tag{5.13}$$

V_d is the displaced volume of one cylinder, N_{cyl} is the number of cylinders and N is the engine speed in rpm. The volumetric efficiency is calculated from

$$\eta_{vol} = \left[\frac{m_{in}}{\left(\frac{P_{atm} V_d}{R_{atm} T_{atm}} \right)} \right]. \tag{5.14}$$

This definition of volumetric efficiency uses the total mass of new air/fuel mixture ingested by the engine during the cycle, excluding residual gas. This provides a lower value than the more commonly used total mass at inlet valve closure.

Other efficiencies calculated include

$$\eta_{mech} = \frac{BMEP}{IMEP} \tag{5.15}$$

The fuel consumption is calculated from

$$\dot{m}_f = \dot{m}_{in} \times \frac{1}{AF+1} \times \frac{2 \times N}{60} \quad \left[\frac{kg}{hr}\right] \tag{5.16}$$

where AF is the air fuel ratio. The specific fuel consumption is then

$$SFC = \frac{\dot{m}_f}{\mathrm{P}} \tag{5.17}$$

The thermal efficiency can be calculated from

$$\eta_{thermal} = \frac{\mathrm{P}}{\frac{2 \cdot N}{60} \cdot Q_{fuel} \cdot m_{fuel}} \tag{5.18}$$

5.5 Computer Implementation

5.5.1 General

The computer code was written in Pascal in the object oriented 32-bit Borland Delphi environment. The in-cylinder thermodynamic, intake and exhaust flow models are each coded in the in the form of self-contained objects called from the main engine simulation interface. The object containing the in-cylinder code calculates the combustion chamber properties from inlet valve closure to exhaust valve opening as well as providing the routines necessary to interface with the manifold flow code during the valve events.

For information on installation and use of the program as well as the engine and environment variables required by the program, the user is referred to

the User Manual for ESA (Engine Simulation and Analysis) in Appendix C. A code listing of the most relevant parts of the in-cylinder code are given in Appendix D.

5.5.2 Numerical Solution Method

The governing equations for the in-cylinder thermodynamics are in the form of a set of linear first order differential equations in standard form

$$\frac{dP}{d\theta} = f_1(\theta, P, T_b, T_u, V_b) \tag{5.19}$$

$$\frac{dT_b}{d\theta} = f_2(\theta, P, T_b, T_u, V_b) \tag{5.20}$$

$$\frac{dT_u}{d\theta} = f_3(\theta, P, T_b, T_u, V_b) \tag{5.21}$$

$$\frac{dV_b}{d\theta} = f_4(\theta, P, T_b, T_u, V_b) \tag{5.22}$$

There are many methods of numerical integration that can be used to solve this system, two of which have been implemented in the code (both from Gerald and Wheatley, 1989). The first is a simple and fast but less accurate algorithm known as the Euler method.

Each of the equations is in the form

$$y_i' = f(y_1, \ldots, y_j, \theta) \tag{5.23}$$

where the subscripts I and j indicate the number of equations in the system. The Euler method is a time stepping method that approximates a value for each y_i at each timestep, n. The value of each y_i at the next timestep, $n+1$ can be estimated using.

$$y_{i,n+1} = y_{i,n} + d\theta \cdot f\left(y_{1,n},...,y_{j,n},\theta_n\right) \tag{5.24}$$

where the second subscript denotes the time step. For each time step, the integration estimates the value for each variable, y_i using the appropriate equation in the system.

A more complex but considerably more accurate method is the fifth-order Runge-Kutta-Fehlberg method, which reduces to the following algorithm

$$y_{i,n+1} = y_{i,n} + \frac{1}{6}\left(k_{i,1} + 2k_{i,2} + 2k_{i,3} + k_{i,4}\right) \tag{5.25}$$

$$k_{i,1} = d\theta \cdot f\left(y_{1,n},...,y_{j,n},\theta_n\right) \tag{5.26}$$

$$k_{i,2} = d\theta \cdot f\left(y_{1,n} + \frac{1}{2}k_{1,1},...,y_{j,n} + \frac{1}{2}k_{j,1},\theta_n + \frac{1}{2}d\theta\right) \tag{5.27}$$

$$k_{i,3} = d\theta \cdot f\left(y_{1,n} + \frac{1}{2}k_{1,2},...,y_{j,n} + \frac{1}{2}k_{j,2},\theta_n + \frac{1}{2}d\theta\right) \tag{5.28}$$

$$k_{i,4} = d\theta \cdot f\left(y_{1,n} + k_{1,3},...,y_{j,n} + k_{j,3},\theta_n + d\theta\right) \tag{5.29}$$

For each equation, the previous k-value is used in implementing the function values, so that there is iteration through the function values occurs before the next k factor is calculated.

The code for the two integrators is given in Appendix D.

5.5.3 Choice of Time Base

One of the primary considerations in the numerical analysis is the choice of the time base or time step that will be used for the integration. The use of a larger time step aids calculation speed but reduces accuracy.

Use of a variable time step would be advantageous so that parts of the cycle requiring more accuracy could have a reduced time step, however, the application of this would be complex. Furthermore, the large range of engine speeds used (often ranging from 500 to 10 000 rpm) would mean that a time step based on real time would also be complex to manage. For these reasons, the code was written based on a crank angle "time" step. This was also coded to allow for a change in the step so that the option was available to use multiples or portions of a single crank angle as the step size.

Once the code had reached a mature stage, an investigation was done where the step size was varied from 0.2° crank angle to 5° crank angle. It was found that a step size smaller than 1° did not offer any accuracy improvements, while the processing time for such a time step was within the desired region (< 5 min for simulation of one operating point on a Pentium II 266MHz). This time step was then chosen and hard-coded into the software. However, this may be changed easily and the code re-complied if required.

It should be noted here that subsequent investigations have shown that the choice of a crank angle based simulation has caused inaccuracies in the manifold flow model at lower engine speeds due to the long time steps. A more detailed discussion of this can be found in the thesis of van Vuuren (2001).

5.5.4 Initial and Boundary Conditions

The boundary conditions of the model were defined as follows:

- Pressure at the plenum side of the inlet is required as an input to the program (air cleaner pressure drop).

- The fuel/air mixture is assumed to be homogeneous when it flows in at the intake.

- The pressure on the underside of the piston is atmospheric.

- Since only the first section of the exhaust is simulated, the program requires an input of exhaust back-pressure and temperature.

The initial conditions are defined as follows:

- The pressure, temperature and velocity in the intake are set to atmospheric values (velocity is zero). The pressure and temperature in the exhaust is set to the back-pressure values.

- The pressure and temperature in the cylinder is atmospheric. There is no residual gas.

- The cycle commences at inlet valve closure. (Start of compression)

5.5.5 One Zone vs Two Zone

The derivation of both the one-zone and the two-zone models has been documented in chapter 2. The two-zone model was originally developed to replace the simple and inaccurate one-zone model. However, it was found during development that the numerical stability of the two-zone model during the first cycles was very reliant upon the initial conditions in the cylinder and inlet and exhaust tracts. Since this initialisation was far from the steady state values, the model tended to become unstable. It was found that, by running two cycles of the one-zone model to initialise the two-zone model, there were no further problems with stability.

The one zone model uses the same integrator as the two-zone model, but with only one equation for pressure being integrated. The bulk temperature is then calculated from the ideal gas law. The ratio of specific heats can be

input to the program, or can be calculated at each cycle point by the gas properties model.

5.5.6 Program Structure

The program structure is best represented by figure 5.1. It should be noted that due to the nature of the Windows Graphical User Interface (GUI), the normal operation of the program when not performing a simulation does not follow a strict linear logic path but that different routines can be initialised and terminated by means of menu and short-cut commands.

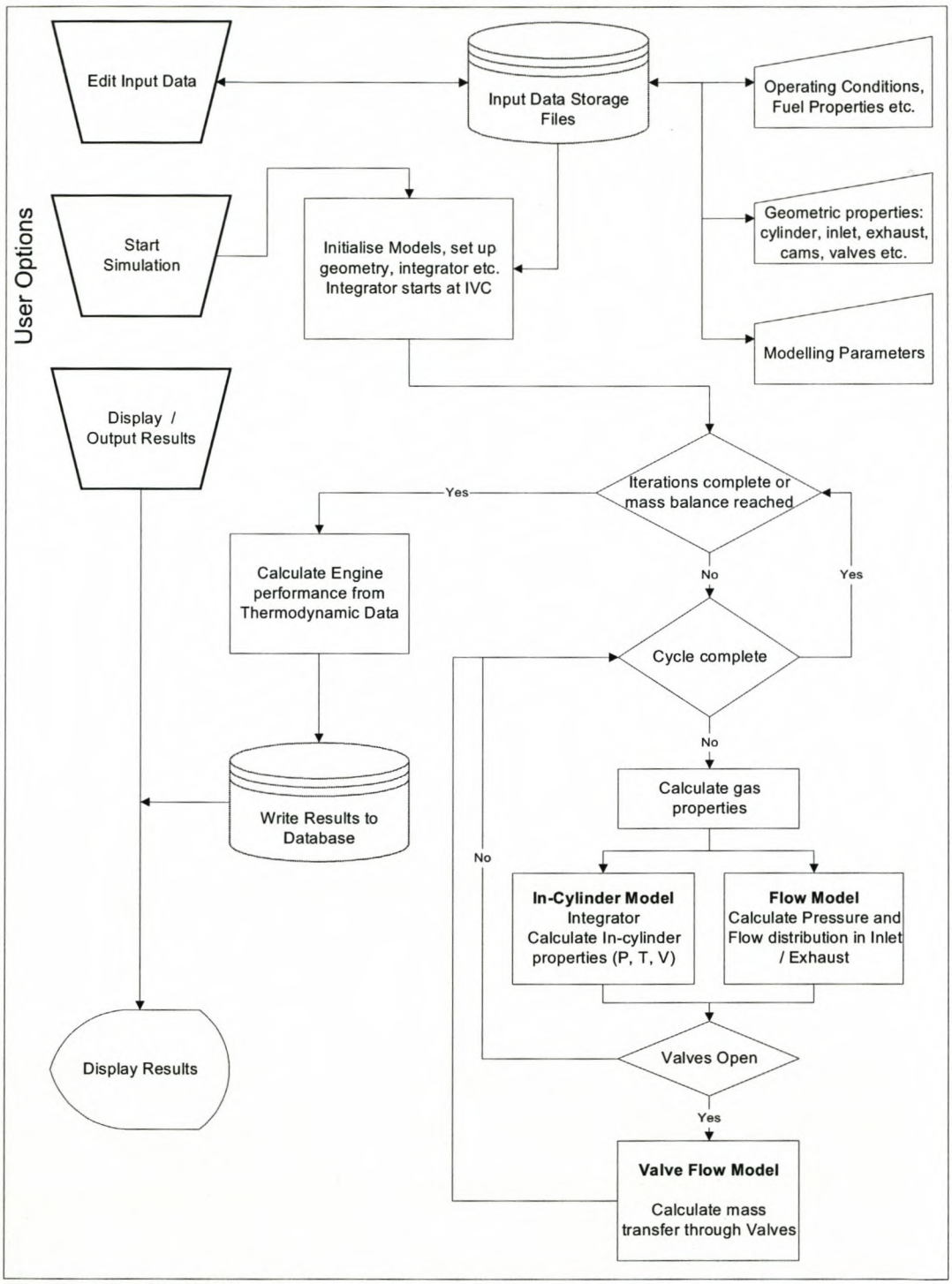

Figure 5.1. ESA program structure

Figure 5.2 shows more detail of the core of the cycle decision and calculation process. The listing of this core code can be found in Appendix D.

```
Determine State: (Overlap, Intake, Compression, Combustion, Expansion,
Exhaust);
If state has changed
       create / destroy second zone
       Zero mass balances if new cycle
       Calculate EGR
       Set integration functions based on state
Integrate
Calculate new gas properties
Calculate new manifold flow state
If valve open
       Calculate mass flow based on new cylinder and manifold state
       Calculate new gas composition based on previous reverse flow
Check for start / end of combustion
       Calculate heat addition (1-zone)
Sum Work done / Pumping work / Heat loss
```

Figure 5.2. Pseudo-code for main program cycle

5.5.7 Data Input.

Data input to the program is in two forms. Dialog boxes can be used to enter the required data, or, in some cases, the names of files containing more detailed information. All of the files are in text format so that the user can modify these outside of the user interface if required.

Details of the format of the input data are given in the User Manual in Appendix C.

5.6 Design Philosophy and Use of The Program.

The structure and implementation of the model has been developed with a particular engine component design strategy in mind. The structure of the models is almost exclusively theoretical, with only a few empirical relations for models such as the engine friction. Although the model is remarkably accurate in predicting the performance of an engine, in order to obtain useable data, one must consider the nature of the models carefully before developing a confidence in the results.

The section on verification testing provides good examples of the use of the program, as well as an indication of the accuracy.

6. VERIFICATION TESTING

6.1 Introduction

Although the models described in the previous chapters are based on sound theory and were carefully implemented in the computer code, the resulting simulation program cannot be used with confidence unless tested against measured engine data. The comparison between test and simulation results should provide indication of the scope of use of the program and the expected accuracy of simulation results.

The testing and verification of the model and associated code implementation was divided into three parts. The first was the independent verification of the robustness of each sub-model and took place as an intricate part of the development of the computer model. The results of each routine were examined and compared with known theory and empirical data to ensure that the theoretical development and the implementation were accurate. These results are not presented here as they are lengthy and the case studies given are deemed sufficient evidence that the program operates correctly.

Once the model had been complete, and combined with the manifold flow model of van Vuuren (2001), the model was evaluated by comparison of simulation results with measured results. A set of tests was devised using a customised engine specifically designed to verify the operation of the model. In these tests, apart from the standard measurements of engine operating condition and performance, measurements were made of the pulsed flow in the inlet manifold. The test schedule was designed to cover various engine configurations, with a single inlet tract isolated to reduce the effects of cylinder interaction.

The third set of verification data is the result of design projects conducted in conjunction with a South African vehicle manufacturer. The parallel use of simulation and engine dynamometer test data produced a set of results that verify the ability of the program to predict the effects of different designs.

6.2 Overview

Section 6.3 contains results obtained from the special engine testing with a customised engine.

Sections 6.4 and 6.5 contain results from two design projects where comparison between measured and simulated results were available.

In each section, the engine configuration, test procedure and model input data are presented, followed by a comparison of the simulated and measured results.

6.3 Sub-Model Verification

Verification of each of the sub models took place as part of the development process. The models were verified using the following checks:

- Hand calculation. The conversion of equations from theory to computer code was checked by running a set of test parameters in which the result of each step of the computation was checked against a hand calculated result.

- Logical parameter variation checks. The result of the variation of important parameters was check to ensure that the result followed the theory. For example, a variation in spark advance shows the well known 'hook' characteristic, with a peak torque at most beneficial timing.

- Results from Literature. Where possible, the models were checked against test cases from the literature.

The full details of this checking are too voluminous for inclusion in this document. The results presented in sections 6.4 and 6.5 provide ample validation of the accuracy of the model.

6.4 Special Engine Testing

The primary method of confirmation of the accuracy of the model was a program of engine dynamometer tests that was designed to show the ability of the program to predict engine performance, as well as the pulsed flow in the inlet and exhaust manifolds.

6.4.1 Engine Configuration

The engine used was a 2.0l, 4-cylinder, 8-valve, over-head cam, cross-flow automotive engine, mounted on a bench dynamometer. The engine was equipped with a purpose-designed, fabricated inlet manifold that allowed the length of the tracts to be varied in 100mm increments from 200 to 400mm (310 to 510mm including port length). The manifold also allowed isolation of a single inlet tract from the remaining 3 tracts when necessary. This isolation was realised by moving the plenum along relative to the outlet pipes so that one pipe (cylinder 1) was left open, while the now open plenum port was blocked.

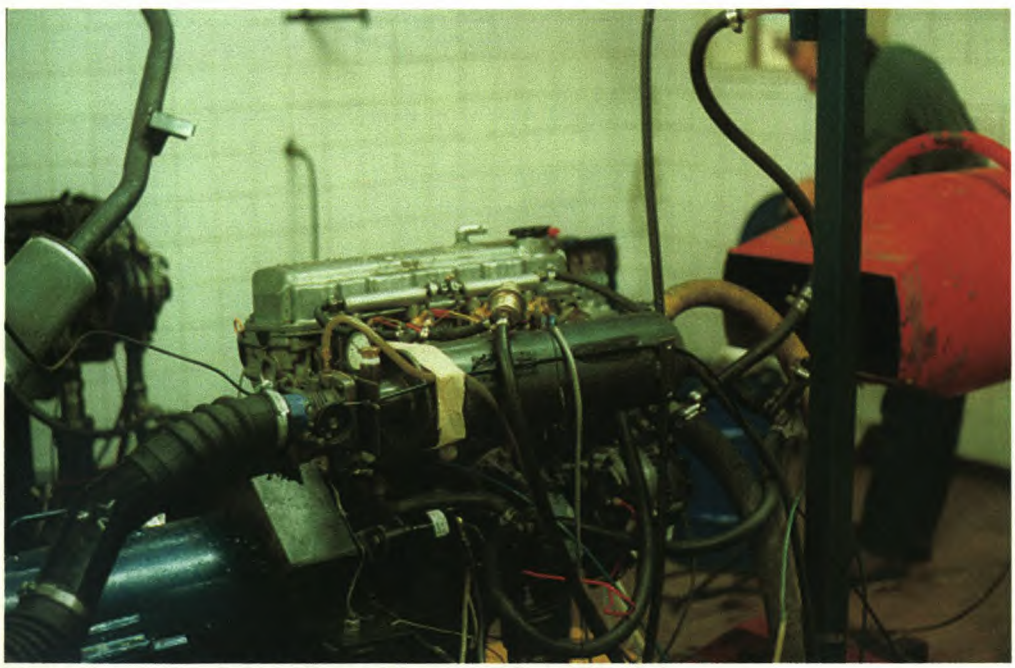

Figure 6.1. Test engine on the dynamometer

These configurations can be seen in Figures 6.2 and 6.3. Detailed drawings are given in Appendix E.

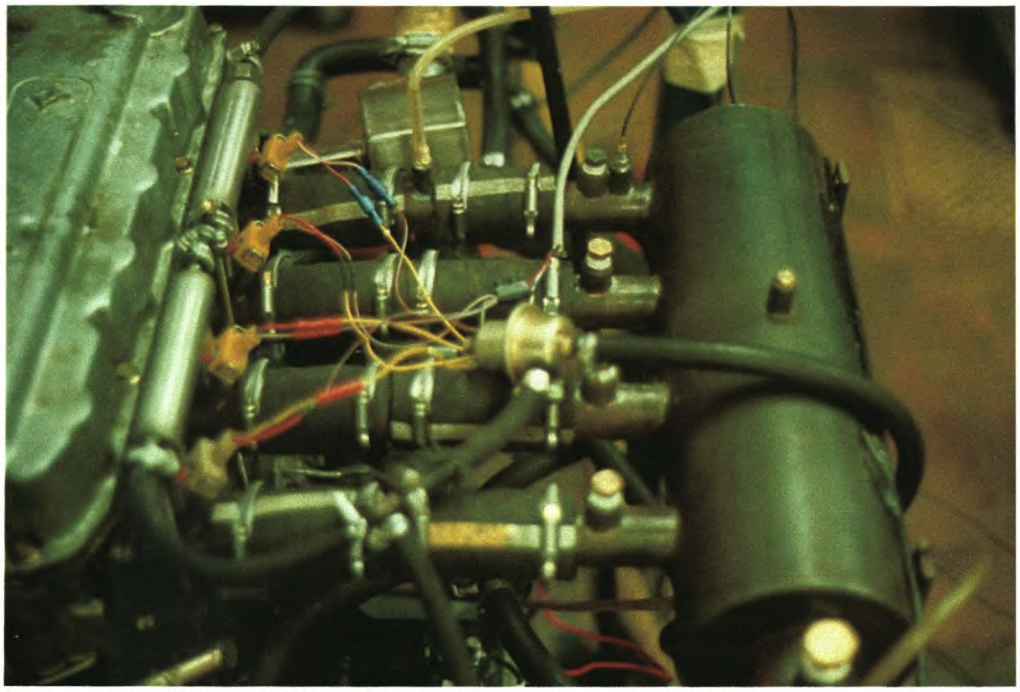

Figure 6.2. Test engine with manifold in normal position.

Engine speed, torque, fuel flow, air flow, air-fuel ratio (Lambda) and spark advance, as well as engine oil and water temperatures were measured using data acquisition hardware coupled to P.C. which saved time averaged data.

The manifold was equipped with high-speed pressure measurement equipment. Hall-effect pickups on a degree-wheel and a TDC mark on the crankshaft provided crank-angle reference. These signals were input into a software package, RACER (Rapid Acquisition of Combustion and Engine Results) designed to average the pressure variations in the manifold over a large number of engine cycles, on a crank-angle basis.

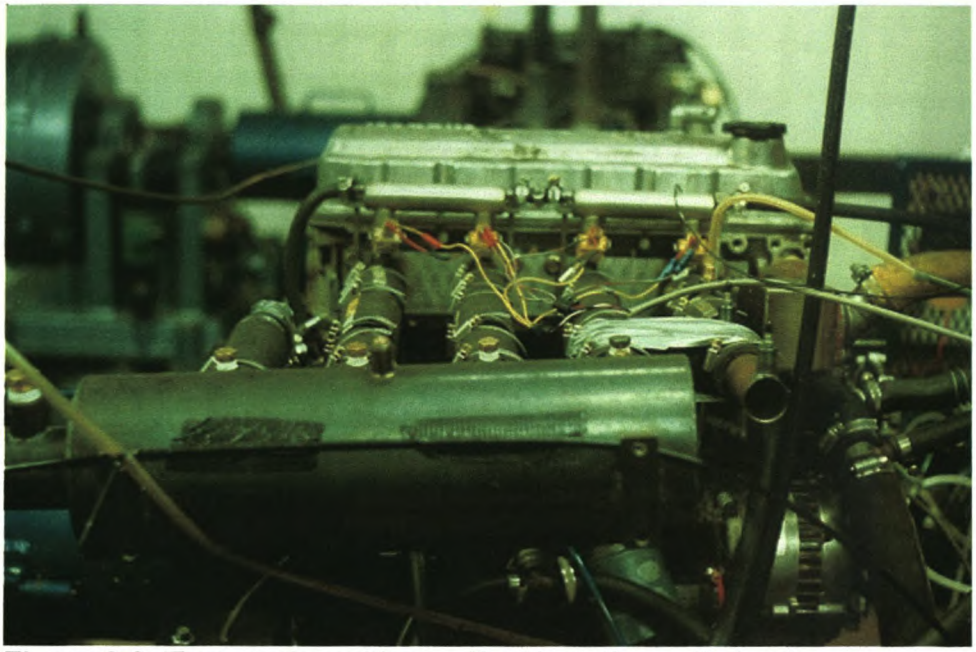

Figure 6.3. Test engine with manifold isolating cylinder 1.

The engine was modified to enable multi-point fuel injection using a DUPEC Defita 2000 Engine Control Unit. The DUPEC software allowed changes to be made to the fuelling and the ignition timing of the engine during operation, so that optimised operation could be guaranteed at each operating point.

An additional exhaust manifold and exhaust system was also fabricated, allowing isolation of one cylinder from pulses present in the other cylinder inlet and exhaust tracts. This modified system can be seen in figure 6.4.

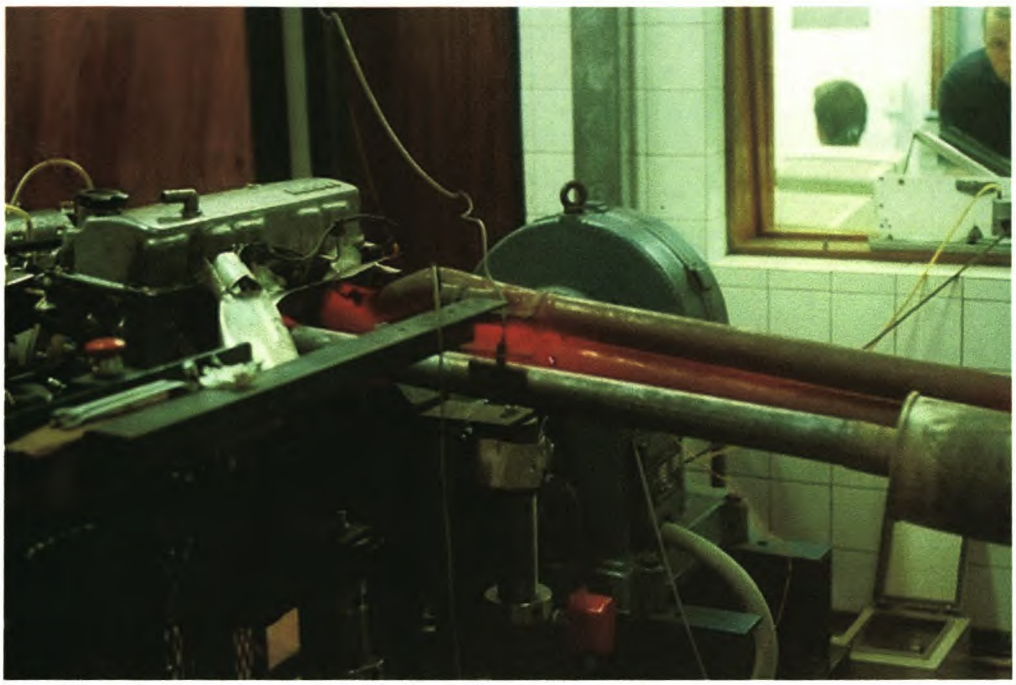

Figure 6.4. Test engine with modified exhaust.

6.4.2 Test Procedure

A test program of seven tests was run. The program was designed to cover the testing requirements of the in-cylinder model as well as the manifold flow model of Van Vuuren (2001).

Test 1: Engine equipped with standard exhaust system (4 into 2 into 1) and fabricated inlet manifold in normal position (all tracts drawing from plenum). The shortest possible inlet manifold tract length of 210mm from cylinder head to plenum was used. This gave a total flow length of approximately 290mm (80mm port length in head). Dynamic pressure measurements were taken at points A (as close as possible to the cylinder head), B (as close as possible to the plenum (±210mm from the head)) and C (at the top of the plenum chamber).

Test 2: The configuration was the same as in test 1 but with the inlet manifold tract length increased by 100mm (310mm from cylinder head to plenum). Dynamic pressure measurements were taken at points A (as close as possible to the cylinder head), B (in the middle of the inlet pipe

(±160mm from the head)), C (as close as possible to the plenum (±210mm from the head)) and D (at the top of the plenum chamber).

Test 3: As in test 1 and 2 but inlet manifold tract length increased by a further 100mm (310mm from cylinder head to plenum). Dynamic pressure measurements were taken at point A (as close as possible to the cylinder head) only. The exhaust system was then modified to isolate cylinder 1 as far as possible. Another pressure trace was measured at point A.

Test 4: As in test 3 (modified exhaust) but with inlet manifold tract on cylinder 1 open to the atmosphere. All four tracts were 410mm long. Dynamic pressure measurements were taken at points A (as close as possible to the cylinder head), B (in the middle of the inlet pipe (±160mm from the head)) and D (at the end of tract 1 open to the atmosphere). The free opening to the plenum was blocked.

Test 5: As in test 4 but inlet length reduced by 100mm. (310mm from cylinder head to atmosphere). Dynamic pressure measurements were taken at point A (as close as possible to the cylinder head)

Test 6: As in test 5 but inlet tract lengths decreased by a further 100mm (210 mm from cylinder head to atmosphere/plenum)

Test 7: As in Test 6. Inlet camshaft indexed by 12° CA. Ignition timing varied in 5° increments.

These configurations are summarised in table 6.1:

Test No	Total Inlet length [mm]	Cyl 4 Inlet Isolated	Cyl 4 Exhaust Isolated	Camshaft Advanced (Crank Angle)	Ignition Timing	Pressure meas. Points
1	290	No	No	0°	Optimised	A, B, C
2	390	No	No	0°	Optimised	A, B, C, D
3a	490	No	No	0°	Optimised	A
3b	490	No	Yes	0°	Optimised	A
4	490	Yes	Yes	0°	Optimised	A, B, D
5	390	Yes	Yes	0°	Optimised	A
6	290	Yes	Yes	0°	Optimised	A
7	290	Yes	Yes	12°	5° Increments	A

Table 6.1. Test summary

The test structure was designed with the following aims:

Test 1 was used to evaluate the ability of the simulation to predict the performance of the engine in standard configuration.

Tests 2 and 3 were used to evaluate the ability of the model, more specifically the manifold flow model, to predict the pressure traces in the inlet and exhaust with varying intake length.

Tests 4 to 6 were used to evaluate the effects of interaction between cylinders. The pressure traces in the isolated cylinder were compared with those from Tests 2 and 3. In this way, the model simplification of no interaction between cylinders could be evaluated.

Test 7 was aimed specifically at evaluating the response of the in-cylinder model to changes in ignition and camshaft timing.

Tests 1,2,3 and 7 form the focus of the following sections, while results from the other tests are discussed briefly. In depth analysis of the results of tests 2 to 6 can be found in the thesis of Van Vuuren (2001).

6.4.3 Model Input Data

The data presented in table 6.2 was used in the computer simulation for all engine configurations. This data was obtained from specifications and drawings supplied by the manufacturer.

Bore	89mm
Stroke	96 mm
Conrod Length	165 mm
Compression Ratio	8.3:1
Inlet Valve Diameter	38 mm
No of Inlet Valves / Cylinder	1
Cam timing: Inlet valve opens	20° BTDC
Cam timing: Inlet valve closes	40° ABDC
Inlet Valve Maximum Lift	9.5 mm
Exhaust Valve Diameter	34 mm
No Exhaust Valves / Cylinder	1
Cam timing: Exhaust valve opens	60° BBDC
Cam timing: Exhaust valve closes	30° ATDC
Exhaust Valve Maximum Lift	9.5 mm
Cam Lift Profiles	From Manufacturers Drawings
Fuel Burn Angle	55° CA
Stoichiometric A/F Ratio	14.5:1
Fuel	Gasoline 97RON
Fuel Combustion Energy	43 MJ/kg
Atmospheric Temperature	25° C
Atmospheric Pressure	1013 mBar

Table 6.2. Simulation input data

This data formed the base for the input files for each test. The full set of input files containing cam profiles, flow areas, and other variable data can be found in the Test Data directory on the accompanying Compact Disc.

6.4.4 Results

Tests 1, 2, and 3 enabled comparison of measured and modelled results for 3 different intake lengths. Figure 6.5. shows these results.

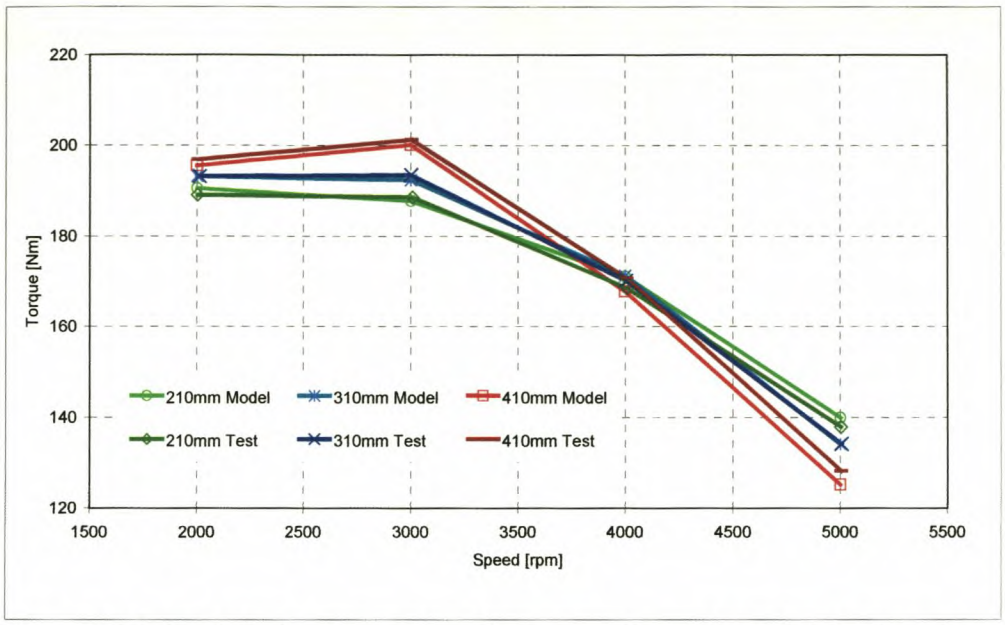

Figure 6.5. Modelled vs tested performance for various intake lengths.

Figure 6.6. shows the response of the model to the change in camshaft timing (Test 7). The camshaft was rotated by one tooth of the drive chain sprocket, resulting in an advance of 12 crankshaft degrees on both inlet and exhaust events.

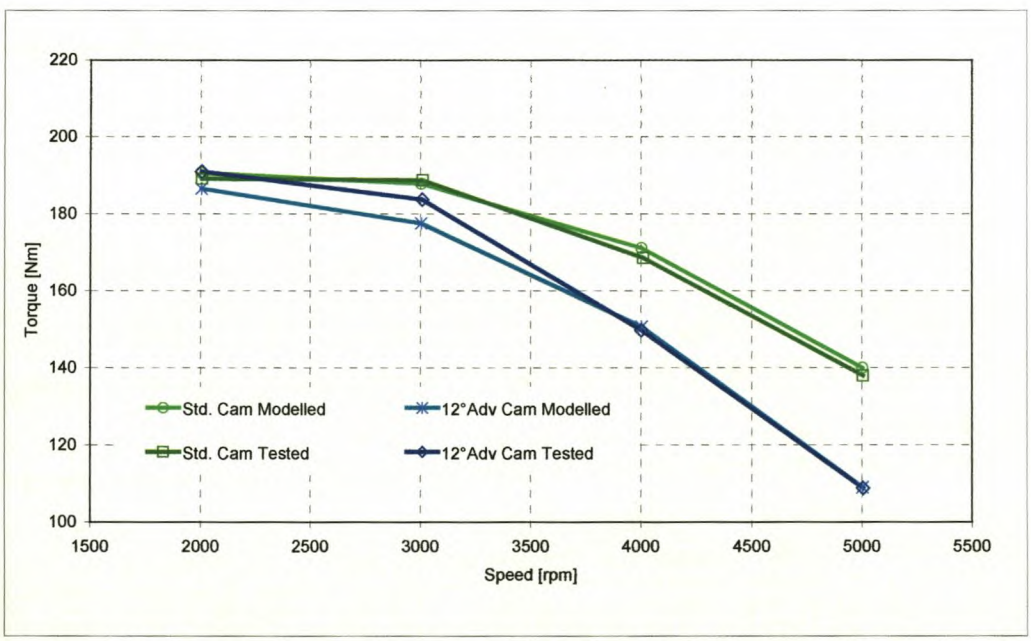

Figure 6.6. Comparison of measured and modelled data with a change in camshaft timing.

Figure 6.7. shows the result of a "timing loop", or variation in ignition angle. It can be seen from the figure that the model predicts the MBT (most beneficial timing) point of 20° BTDC very well, with a 2.3% error in peak torque.

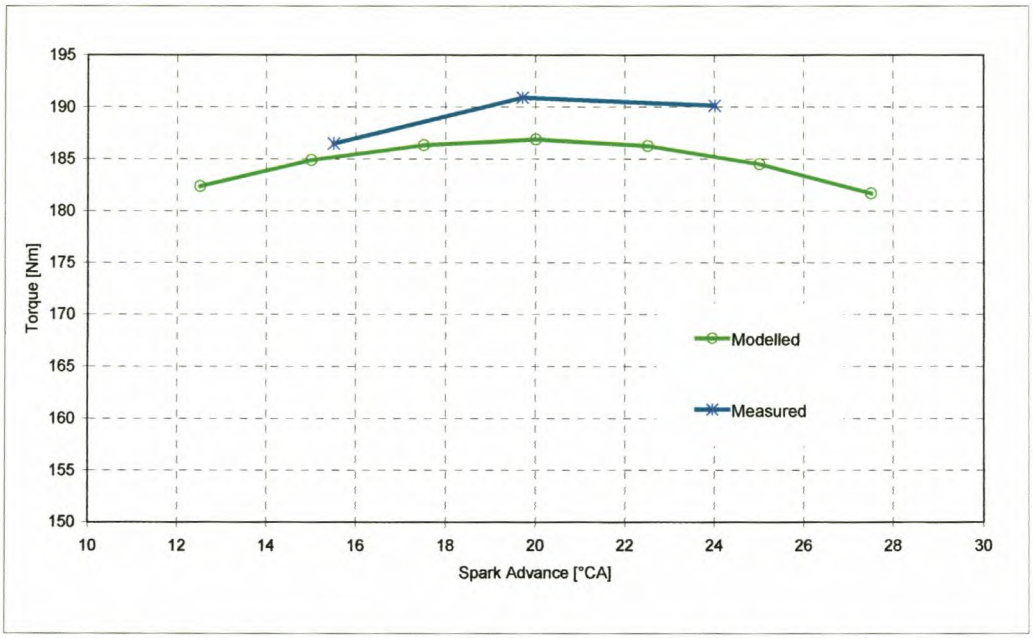

Figure 6.7. Comparison of measured and modelled data with variation in ignition timing.

From these figures we can deduce the following:

- The model has the ability to closely simulate engine performance. Modelled torque is within 4% of measured torque (corrected) for all test points.

- The model has the ability to predict the influence of changes in intake length. The similarity of the results for modelled and measured torque for each different length is clearly visible in figure 6.5.

- The model has the ability to predict the influence of changes to camshaft timing.

- The model has the ability to predict the effects of ignition timing variation, as well as the optimum ignition angle (MBT).

Figure 6.8. shows an example of a comparison of measured and predicted pressure wave motion in the inlet manifold. This is one of many such comparisons that were made for the three different intake lengths and various engine speeds. In all cases, a remarkable correlation exists, with very close frequency correspondence. There is, however, a slight difference in pulse amplitude at some speeds.

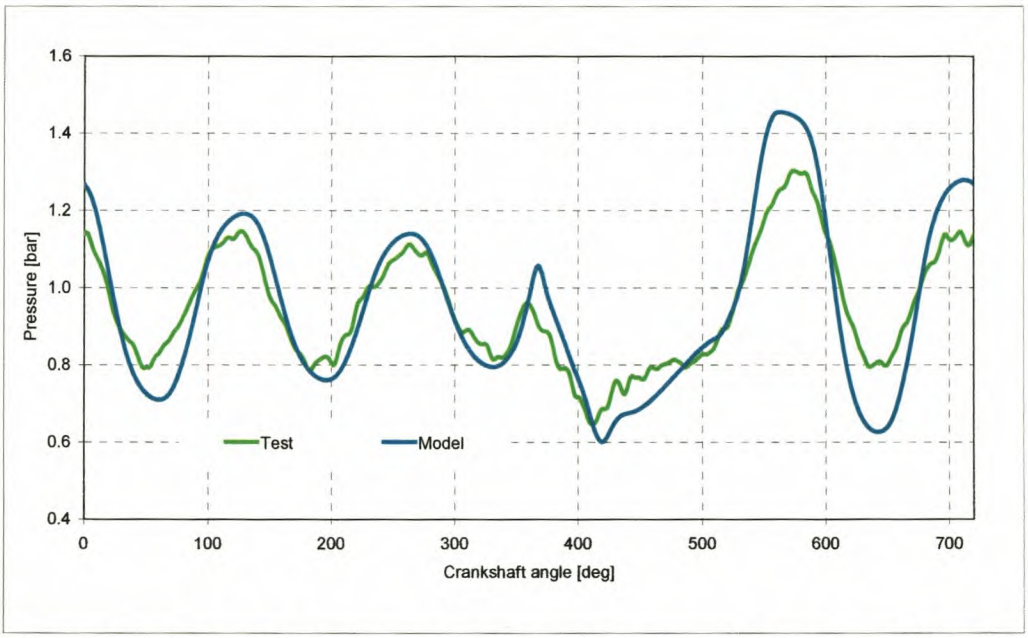

Figure 6.8. Comparison of measured and modelled pressure pulses in the inlet manifold at point A, 5000 rpm, 310mm inlet length.

From this figure we can deduce the following:

- The intake and exhaust flow models of van Vuuren (2001) are able to predict the manifold flow quite well.

- The interaction between the flow models and the in-cylinder combustion models at the valve events is good. The energy carry-over as well as mass flow into the cylinder is adequately modelled.

6.5 Design Project 1

In this project, the model was utilised in the development of an inlet manifold as well as the selection of a camshaft from a given parts bin. The model was

used to reduce the amount of engine dynamometer testing necessary to establish the optimum inlet manifold tract lengths and diameters, and camshaft timing. The primary aim of the development was to obtain maximum torque at low engine speed (below 3000 rpm) while maintaining a set power target.

6.5.1 Engine Configuration

The engine used was a Volkswagen 1,6L EA113 series production engine with 4 cylinders and 8 Valves in a counter-flow configuration. The engine was equipped with a DUPEC development Engine Management System allowing optimisation of timing and fuelling. Air cleaner and exhaust parts were representative of proposed production.

Figure 6. 9. New inlet manifold developed during design project 1.

6.5.2 Development Procedure

The development process can be described as follows:

- Engine tests were performed with two available inlet manifolds and various camshafts. Simulations of these configurations were run, allowing baseline torque curves to be established.

- Two prototype manifolds were fabricated, with the shortest possible and longest possible tract length respectively. The diameters were kept constant and were based on the diameter of an existing manifold for the engine. The manifold tracts were equipped with a trumpet section at the plenum end designed to reduce pressure loss. The manifolds were tested on dynamometer with various cams and the camshaft selection was reduced to the 3 camshafts showing the best torque characteristics.

- Multiple computer simulations were run at 10mm tract length intervals and 1mm tract diameter intervals with the reduced camshaft set. It was shown that the variation in tract length had a greater effect than the variation in tract diameter.

- The 640mm and 680mm lengths were highlighted as having the best bottom-end torque while still maintaining power. Two diameter options for each of these lengths were selected from modelled. Prototypes were constructed with the resulting four options. The optimum camshaft was selected.

- Engine tests of the prototypes highlighted the best option, which was selected for production. The torque and power targets were met.

6.5.3 Model Input Data

Details of the model input data can be found in the Test Data directory of the accompanying CD.

6.5.4 Results

The following two examples of data from this project demonstrate the ability of the model to predict both absolute engine performance as well as the effect of changes to the engine configuration.

Figure 6.10 shows the predicted vs. measured torque curves for the final manifold design and camshaft choice. It can be seen that the model predicts the torque well above 2500rpm but deviates somewhat from the measured values at low engine speed. This deviation can be attributed to the time step size used in the CFD inlet manifold model, and is discussed in detail in the thesis of van Vuuren (2001). The time step size is based on a constant crank angle step so that at low engine speed, the time-step, and thus the grid size of the inlet manifold is also larger.

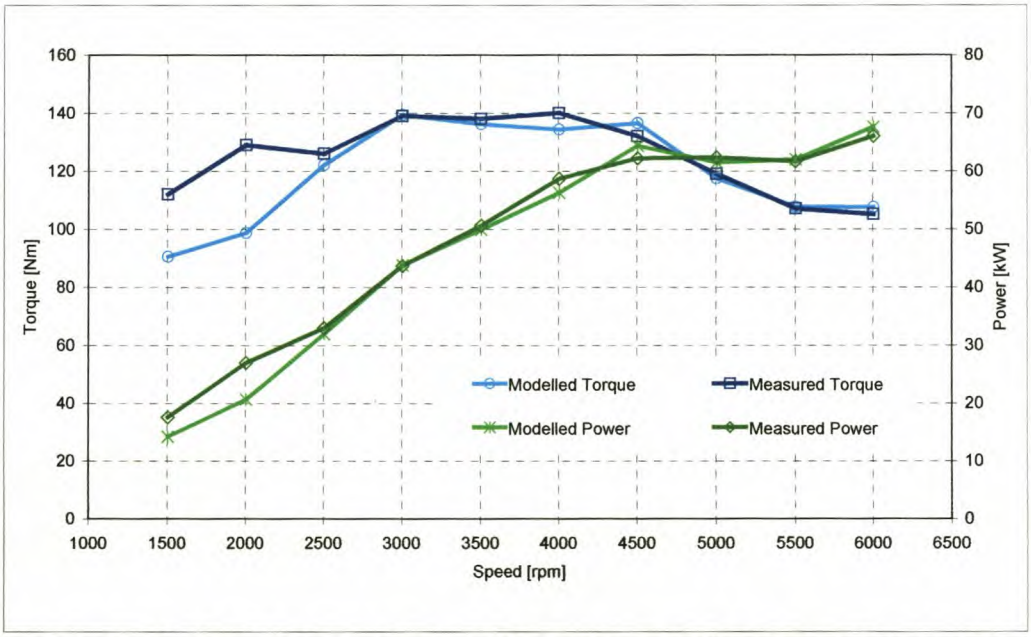

Figure 6.10. Correlation of measured and predicted torque curves for development engine 1.

Of special interest is the torque at 6000rpm, which is higher than expected, based on the trend of the 4000, 4500 and 5000 rpm values. The deviation of this curve from the expected trend caused some scepticism of the validity of the test results. This "kick up", however, was reflected in the model, which provided enough detail data of the engine and manifold conditions to enable an explanation of this effect, which can be attributed to favourable manifold pulsations at the higher engine speeds.

Figure 6.11 shows the ability of the model to predict the result of changes to the design of an engine, in this case, the change of a camshaft. The

graph shows the difference in measured and predicted torque when the camshaft was changed from Cam A to Cam B shown in table 6.3.

Camshaft	Lift [mm]	IVO [BTDC]	IVC [ABDC]	EVO [BBDC]	EVC [ATDC]	Duration at 1mm lift [°CA]
Cam A	8.6	23	66	51	38	202
Cam B	10	29	75	71	33	216

Table 6.3: Camshaft data.

Figure 6.11 once again shows a close correlation between predicted and measured values, demonstrating the effectiveness of the program in such engine developments.

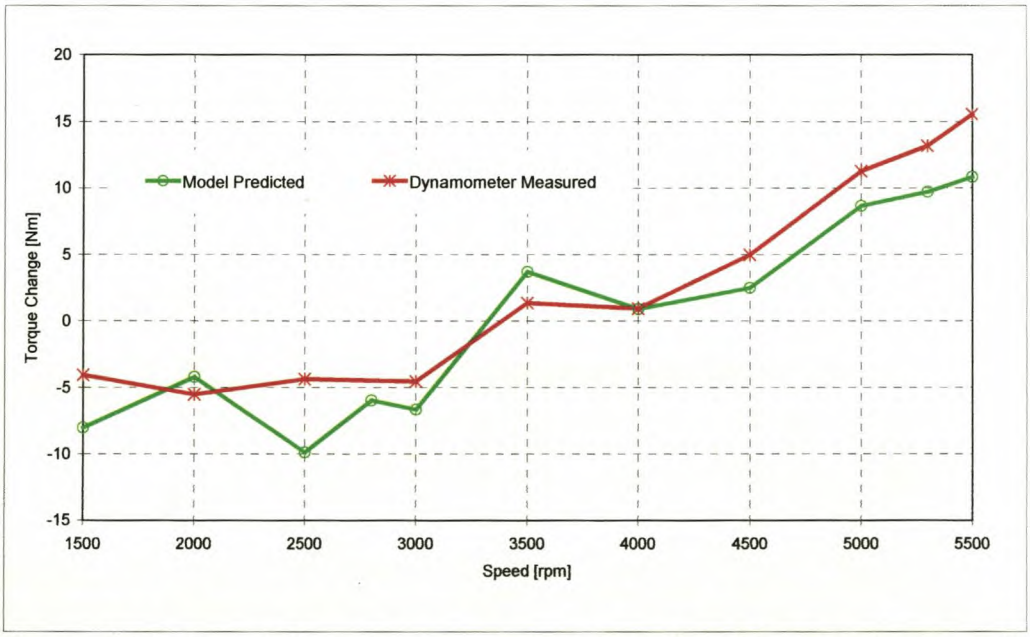

Figure 6.11. Correlation of measured and predicted torque change with a camshaft change.

The results of the modelling illustrate the ability of the application to predict the relative performance of different design options with reasonable accuracy, and so reduce the development time of an engine.

6.6 Design Project 2

6.6.1 Project Description

The second design project discussed here was also an engine development project in which an existing production engine was upgraded. The design brief was to improve full load performance of the baseline engine so as to meet given performance specifications. The new engine was to be packaged inside a different vehicle to that of the baseline engine. The following design changes formed part of the project specification:

- New piston design with compression ratio to be selected within the range 9.3 to 10.3:1.
- New inlet manifold.
- Selection of camshafts with incorporation of an existing variable valve timing mechanism (VVT), enabling switching of the inlet camshaft.
- New exhaust down-pipe and selection of exhaust rear section.

The targets of the development were that power was to be increased from 74kW to 78kW while torque was to be maintained at 150Nm, with a targeted peak torque point below 4000 rpm.

6.6.2 Engine Configuration

The engine developed had an in-line 4-cylinder double overhead cam configuration, a capacity of 1,6L and 5 valves per cylinder. A Bosch M.1.5.4 engine management system was used for initial development enabling tight control of timing and fuelling.

6.6.3 Development Procedure

Timing constraints of the project prohibited the design team from following a joint optimisation process with the design of the different components. A compression ratio had to be selected before manifold prototypes were available. Initial modelling and testing showed that the higher compression ratios boosted peak power quite considerably while having little effect on the peak torque. Because of the necessity to meet the power target, as well as the obvious efficiency gains, the compression ratio was chosen to be 10.3:1 very early in the project. At this stage of the project it was also found that the engine was extremely knock sensitive at full load with this compression ratio, so much so that 90% of the torque curve had to be obtained at KLSA rather that MBT. The use of a modern engine management system with good knock detection made this a viable solution for production. Manifold and other component designs were then done with this compression ratio.

The primary downside to this decision was that it became very difficult to use the model for simulation of induction changes as the performance effects of changes to the breathing were often negated by resulting changes to the KLSA curve. This highlighted the need for the program to have the ability to predict the onset of knock. The following examples show areas in which simulation was possible.

6.6.4 Model Input Data

Engine data was available for all required parameters with the exception of the flow coefficients of the 5-valve-per-cylinder head. Timing restraints forced the design team to use estimated data, as a full 3-D flow analysis would have been too time consuming. The data used can be found on the accompanying CD.

6.6.5 Results

The first stage of the project involved modelling of the baseline performance using the ESA code so that initial possibilities could be investigated before the first prototypes were built. Figure 6.12 shows a comparison between the modelled and tested data from the baseline engine (before development)

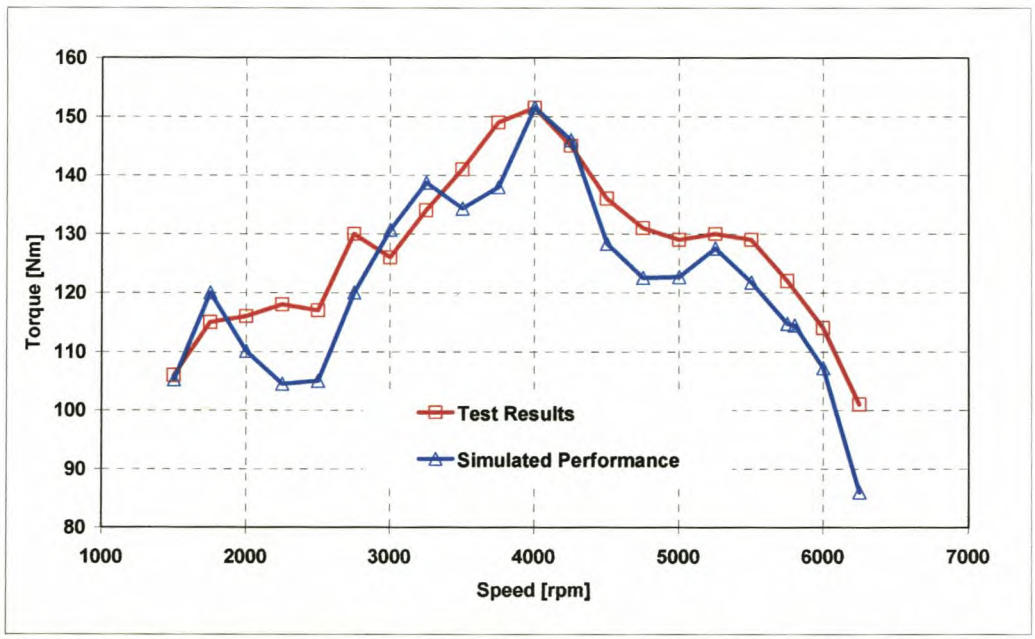

Figure 6.12. Simulated and measured baseline engine performance.

It is clear that the model had captured the primary aspects of the engine operation. The deviation at engine speeds below 3000 rpm is due to the fact that the model is based on a fixed crank angle step, causing the time step to be too large at these low engine speeds.

The first step once the baseline simulation had been verified was the selection of a compression ratio. The specification allowed for a compression ratio between 9.3:1 and 10.3:1. The engine had to be designed for best operation on 95 RON fuel. Figure 6.13 shows the comparison between the measured and predicted data for 9.3:1 and 10.3:1 compression ratios. It is clear that the model predicts the trend well but the engine was unable to obtain the high torque due to the knock limit without the use of the higher octane fuel.

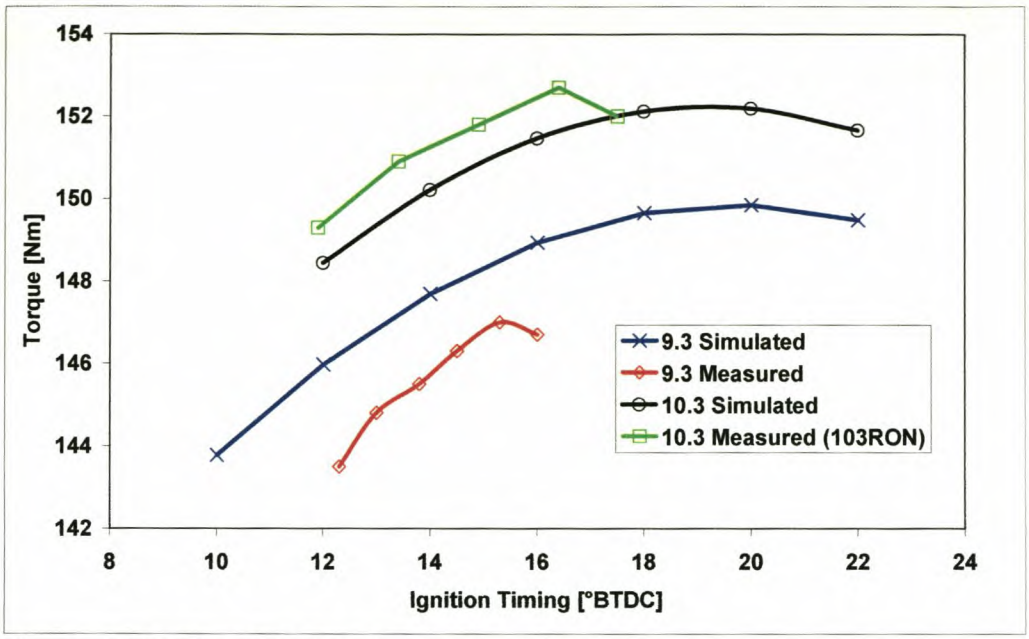

Figure 6.13. Simulated and measured timing loops.

Once the baseline model had been established, and the compression ratio had been selected, time was spent on the design of the inlet manifold. The packaging of the engine forced the tract length to be fixed at 686mm (total flow length) so that existing clean air supply parts could be utilised. The parameters left for selection were the diameter of the tracts as well as the design of a "trumpet" shape at the plenum end to aid pressure recovery. The program was utilised to compare the predicted effects of various intake diameters. Figure 6.13 shows the predicted results for diameters of 35.5 and 41mm, which were selected for the first two prototypes. These results are presented compared to dynamometer-tested results showing that the program predicts the effects of the diameter differences well.

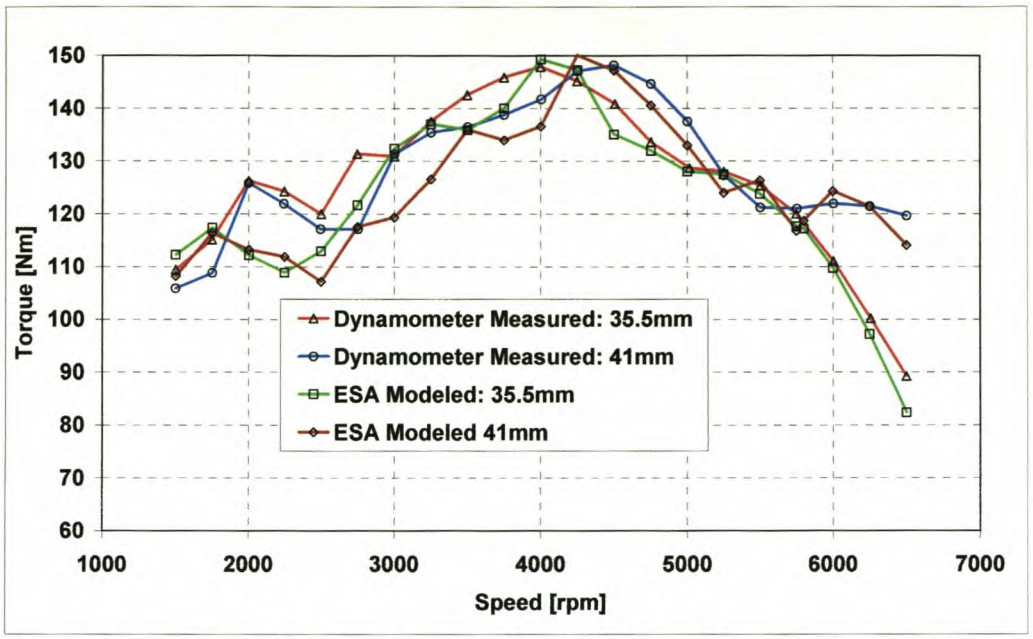

Figure 6.14. Simulated and measured performance with varying inlet diameter.

At the conclusion of the design phase of the project, a final simulation was made of the final prototype engine. This result is shown in figure 6.15, again confirming the usefulness of the program in this type of development.

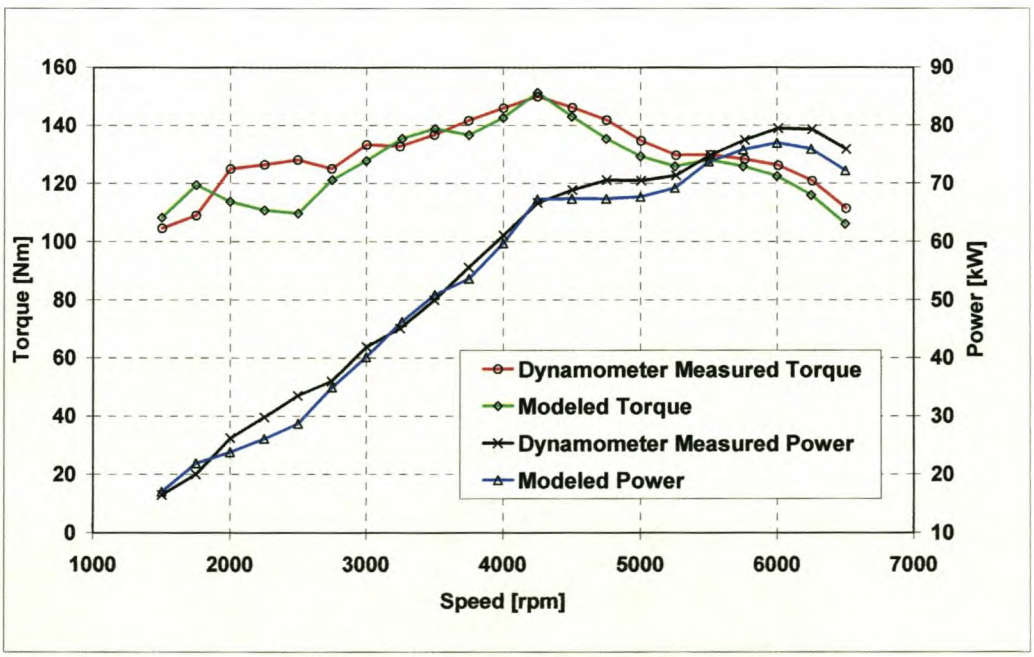

Figure 6.15. Simulated and measured final engine performance.

One point to note about these last two comparisons is that fixed ignition timing and fueling was used. This was necessary because of the inability

of the program to predict knock. Since the engine has a high compression ratio, and a very high volumetric efficiency, and has to operate with 95 RON fuel, the knock limit at most engine speeds is at timing values well below the optimum. If timing was optimised at each modelled point, the predicted torque was much higher than practically obtainable.

7. CONCLUSIONS AND RECOMENDATIONS

7.1 Conclusions

A computer model for simulation of in-cylinder thermodynamics has been developed and successfully mated with a CFD model of inlet and exhaust pulsated flow. These models have been implemented in a Windows based application that can be easily run on a desktop PC. The run-time of an operating point simulation is short enough to enable an interactive development process.

The test results show that the application has the ability to predict the behaviour of a 4-cylinder, 4-stroke spark ignition engine with enough accuracy to enable the reduction of the amount of engine dynamometer testing necessary in an engine development. The application is especially useful in predicting "relative" values before and after changes.

7.2 Restrictions of the Model

The following should be noted when using the model.

7.2.1 Exhaust Temperatures and Pressures

It is often impossible to obtain variables such as exhaust backpressures and temperatures that are inputs to the model, without testing an engine on the dynamometer. In this case, the model can be used after initial testing to investigate effects of other variables.

7.2.2 Ignition Angle

The ignition or spark angle of the engine is an input to the model. The angle given to the model is used as the start of combustion and does not take delays inherent in the ignition system or in the ignition of the fuel mixture by the spark into account.

7.2.3 Knock

The model does not have the ability to predict knock ("pinging" or pre-detonation). This means that the user can easily use a timing advance angle exceeding that at which the engine is able to operate without knock and a given fuel octane. If the engine being studied is knock limited, the user should be very careful to provide the model with spark advance values that are correct for the engine configuration being studied. If the model is being used for pre-development studies, this information is often not available, and the user must take possible restrictions to the optimal timing into account.

7.3 Recommendations for Future Development

The following developments to the ESA model and program are recommended.

- The time base of the manifold model should be adjusted to compensate for the increased time step at low engine speeds. This will increase the accuracy at low speed.

- Different models for heat release rate should be developed, including the facility for a custom "user input" rate curve.

- The ability to model two-stroke engine cycles should be added.

- The inlet and exhaust flow models should be expanded to include the effects of interaction between cylinders in a multi-cylinder engine.

- Models for turbo and supercharging should be added and integrated.

- The ability to predict the onset of knock should be added. An optimisation routine could then provide the optimum spark advance and fuelling at each modelled point.

- Models should be developed for exhaust systems allowing calculation of backpressures and temperatures based on the state of the cylinder gasses.

The following developments to the ESACam model and program are recommended. This program would then be useful not only to provide inputs to the ESA model but also as a design tool for cam profiles.

- The model should be extended to multiple degrees of freedom so that the effects of spring clash can also be simulated.

- A model for hydraulic tappets should be included.

Audie Technology Inc. and V.P. Engineering Inc., ***"DYNOMATION – Four Cycle Wave Action Simulator"***, Audie Technology Inc. and V.P. Engineering Inc., 1994

Bell, A. J., ***The effect of Fuel Formulation on the Exhaust Emissions of Spark Ignition Engines***, Unpublished M.Eng degree thesis, University of Stellenbosch, 1998.

Benson, R. S., ***The Thermodynamics and Gas Dynamics of Internal Combustion Engines***, Volumes 1 and 2, Clarendon Press, Oxford, 1982.

Blair, G. P., ***Design and Simulation of Four-Stroke Engines***, Society of Automotive Engineers Inc.,Warrendale, 1998.

Blair, G. P. and Drouin, F. M. M., ***Relationship Between Discharge Coefficients and Accuracy of Engine Simulation.***, SAE Paper 962527, 1996.

Charlton, S. J., "***SPICE II – Simulation Program for Internal Combustion Engines***", University of Bath, 1990

Dent, J. C. and Chen, A., ***An Investigation of Steady Flow Through a Curved Inlet Port***, SAE Paper 940522, 1994.

Enomoto, Y. and Furuhama, S**.**, ***Heat Transfer into Ceramic Combustion Chamber Wall of Internal Combustion Engines.***, SAE Paper 861276, 1986.

Ferguson, C. R., ***Internal Combustion Engines.***, John Wiley & Sons, New York, 1986.

Gerald, C. F. and Wheatley, P. O., ***Applied Numerical Analysis***., Fourth Edition, Addison-Wesley, 1989.

Gordon, S. and McBride, B. J., ***"Computer Program for the Calculation of Complex Chemical Equilibrium Composition, Rocket Performance, Incident and Reflected Shocks and Chapman-Jouquet Detonations,"*** NASA publication SP-273, 1971 (NTIS number N71-37775).

Heisler, H., ***Advanced Engine Technology***, Edward Arnold, London, 1995.

Heywood, J. B., ***Internal Combustion Engine Fundamentals***, McGraw-Hill, Singapore, 1988.

Hohenberg, G. H., ***Advanced Approaches for Heat Transfer Calculations***., SAE Technical Paper 790825, 1979.

Kanesaka, H., Akiba, K., and Sakai, H., ***A New Method of Valve Cam Design-HYSDYNE Cam***, SAE Technical Paper 770777, Society of Automotive Engineers, 1977.

Koster, MP, ***Vibrations of Cam Mechanisms***, McMillan Press, London UK, 1974

Krieger, R. B. and Borman, G. L., ***The Computation of Apparent Heat Release for Internal Combustion Engines***, ASME paper 66-WA/DGP-4, 1966.

Lee, W. and Schaefer, H. J., ***An Analysis of Local Pressures, Surface Temperatures and Engine Damage under Knock Conditions***., SAE Technical Paper 830508, 1983.

Olikara, C. and Borman, G. L., ***A Computer Program for Calculating Properties of Equilibrium Combustion Products with Some Applications to I. C. Engines***, SAE Technical Paper 750468, Society of Automotive Engineers, 1975.

Ramos, J. I., ***Internal Combustion Engine Modelling***, Hemisphere Publishing Corporation, New York, 1989.

Philips, P. J., Schamel, A. R. and Meyer, J., ***An Efficient Model for Valvetrain and Spring Dynamics***, SAE Technical Paper 890619, Society of Automotive Engineers, 1989.

Schamel, A. R., Hammacher, J. And Utsch, D., ***Modelling and Measurement Techniques for Valve Spring Dynamics in High Revving Internal Combustion Engines***, SAE Technical Paper 930615, Society of Automotive Engineers, 1993.

Taylor, A. B., ***Internal Combustion Engines***, Class notes: Binnebrandenjins 414, Department of Mechanical Engineering, University of Stellenbosch, 1996.

Theron, N. J., ***Direkte Integrasie-Algoritmes vir gebruik in Struktuurdinamise-Analise met die Eindige Element-Metode***, Class Notes: Advanced Dynamics 834 (M.Sc.Ing), University of Stellenbosch, 1996.

Thomson, W. T., ***Theory of Vibration with Applications***, Fourth Edition, Chapman and Hall, 1993

van Vuuren, C. M., ***CFD Modelling of Internal Combustion Engine Intake and Exhaust Processes***, M.Sc. Ing Thesis, University of Stellenbosch, 2001.

Wagstaff, P. R., ***Analysis of Valve Gear Dynamics with a Digital Computer.***, Procedings 1967-68 Volume 182 Part 3L, Symposium on Computers in Internal Combustion Engine Design, Institution of Mechanical Engineers, London, 1968.

White, R. A. and Peters, J. E., ***Combustion Chamber Temperature and instantaneous Local Heat Flux Measurements in a Spark Ignition Engine.***, SAE Paper 930217, 1993.

Winterbourne, D. E. and Pearson, R. J., ***Design Techniques for Engine Manifolds: Wave Action Methods for IC engines***., Society of Automotive Engineers, Inc., Pennsylvania, USA, 1999.

Woschni, G., ***A Universally Applicable Equation for the Instantaneous Heat Transfer Coefficient in the Internal Combustion Engine***., SAE Paper 670931, 1967.

Zou, D. and McCormick, H. E., ***Dynamic Model and Computer Simulation of Valve Train Assemblies with Hydraulic Lash Adjuster***., SAE Paper 960351, 1996.

Zucrow, M. J. and Hoffman, J. D., ***Gas Dynamics***, Volume I, John Wiley and Sons, New York, 1976.

APPENDIX A: SOLUTION OF IN-CYLINDER EQUATIONS

The solution for the two-zone in-cylinder equations is similar for the case with and without mass transfer. The case with mass transfer is shown here.

The equations derived in the text are rearranged as follows:

From equation 2.60

$$\dot{m}_{in}(u_u - h_{in}) + m_u \frac{\partial u_u}{\partial T_u}\dot{T}_u = \dot{Q}_u - p\dot{V} + p\dot{V}_b \qquad \text{(A.1.)}$$

$$\therefore -p\dot{V}_b + m_u \frac{\partial u_u}{\partial T_u}\dot{T}_u = \dot{Q}_u - p\dot{V} - \dot{m}_{in}(u_u - h_{in}) \qquad \text{(A. 2.)}$$

From equation 2.63

$$\dot{m}_{out}(h_{out} - u_b) = \dot{Q}_b - p\dot{V}_b - m_b \frac{\partial u_b}{\partial T_b}\dot{T}_b \qquad \text{(A. 3.)}$$

$$\therefore p\dot{V}_b + m_b \frac{\partial u_b}{\partial T_b}\dot{T}_b = \dot{Q}_b - \dot{m}_{out}(h_{out} - u_b) \qquad \text{(A. 4.)}$$

From equation 2.65 (note change of symbol for consistency in flow direction)

$$\frac{\dot{p}}{p} = \frac{-\dot{m}_{out}}{m_b} + \frac{\dot{T}_b}{T_b} - \frac{\dot{V}_b}{V_b} \qquad \text{(A. 5.)}$$

$$\therefore \frac{\dot{V}_b}{V_b} + \frac{\dot{p}}{p} - \frac{\dot{T}_b}{T_b} = \frac{-\dot{m}_{out}}{m_b} \qquad \text{(A. 6.)}$$

From equation 2.68.

$$\frac{\dot{p}}{p} = \frac{\dot{m}_{in}}{m_u} + \frac{\dot{T}_u}{T_u} - \frac{\dot{V}}{V_u} + \frac{\dot{V}_b}{V_u} \qquad \text{(A. 7.)}$$

$$\therefore -\frac{\dot{V}_b}{V_u} + \frac{\dot{p}}{p} - \frac{\dot{T}_u}{T_u} = \frac{\dot{m}_{in}}{m_u} - \frac{\dot{V}}{V_u} \qquad \text{(A. 8.)}$$

This system is in the form

$$\begin{bmatrix} A & B & C & D \\ E & F & G & H \\ I & J & K & L \\ M & N & O & P \end{bmatrix} \begin{bmatrix} w \\ x \\ y \\ z \end{bmatrix} = \begin{bmatrix} Q \\ R \\ S \\ T \end{bmatrix}$$

where $w = \frac{dV_b}{d\theta}$, $x = \frac{dp}{d\theta}$, $y = \frac{dT_b}{d\theta}$, $z = \frac{dT_u}{d\theta}$ and the matrix coefficients are as follows

$A = -p$

$B = 0$

$C = 0$

$D = m_u \frac{\partial u_u}{\partial \mathrm{T}_u}$

$Q = \dot{Q}_u - p\dot{V} - \dot{m}_{in}(u_u - h_{in})$

$E = p$

$F = 0$

$G = m_b \frac{\partial u_b}{\partial \mathrm{T}_b}$

$H = 0$

$R = \dot{Q}_b - \dot{m}_{out}(h_{out} - u_b)$

$$I = \frac{1}{V_b}$$

$$J = \frac{1}{p}$$

$$K = -\frac{1}{T_b}$$

$$L = 0$$

$$S = \frac{-\dot{m}_{out}}{m_b}$$

$$M = -\frac{1}{V_u}$$

$$N = \frac{1}{p}$$

$$O = 0$$

$$P = -\frac{1}{T_u}$$

$$T = \frac{\dot{m}_{in}}{m_u} - \frac{\dot{V}}{V_u} \qquad \text{(A.9.)}$$

The system to be solved can thus be reduced to

$$\begin{bmatrix} A & 0 & 0 & D \\ E & 0 & G & 0 \\ I & J & K & 0 \\ M & N & 0 & P \end{bmatrix} \begin{bmatrix} w \\ x \\ y \\ z \end{bmatrix} = \begin{bmatrix} Q \\ R \\ S \\ T \end{bmatrix} \text{ or in matrix notation } \mathbf{P}_1\mathbf{X} = \mathbf{Q}_1, \qquad \text{(A.10.)}$$

the solution of which is

$$\mathbf{X} = \mathbf{P}_1^{-1}\mathbf{Q}_1 \qquad \text{(A.11.)}$$

This was solved by MATLAB as follows

```
P1=sym('[A,0,0,D;E,0,G,0;I,J,K,0;M,N,0,P]')
Q1=sym(['Q;R;S;T'])
R1=symmul(inverse(P1), Q1)
```

(A.12.)

This returned

```
R1 =

[-(-J*G*P*Q+D*R*K*N-N*D*G*S+J*D*G*T)/(A*J*G*P-E*N*D*K+I*N*D*G-
M*J*D*G)]

[(P*Q*E*K-P*Q*I*G-R*A*K*P+R*M*D*K+S*A*G*P-S*M*D*G-
D*T*E*K+D*T*I*G)/(A*J*G*P-E*N*D*K+I*N*D*G-M*J*D*G)]

[(-E*J*P*Q+R*A*J*P+R*I*D*N-R*M*D*J-E*D*N*S+E*D*J*T)/(A*J*G*P-
E*N*D*K+I*N*D*G-M*J*D*G)]

[(-Q*E*K*N+Q*I*G*N-Q*M*G*J+A*R*K*N-A*G*N*S+A*G*J*T)/(A*J*G*P-
E*N*D*K+I*N*D*G-M*J*D*G)]
```

(A.13.)

The result is then four equations of the form

$$\frac{dP}{d\theta} = f_1(\theta, P, T_b, T_u, V_b) \tag{5.1}$$

$$\frac{dT_b}{d\theta} = f_2(\theta, P, T_b, T_u, V_b) \tag{5.2}$$

$$\frac{dT_u}{d\theta} = f_3(\theta, P, T_b, T_u, V_b) \tag{5.3}$$

$$\frac{dV_b}{d\theta} = f_4(\theta, P, T_b, T_u, V_b) \tag{5.4}$$

which can be easily solved numerically in the computer code.

APPENDIX B : EQUATIONS OF MOTION FOR THE MDOF MODEL.

The multiple degree of freedom model was not used in the simulation for reasons as discussed in section 4.3. However, as the required derivation was completed it is presented here should a later expansion of the model be required. The development is based on figure A.1. m_1 is the combined masses of the follower and pushrod (where utilised). m_2, k_2 and c_2 represent the rocker, collets and valve stem. m_3 represents the mass of the head of the valve as well as a portion of the valve stem. The spring is simulated by N masses making a total of M=N+3 degrees of freedom.

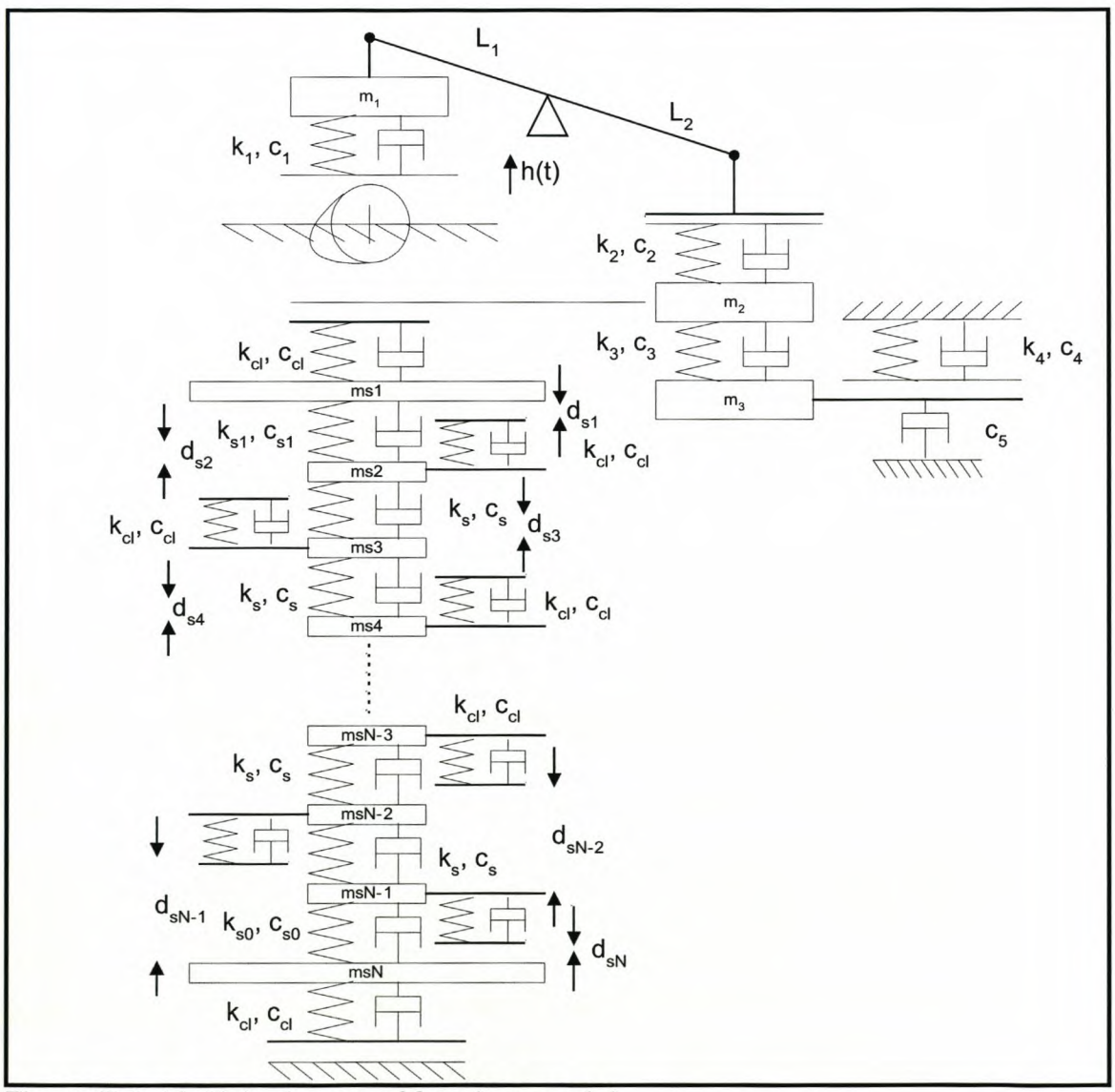

Figure B.1. Multiple degree of freedom model

The equations of motion are written in the form

$$\mathbf{M}\ddot{\mathbf{X}} + \mathbf{C}\dot{\mathbf{X}} + \mathbf{K}\mathbf{X} = \mathbf{F}$$

where

$$\ddot{\mathbf{X}} = \begin{bmatrix} \ddot{x}_1 & \ddot{x}_2 & \ddot{x}_3 & \ddot{x}_{s1} & \ddot{x}_{s2} & \ddot{x}_{s3} & \dots & \ddot{x}_{si} & \dots & \ddot{x}_M \end{bmatrix}^T$$

$$\dot{\mathbf{X}} = \begin{bmatrix} \dot{x}_1 & \dot{x}_2 & \dot{x}_3 & \dot{x}_{s1} & \dot{x}_{s2} & \dot{x}_{s3} & \dots & \dot{x}_{si} & \dots & \dot{x}_M \end{bmatrix}^T$$

$$\mathbf{X} = \begin{bmatrix} x_1 & x_2 & x_3 & x_{s1} & x_{s2} & x_{s3} & \dots & x_{si} & \dots & x_M \end{bmatrix}^T$$

$$\mathbf{F} = \begin{bmatrix} F_1 & F_2 & F_3 & F_{s1} & F_{s2} & F_{s3} & \dots & F_{si} & \dots & F_M \end{bmatrix}^T$$

and

$$\mathbf{M} = \begin{bmatrix} m_1 & 0 & 0 & 0 & 0 & \dots & 0 & \dots & 0 & 0 \\ 0 & m_2 & 0 & 0 & 0 & \dots & 0 & \dots & 0 & 0 \\ 0 & 0 & m_3 & 0 & 0 & \dots & 0 & \dots & 0 & 0 \\ 0 & 0 & 0 & m_{s1} & 0 & \dots & 0 & \dots & 0 & 0 \\ 0 & 0 & 0 & 0 & m_{s2} & \dots & 0 & \dots & 0 & 0 \\ \dots & \dots & \dots & \dots & \dots & \dots & \dots & \dots & \dots & \dots \\ 0 & 0 & 0 & 0 & 0 & \dots & m_{si} & \dots & 0 & 0 \\ \dots & \dots & \dots & \dots & \dots & \dots & \dots & \dots & \dots & \dots \\ 0 & 0 & 0 & 0 & 0 & \dots & 0 & \dots & m_{sN-1} & 0 \\ 0 & 0 & 0 & 0 & 0 & \dots & 0 & \dots & 0 & m_{sN1} \end{bmatrix}$$

$$\mathbf{C} = \begin{bmatrix} C_{11} & C_{12} & C_{13} & C_{14} & C_{15} & \cdots & C_{1,i+3} & \cdots & C_{1,N+2} & C_{1,N+3} \\ C_{21} & C_{22} & \cdots & \cdots & \cdots & \cdots & \cdots & \cdots & \cdots & \cdots \\ C_{31} & \cdots & \cdots & \cdots & \cdots & \cdots & \cdots & \cdots & \cdots & \cdots \\ C_{41} & \cdots & \cdots & \cdots & \cdots & \cdots & \cdots & \cdots & \cdots & \cdots \\ C_{51} & \cdots & \cdots & \cdots & \cdots & \cdots & \cdots & \cdots & \cdots & \cdots \\ \cdots & \cdots & \cdots & \cdots & \cdots & \cdots & \cdots & \cdots & \cdots & \cdots \\ C_{i+3,1} & \cdots & \cdots & \cdots & \cdots & \cdots & \cdots & \cdots & \cdots & \cdots \\ \cdots & \cdots & \cdots & \cdots & \cdots & \cdots & \cdots & \cdots & \cdots & \cdots \\ C_{N+2,1} & \cdots & \cdots & \cdots & \cdots & \cdots & \cdots & \cdots & \cdots & \cdots \\ C_{N+3,1} & \cdots & \cdots & \cdots & \cdots & \cdots & \cdots & \cdots & \cdots & C_{N+3,N+3} \end{bmatrix}$$

$$\mathbf{K} = \begin{bmatrix} K_{11} & K_{12} & K_{13} & K_{14} & K_{15} & \cdots & K_{1,i+3} & \cdots & K_{1,N+2} & K_{1,N+3} \\ K_{21} & K_{22} & \cdots & \cdots & \cdots & \cdots & \cdots & \cdots & \cdots & \cdots \\ K_{31} & \cdots & \cdots & \cdots & \cdots & \cdots & \cdots & \cdots & \cdots & \cdots \\ K_{41} & \cdots & \cdots & \cdots & \cdots & \cdots & \cdots & \cdots & \cdots & \cdots \\ K_{51} & \cdots & \cdots & \cdots & \cdots & \cdots & \cdots & \cdots & \cdots & \cdots \\ \cdots & \cdots & \cdots & \cdots & \cdots & \cdots & \cdots & \cdots & \cdots & \cdots \\ K_{i+3,1} & \cdots & \cdots & \cdots & \cdots & \cdots & \cdots & \cdots & \cdots & \cdots \\ \cdots & \cdots & \cdots & \cdots & \cdots & \cdots & \cdots & \cdots & \cdots & \cdots \\ K_{N+2,1} & \cdots & \cdots & \cdots & \cdots & \cdots & \cdots & \cdots & \cdots & \cdots \\ K_{N+3,1} & \cdots & \cdots & \cdots & \cdots & \cdots & \cdots & \cdots & \cdots & K_{N+3,N+3} \end{bmatrix}$$

The equation of motion of each mass is written by considering Newton's law

$$\sum F = m\ddot{x}$$

for each mass. The displacement of each mass in the positive valve lift direction is haven as m_j. The i^{th} spring mass is indicated by m_{si} with the index j used to number the matrix coefficients. The result for each mass is thus

Mass 1 : Follower:

$$m_1\ddot{x}_1 = k_1(h - x_1) + c_1(\dot{h} - \dot{x}_1) + \left[k_2\left(x_2 - \frac{l_2}{l_1}x_1 + \frac{l_2}{l_1}d\right) + c_2\left(\dot{x}_2 - \frac{l_2}{l_1}\dot{x}_1\right)\right]S_t$$

$$\therefore m_1\ddot{x}_1 = k_1 h - k_1 x_1 + c_1\dot{h} - c_1\dot{x}_1$$
$$+ S_t k_2 x_2 - S_t \frac{l_2}{l_1} k_2 x_1 + S_t \frac{l_2}{l_1} k_2 d + S_t c_2 \dot{x}_2 - S_t \frac{l_2}{l_1} c_2 \dot{x}_1$$

$$\therefore m_1\ddot{x}_1 - k_1 h + k_1 x_1 - c_1\dot{h} + c_1\dot{x}_1$$
$$- S_t k_2 x_2 + S_t \frac{l_2}{l_1} k_2 x_1 - S_t \frac{l_2}{l_1} k_2 d - S_t c_2 \dot{x}_2 + S_t \frac{l_2}{l_1} c_2 \dot{x}_1 = 0$$

$$\therefore m_1\ddot{x}_1$$
$$+ c_1\dot{x}_1 + S_t R c_2 \dot{x}_1 - S_t c_2 \dot{x}_2$$
$$+ k_1 x_1 + S_t R k_2 x_1 - S_t k_2 x_2$$
$$= +k_1 h + c_1\dot{h} + S_t R k_2 d$$

the matrix coefficients for this mass are thus,

$$C_{11} = +c_1 + S_t R c_2$$
$$C_{12} = -S_t c_2$$
$$K_{11} = +k_1 + S_t R k_2$$
$$K_{12} = -S_t k_2$$
$$F_1 = +k_1 h + c_1\dot{h} + S_t R k_2 d$$

where

$$R = \frac{l_2}{l_1}$$

Mass2 : Rocker :

$$m_2\ddot{x}_2 = \frac{l_2}{l_1}\left[k_2\left(\frac{l_2}{l_1}x_1 - x_2 - \frac{l_2}{l_1}d\right) + c_2\left(\frac{l_2}{l_1}\dot{x}_1 - \dot{x}_2\right)\right]S_t$$
$$+ k_3(x_3 - x_2) + c_2(\dot{x}_3 - \dot{x}_2)$$
$$+ \left[k_{cl}(x_{s1} - x_2) + c_{cl}(\dot{x}_{s1} - \dot{x}_2)\right]S_{st}$$

$$\therefore m_2\ddot{x}_2 = S_t k_2\left(\frac{l_2}{l_1}\right)^2 x_1 - S_t\frac{l_2}{l_1}k_2x_2 - S_t k_2\left(\frac{l_2}{l_1}\right)^2 d + S_t\left(\frac{l_2}{l_1}\right)^2 c_2\dot{x}_1 - S_t\frac{l_2}{l_1}c_2\dot{x}_2$$
$$+ k_3x_3 - k_3x_2 + c_2\dot{x}_3 - c_2\dot{x}_2$$
$$+ S_{st}k_{cl}x_{s1} - S_{st}k_{cl}x_2 + S_{st}c_{cl}\dot{x}_{s1} - S_{st}c_{cl}\dot{x}_2$$

$$\therefore m_2\ddot{x}_2 - S_t k_2\left(\frac{l_2}{l_1}\right)^2 x_1 + S_t\frac{l_2}{l_1}k_2x_2 + S_t k_2\left(\frac{l_2}{l_1}\right)^2 d - S_t\left(\frac{l_2}{l_1}\right)^2 c_2\dot{x}_1 + S_t\frac{l_2}{l_1}c_2\dot{x}_2$$
$$- k_3x_3 + k_3x_2 - c_2\dot{x}_3 + c_2\dot{x}_2$$
$$- S_{st}k_{cl}x_{s1} + S_{st}k_{cl}x_2 - S_{st}c_{cl}\dot{x}_{s1} + S_{st}c_{cl}\dot{x}_2 = 0$$

$$\therefore m_2\ddot{x}_2$$
$$- S_t k_2R^2x_1 + S_tRk_2x_2 + k_3x_2 + S_{st}k_{cl}x_2 - k_3x_3 - S_{st}k_{cl}x_{s1}$$
$$- S_tR^2c_2\dot{x}_1 + S_tRc_2\dot{x}_2 + c_2\dot{x}_2 + S_{st}c_{cl}\dot{x}_2 - c_2\dot{x}_3 - S_{st}c_{cl}\dot{x}_{s1}$$
$$= -S_t k_2R^2d$$

the matrix coefficients are thus,

$$K_{21} = -S_t k_2R^2$$
$$K_{22} = +S_tRk_2 + k_3 + S_{st}k_{cl}$$
$$K_{23} = -k_3$$
$$K_{24} = -S_{st}k_{cl}$$
$$C_{21} = -S_tR^2c_2$$
$$C_{22} = +S_tRc_2 + c_2 + S_{st}c_{cl}$$
$$K_{23} = -c_2$$
$$K_{24} = -S_{st}c_{cl}$$
$$F_2 = -S_t k_2R^2d$$

Mass 3 : Valve :

$$m_3\ddot{x}_3 = k_3(x_2 - x_3) + c_3(\dot{x}_2 - \dot{x}_3)$$
$$+ c_5(-\dot{x}_3)$$
$$+ [k_4(-x_3) + c_4(-\dot{x}_3)]S_s$$

$$\therefore m_3\ddot{x}_3 = k_3x_2 - k_3x_3 + c_3\dot{x}_2 - c_3\dot{x}_3$$
$$- \dot{x}_3c_5$$
$$- S_sk_4x_3 - S_sc_4\dot{x}_3$$

$$\therefore m_3\ddot{x}_3 - k_3x_2 + k_3x_3 - c_3\dot{x}_2 + c_3\dot{x}_3$$
$$+ \dot{x}_3c_5 + S_sk_4x_3 + S_sc_4\dot{x}_3 = 0$$

$$\therefore m_3\ddot{x}_3$$
$$- k_3x_2 + k_3x_3 + S_sk_4x_3$$
$$- c_3\dot{x}_2 + c_3\dot{x}_3 + c_5\dot{x}_3 + S_sc_4\dot{x}_3$$
$$= 0$$

the matrix coefficients are thus,

$$K_{32} = -k_3$$
$$K_{33} = +k_3 + S_sk_4$$
$$C_{32} = -c_3$$
$$C_{33} = +c_3 + c_5 + S_sc_4$$
$$F_3 = 0$$

M_{s1} : Spring Top Mass :

$$m_{s1}\ddot{x}_{s1} = \left[k_{cl}\left(x_2 - x_{s1}\right) + c_{cl}\left(\dot{x}_2 - \dot{x}_{s1}\right)\right]S_{springtop}$$
$$+ k_{s1}\left(x_{s2} - x_{s1}\right) + c_{s1}\left(\dot{x}_{s2} - \dot{x}_{s1}\right)$$
$$+ \left[k_{cl}\left(x_{s2} - x_{s1} + d_{s1}\right) + c_{cl}\left(\dot{x}_{s2} - \dot{x}_{s1}\right)\right]C_{12}$$
$$+ \left[k_{cl}\left(x_{s3} - x_{s1} + d_{s2}\right) + c_{cl}\left(\dot{x}_{s3} - \dot{x}_{s1}\right)\right]C_{13}$$

$$\therefore m_{s1}\ddot{x}_{s1} = S_{st}k_{cl}x_2 - S_{st}k_{cl}x_{s1} + S_{st}c_{cl}\dot{x}_2 - S_{st}c_{cl}\dot{x}_{s1}$$
$$+ k_{s1}x_{s2} - k_{s1}x_{s1} + c_{s1}\dot{x}_{s2} - c_{s1}\dot{x}_{s1}$$
$$+ C_{12}k_{cl}x_{s2} - C_{12}k_{cl}x_{s1} + C_{12}k_{cl}d_{s1} + C_{12}c_{cl}\dot{x}_{s2} - C_{12}c_{cl}\dot{x}_{s1}$$
$$+ C_{13}k_{cl}x_{s3} - C_{13}k_{cl}x_{s1} + C_{13}k_{cl}d_{s2} + C_{13}c_{cl}\dot{x}_{s3} - C_{13}c_{cl}\dot{x}_{s1}$$

$$\therefore m_{s1}\ddot{x}_{s1} - S_{st}k_{cl}x_2 + S_{st}k_{cl}x_{s1} - S_{st}c_{cl}\dot{x}_2 + S_{st}c_{cl}\dot{x}_{s1}$$
$$- k_{s1}x_{s2} + k_{s1}x_{s1} - c_{s1}\dot{x}_{s2} + c_{s1}\dot{x}_{s1}$$
$$- C_{12}k_{cl}x_{s2} + C_{12}k_{cl}x_{s1} - C_{12}k_{cl}d_{s1} - C_{12}c_{cl}\dot{x}_{s2} + C_{12}c_{cl}\dot{x}_{s1}$$
$$- C_{13}k_{cl}x_{s3} + C_{13}k_{cl}x_{s1} - C_{13}k_{cl}d_{s2} - C_{13}c_{cl}\dot{x}_{s3} + C_{13}c_{cl}\dot{x}_{s1} = 0$$

$$\therefore m_{s1}\ddot{x}_{s1}$$
$$-S_{st}k_{cl}x_2 + S_{st}k_{cl}x_{s1} + k_{s1}x_{s1} + C_{12}k_{cl}x_{s1} + C_{13}k_{cl}x_{s1} - k_{s1}x_{s2} - C_{12}k_{cl}x_{s2} - C_{13}k_{cl}x_{s3}$$
$$-S_{st}c_{cl}\dot{x}_2 + S_{st}c_{cl}\dot{x}_{s1} + c_{s1}\dot{x}_{s1} + C_{12}c_{cl}\dot{x}_{s1} + C_{13}c_{cl}\dot{x}_{s1} - c_{s1}\dot{x}_{s2} - C_{12}c_{cl}\dot{x}_{s2} - C_{13}c_{cl}\dot{x}_{s3}$$
$$= +C_{12}k_{cl}d_{s1} + C_{13}k_{cl}d_{s2}$$

the matrix coefficients are thus,

$$K_{42} = -S_{st}k_{cl}$$
$$K_{43} = 0$$
$$K_{44} = +S_{st}k_{cl} + k_{s1} + C_{12}k_{cl} + C_{13}k_{cl}$$
$$K_{45} = -k_{s1} - C_{12}k_{cl}$$
$$K_{46} = -C_{13}k_{cl}$$
$$C_{42} = -S_{st}c_{cl}$$
$$C_{43} = 0$$
$$C_{44} = +S_{st}c_{cl} + c_{s1} + C_{12}c_{cl} + C_{13}c_{cl}$$
$$C_{45} = -c_{s1} - C_{12}c_{cl}$$
$$C_{46} = -C_{13}c_{cl}$$
$$F_4 = +C_{12}k_{cl}d_{s1} + C_{13}k_{cl}d_{s2}$$

M_{s2} : Spring Second Mass :

$$m_{s2}\ddot{x}_{s2} = k_{s1}(x_{s1} - x_{s2}) + c_s(\dot{x}_{s1} - \dot{x}_{s2})$$
$$+ k_s(x_{s3} - x_{s2}) + c_s(\dot{x}_{s3} - \dot{x}_{s2})$$
$$+ [k_{cl}(x_{s1} - x_{s2} - d_{s1}) + c_{cl}(\dot{x}_{s1} - \dot{x}_{s2})]C_{1,2}$$
$$+ [k_{cl}(x_{s4} - x_{s2} + d_{s3}) + c_{cl}(\dot{x}_{s4} - \dot{x}_{s2})]C_{2,3}$$

$$\therefore m_{s2}\ddot{x}_{s2} = k_{s1}x_{s1} - k_{s1}x_{s2} + c_s\dot{x}_{s1} - c_s\dot{x}_{s2}$$
$$+ k_s x_{s3} - k_s x_{s2} + c_s\dot{x}_{s3} - c_s\dot{x}_{s2}$$
$$+ C_{1,2}k_{cl}x_{s1} - C_{1,2}k_{cl}x_{s2} - C_{1,2}k_{cl}d_{s1} + C_{1,2}c_{cl}\dot{x}_{s1} - C_{1,2}c_{cl}\dot{x}_{s2}$$
$$+ C_{2,3}k_{cl}x_{s4} - C_{2,3}k_{cl}x_{s2} + C_{2,3}k_{cl}d_{s3} + C_{2,3}c_{cl}\dot{x}_{s4} - C_{2,3}c_{cl}\dot{x}_{s2}$$

$$\therefore m_{s2}\ddot{x}_{s2} - k_{s1}x_{s1} + k_{s1}x_{s2} - c_s\dot{x}_{s1} + c_s\dot{x}_{s2}$$
$$- k_s x_{s3} + k_s x_{s2} - c_s\dot{x}_{s3} + c_s\dot{x}_{s2}$$
$$- C_{1,2}k_{cl}x_{s1} + C_{1,2}k_{cl}x_{s2} + C_{1,2}k_{cl}d_{s1} - C_{1,2}c_{cl}\dot{x}_{s1} + C_{1,2}c_{cl}\dot{x}_{s2}$$
$$- C_{2,3}k_{cl}x_{s4} + C_{2,3}k_{cl}x_{s2} - C_{2,3}k_{cl}d_{s3} - C_{2,3}c_{cl}\dot{x}_{s4} + C_{2,3}c_{cl}\dot{x}_{s2} = 0$$

$$\therefore m_{s2}\ddot{x}_{s2}$$
$$-k_{s1}x_{s1} - C_{1,2}k_{cl}x_{s1} + k_{s1}x_{s2} + k_s x_{s2} + C_{1,2}k_{cl}x_{s2} + C_{2,3}k_{cl}x_{s2} - k_s x_{s3} - C_{2,3}k_{cl}x_{s4}$$
$$-c_s\dot{x}_{s1} - C_{1,2}c_{cl}\dot{x}_{s1} + c_s\dot{x}_{s2} + c_s\dot{x}_{s2} + C_{1,2}c_{cl}\dot{x}_{s2} + C_{2,3}c_{cl}\dot{x}_{s2} - c_s\dot{x}_{s3} - C_{2,3}c_{cl}\dot{x}_{s4}$$
$$= -C_{1,2}k_{cl}d_{s1} + C_{2,3}k_{cl}d_{s3}$$

the matrix coefficients are thus :

$$K_{54} = -k_{s1} - C_{1,2}k_{cl}$$
$$K_{55} = +k_{s1} + k_s + C_{1,2}k_{cl} + C_{2,3}k_{cl}$$
$$K_{56} = -k_s$$
$$K_{57} = -C_{2,3}k_{cl}$$
$$C_{54} = -c_s - C_{1,2}c_{cl}$$
$$C_{55} = +c_s + c_s + C_{1,2}c_{cl} + C_{2,3}c_{cl}$$
$$C_{56} = -c_s$$
$$C_{57} = -C_{2,3}c_{cl}$$
$$F_5 = -C_{1,2}k_{cl}d_{s1} + C_{2,3}k_{cl}d_{s3}$$

Msi : Spring General Mass :

$$\begin{aligned} m_{si}\ddot{x}_{si} &= k_s(x_{si-1} - x_{si}) + c_s(\dot{x}_{si-1} - \dot{x}_{si}) \\ &+ k_s(x_{si+1} - x_{si}) + c_s(\dot{x}_{si+1} - \dot{x}_{si}) \\ &+ [k_{cl}(x_{si-2} - x_{si} - d_{si-1}) + c_{cl}(\dot{x}_{si-2} - \dot{x}_{si})]C_{i-2,i} \\ &+ [k_{cl}(x_{si+2} - x_{si} + d_{si+1}) + c_{cl}(\dot{x}_{si+2} - \dot{x}_{si})]C_{i,i+2} \end{aligned}$$

$$\begin{aligned} \therefore m_{si}\ddot{x}_{si} &= k_s x_{si-1} - k_s x_{si} + c_s\dot{x}_{si-1} - c_s\dot{x}_{si} \\ &+ k_s x_{si+1} - k_s x_{si} + c_s\dot{x}_{si+1} - c_s\dot{x}_{si} \\ &+ C_{i-2,i}k_{cl}x_{si-2} - C_{i-2,i}k_{cl}x_{si} - C_{i-2,i}k_{cl}d_{si-1} + C_{i-2,i}c_{cl}\dot{x}_{si-2} - C_{i-2,i}c_{cl}\dot{x}_{si} \\ &+ C_{i,i+2}k_{cl}x_{si+2} - C_{i,i+2}k_{cl}x_{si} + C_{i,i+2}k_{cl}d_{si+1} + C_{i,i+2}c_{cl}\dot{x}_{si+2} - C_{i,i+2}c_{cl}\dot{x}_{si} \end{aligned}$$

$$\begin{aligned} \therefore m_{si}\ddot{x}_{si} &- k_s x_{si-1} + k_s x_{si} - c_s\dot{x}_{si-1} + c_s\dot{x}_{si} \\ &- k_s x_{si+1} + k_s x_{si} - c_s\dot{x}_{si+1} + c_s\dot{x}_{si} \\ &- C_{i-2,i}k_{cl}x_{si-2} + C_{i-2,i}k_{cl}x_{si} + C_{i-2,i}k_{cl}d_{si-1} - C_{i-2,i}c_{cl}\dot{x}_{si-2} + C_{i-2,i}c_{cl}\dot{x}_{si} \\ &- C_{i,i+2}k_{cl}x_{si+2} + C_{i,i+2}k_{cl}x_{si} - C_{i,i+2}k_{cl}d_{si+1} - C_{i,i+2}c_{cl}\dot{x}_{si+2} + C_{i,i+2}c_{cl}\dot{x}_{si} = 0 \end{aligned}$$

$$\therefore m_{si}\ddot{x}_{si}$$
$$-C_{i-2,i}k_{cl}x_{si-2}-k_s x_{si-1}+k_s x_{si}+k_s x_{si}+C_{i-2,i}k_{cl}x_{si}+C_{i,i+2}k_{cl}x_{si}-k_s x_{si+1}-C_{i,i+2}k_{cl}x_{si+2}$$
$$-C_{i-2,i}c_{cl}\dot{x}_{si-2}-c_s\dot{x}_{si-1}+c_s\dot{x}_{si}+c_s\dot{x}_{si}+C_{i-2,i}c_{cl}\dot{x}_{si}+C_{i,i+2}c_{cl}\dot{x}_{si}-c_s\dot{x}_{si+1}-C_{i,i+2}c_{cl}\dot{x}_{si+2}$$
$$=-C_{i-2,i}k_{cl}d_{si-1}+C_{i,i+2}k_{cl}d_{si+1}$$

the matrix coefficients are thus :

$$K_{j,j-2}=-C_{i-2,i}k_{cl}$$
$$K_{j,j-1}=-k_s$$
$$K_{j,j}=+k_s+k_s+C_{i-2,i}k_{cl}+C_{i,i+2}k_{cl}$$
$$K_{j,j+1}=-k_s$$
$$K_{j,j+2}=-C_{i,i+2}k_{cl}$$
$$C_{j,j-2}=-C_{i-2,i}c_{cl}$$
$$C_{j,j-1}=-c_s$$
$$C_{j,j}=+c_s+c_s+C_{i-2,i}c_{cl}+C_{i,i+2}c_{cl}$$
$$C_{j,j+1}=-c_s$$
$$C_{j,j+2}=-C_{i,i+2}c_{cl}$$
$$F_j=-C_{i-2,i}k_{cl}d_{si-1}+C_{i,i+2}k_{cl}d_{si+1}$$

M_{sN-1} : Spring Second Last Mass :

$$\begin{aligned}m_{sN-1}\ddot{x}_{sN-1}&=k_s\left(x_{sN-2}-x_{sN-1}\right)+c_s\left(\dot{x}_{sN-2}-\dot{x}_{sN-1}\right)\\&+k_{s0}\left(x_{sN}-x_{sN-1}\right)+c_{s0}\left(\dot{x}_{sN}-\dot{x}_{sN-1}\right)\\&+\left[k_{cl}\left(x_{sN-3}-x_{sN-1}-d_{sN-2}\right)+c_{cl}\left(\dot{x}_{sN-3}-\dot{x}_{sN-1}\right)\right]C_{N-1,N-3}\\&+\left[k_{cl}\left(x_{sN}-x_{sN-1}+d_{sN}\right)+c_{cl}\left(\dot{x}_{sN}-\dot{x}_{sN-1}\right)\right]C_{N,N-1}\end{aligned}$$

$$\begin{aligned}\therefore m_{sN-1}\ddot{x}_{sN-1}&=k_s x_{sN-2}-k_s x_{sN-1}+c_s\dot{x}_{sN-2}-c_s\dot{x}_{sN-1}\\&+k_{s0}x_{sN}-k_{s0}x_{sN-1}+c_{s0}\dot{x}_{sN}-c_{s0}\dot{x}_{sN-1}\\&+C_{N-1,N-3}k_{cl}x_{sN-3}-C_{N-1,N-3}k_{cl}x_{sN-1}-C_{N-1,N-3}k_{cl}d_{sN-2}+C_{N-1,N-3}c_{cl}\dot{x}_{sN-3}-C_{N-1,N-3}c_{cl}\dot{x}_{sN-1}\\&+C_{N,N-1}k_{cl}x_{sN}-C_{N,N-1}k_{cl}x_{sN-1}+C_{N,N-1}k_{cl}d_{sN}+C_{N,N-1}c_{cl}\dot{x}_{sN}-C_{N,N-1}c_{cl}\dot{x}_{sN-1}\end{aligned}$$

$$\therefore m_{sN-1}\ddot{x}_{sN-1} - k_s x_{sN-2} + k_s x_{sN-1} - c_s \dot{x}_{sN-2} + c_s \dot{x}_{sN-1}$$
$$- k_{s0} x_{sN} + k_{s0} x_{sN-1} - c_{s0} \dot{x}_{sN} + c_{s0} \dot{x}_{sN-1}$$
$$- C_{N-1,N-3} k_{cl} x_{sN-3} + C_{N-1,N-3} k_{cl} x_{sN-1} + C_{N-1,N-3} k_{cl} d_{sN-2}$$
$$- C_{N-1,N-3} c_{cl} \dot{x}_{sN-3} + C_{N-1,N-3} c_{cl} \dot{x}_{sN-1}$$
$$- C_{N,N-1} k_{cl} x_{sN} + C_{N,N-1} k_{cl} x_{sN-1}$$
$$- C_{N,N-1} k_{cl} d_{sN} - C_{N,N-1} c_{cl} \dot{x}_{sN} + C_{N,N-1} c_{cl} \dot{x}_{sN-1} = 0$$

$$\therefore m_{sN-1}\ddot{x}_{sN-1}$$
$$- C_{N-1,N-3} k_{cl} x_{sN-3} - k_s x_{sN-2} + k_s x_{sN-1} + k_{s0} x_{sN-1}$$
$$+ C_{N-1,N-3} k_{cl} x_{sN-1} + C_{N,N-1} k_{cl} x_{sN-1} - k_{s0} x_{sN} - C_{N,N-1} k_{cl} x_{sN}$$
$$- C_{N-1,N-3} c_{cl} \dot{x}_{sN-3} - c_s \dot{x}_{sN-2} + c_s \dot{x}_{sN-1} + c_{s0} \dot{x}_{sN-1}$$
$$+ C_{N-1,N-3} c_{cl} \dot{x}_{sN-1} + C_{N,N-1} c_{cl} \dot{x}_{sN-1} - c_{s0} \dot{x}_{sN} - C_{N,N-1} c_{cl} \dot{x}_{sN}$$
$$= -C_{N-1,N-3} k_{cl} d_{sN-2} + C_{N,N-1} k_{cl} d_{sN}$$

the matrix coefficients are thus :

$$K_{M-1,M-3} = -C_{N-1,N-3} k_{cl}$$
$$K_{M-1,M-2} = -k_s$$
$$K_{M-1,M-1} = +k_s + k_{s0} + C_{N-1,N-3} k_{cl} + C_{N,N-1} k_{cl}$$
$$K_{M-1,M} = -k_{s0} - C_{N,N-1} k_{cl}$$
$$C_{M-1,M-3} = -C_{N-1,N-3} c_{cl}$$
$$C_{M-1,M-2} = -c_s$$
$$C_{M-1,M-1} = +c_s + c_{s0} + C_{N-1,N-3} c_{cl} + C_{N,N-1} c_{cl}$$
$$C_{M-1,M} = -c_{s0} - C_{N,N-1} c_{cl}$$
$$F_{M-1} = -C_{N-1,N-3} k_{cl} d_{sN-2} + C_{N,N-1} k_{cl} d_{sN}$$

Mass N : Last Mass

$$m_{sN}\ddot{x}_{sN} = k_{s0}(x_{sN-1} - x_{sN}) + c_{s0}(\dot{x}_{sN-1} - \dot{x}_{sN})$$
$$+ [k_{cl}(-x_{sN}) + c_{cl}(-\dot{x}_{sN})] S_{springbottom}$$
$$+ [k_{cl}(x_{sN-1} - x_{sN} - d_{sN}) + c_{cl}(\dot{x}_{sN-1} - \dot{x}_{sN})] C_{N,N-1}$$
$$+ [k_{cl}(x_{sN-2} - x_{sN} - d_{sN-1}) + c_{cl}(\dot{x}_{sN-2} - \dot{x}_{Ni})] C_{N,N-2}$$

$$
\begin{aligned}
\therefore m_{sN}\ddot{x}_{sN} &= k_{s0}x_{sN-1} - k_{s0}x_{sN} + c_{s0}\dot{x}_{sN-1} - c_{s0}\dot{x}_{sN} \\
&\quad - S_{sb}k_{cl}x_{sN} - S_{sb}c_{cl}\dot{x}_{sN} \\
&\quad + C_{N,N-1}k_{cl}x_{sN-1} - C_{N,N-1}k_{cl}x_{sN} - C_{N,N-1}k_{cl}d_{sN} \\
&\quad + C_{N,N-1}c_{cl}\dot{x}_{sN-1} - C_{N,N-1}c_{cl}\dot{x}_{sN} \\
&\quad + C_{N,N-2}k_{cl}x_{sN-2} - C_{N,N-2}k_{cl}x_{sN} - C_{N,N-2}k_{cl}d_{sN-1} \\
&\quad + C_{N,N-2}c_{cl}\dot{x}_{sN-2} - C_{N,N-2}c_{cl}\dot{x}_{Ni}
\end{aligned}
$$

$$
\begin{aligned}
\therefore m_{sN}\ddot{x}_{sN} &- k_{s0}x_{sN-1} + k_{s0}x_{sN} - c_{s0}\dot{x}_{sN-1} + c_{s0}\dot{x}_{sN} \\
&\quad + S_{sb}k_{cl}x_{sN} + S_{sb}c_{cl}\dot{x}_{sN} \\
&\quad - C_{N,N-1}k_{cl}x_{sN-1} + C_{N,N-1}k_{cl}x_{sN} + C_{N,N-1}k_{cl}d_{sN} \\
&\quad - C_{N,N-1}c_{cl}\dot{x}_{sN-1} + C_{N,N-1}c_{cl}\dot{x}_{sN} \\
&\quad - C_{N,N-2}k_{cl}x_{sN-2} + C_{N,N-2}k_{cl}x_{sN} \\
&\quad + C_{N,N-2}k_{cl}d_{sN-1} - C_{N,N-2}c_{cl}\dot{x}_{sN-2} + C_{N,N-2}c_{cl}\dot{x}_{Ni} = 0
\end{aligned}
$$

$$
\begin{aligned}
&\therefore m_{sN}\ddot{x}_{sN} \\
&- C_{N,N-2}k_{cl}x_{sN-2} - k_{s0}x_{sN-1} - C_{N,N-1}k_{cl}x_{sN-1} \\
&\quad + k_{s0}x_{sN} + S_{sb}k_{cl}x_{sN} + C_{N,N-1}k_{cl}x_{sN} + C_{N,N-2}k_{cl}x_{sN} \\
&- C_{N,N-2}c_{cl}\dot{x}_{sN-2} - c_{s0}\dot{x}_{sN-1} - C_{N,N-1}c_{cl}\dot{x}_{sN-1} \\
&\quad + c_{s0}\dot{x}_{sN} + S_{sb}c_{cl}\dot{x}_{sN} + C_{N,N-1}c_{cl}\dot{x}_{sN} + C_{N,N-2}c_{cl}\dot{x}_{Ni} \\
&= -C_{N,N-1}k_{cl}d_{sN} - C_{N,N-2}k_{cl}d_{sN-1}
\end{aligned}
$$

the matrix coefficients are thus:

$$
\begin{aligned}
K_{M,M-2} &= -C_{N,N-2}k_{cl} \\
K_{M,M-1} &= -k_{s0} - C_{N,N-1}k_{cl} \\
K_{M,M} &= +k_{s0} + S_{sb}k_{cl} + C_{N,N-1}k_{cl} + C_{N,N-2}k_{cl} \\
C_{M,M-2} &= -C_{N,N-2}c_{cl} \\
C_{M,M-1} &= -c_{s0} - C_{N,N-1}c_{cl} \\
C_{M,M} &= +c_{s0} + S_{sb}c_{cl} + C_{N,N-1}c_{cl} + C_{N,N-2}c_{cl} \\
K_{M} &= -C_{N,N-1}k_{cl}d_{sN} - C_{N,N-2}k_{cl}d_{sN-1}
\end{aligned}
$$

The rest of the coefficients of the K and C matrices are zero.

(Page intentionally blank)

USER MANUAL

Engine Simulation and Analysis

Software for Personal Computer Based Numeric Simulation of Engine Performance

Paul Williams
Christie van Vuuren

University of Stellenbosch
1996-2001

1. Introduction

ESA is an internal combustion engine simulation package written by post-graduate students of the University of Stellenbosch as part of their studies. The simulation package consists of a two-zone thermodynamic combustion model linked to a computation fluid dynamics (CFD) manifold and pipe flow model and integrated with a camshaft analysis model. The combination of these three models allows accurate simulation of all the effects of variation of cam profiles, manifold and exhaust pipe dimensions as well as geometric, fuel and other properties of the engine and its environment. The program was written in Borland Delphi 4 and compiled to a user friendly, full 32 bit Windows 95/98 and NT application.

2. Disclaimer

The authors, the CAE and the University of Stellenbosch, make no warranty of any kind, expressed or implied, including without limitation any warranties of merchantability and/or fitness for a particular purpose. The authors do not assume any liability for the use of ESA, as will be displayed on initialising the program.

In no event will the authors be liable for any additional damages. This include any lost profits, lost savings, or other incidental or consequential damages arising from the use of, or inability to use, this software and its accompanying documentation, even if the authors have been advised of the possibility of such damages.

Please note that the software is still in the developmental phase.

3. Installation and Setup

The computer installation code is supplied on a CD-ROM disc. The program can be installed on the computer of the user by the standard Windows method of running SETUP.EXE on the CD. This is accomplished either by selecting

Start, Settings, Control Panel, Add/Remove Programs and then clicking ***Install*** or by selecting ***Start, Run*** typing X:\ESA\SETUP.EXE in the open box and then clicking ***Ok*** (X is the letter of the appropriate disk drive, normally *D* for the CD-ROM drive). Once the Install Wizard is running, the user should follow the instructions as given, remembering to type the user details and serial number supplied with the program in the required dialog. ESA installs by default into the C:\ESA directory, but this can be changed by the user if so desired.

The Install Wizard installs the following files into the selected folder of the user. A description of the exact nature of the user adjustable files is given later in this document.

ESA.exe - the executable file to run the program

Default.eng - a default engine setup file

Default.cwt - a default head, piston and liner temperature vs. speed file

Default.spk - a default ignition timing vs. speed file

Default_Inl.maf - a default inlet manifold and pipe geometric profile file

Default_Exh.maf - a default exhaust manifold and pipe geometric profile file

Default.exh - a default exhaust gas temperature and pressure vs. speed file

Default_Inl.cam - a default inlet valve lift profile file

Default_Exh.cam - a default exhaust valve lift profile file

Default_IV.vcd - a default inlet valve C_d map (forward flow) file

Default_IVRev.vcd - a default inlet valve C_d map (reverse flow) file

Default_EV.vcd - a default exhaust valve C_d map (forward flow) file

Default_EVRev.vcd - a default exhaust valve C_d map (reverse flow) file

Errorlog.err - a file used to log errors that may occur in the simulation

ESA.ini - a program setup file installed into the C:\Windows directory.

Once the installation has been completed, the user can run the program by clicking on the ESA icon under the **Start Menu / Programs** folder. No further user setup is required at this time. The program runs best in a screen resolution of 800x600 or 1024x768 with at least 256 colours.

4. Program and Menu Overview

A short description of the menu items and functions as well as basic operation of the program is given in this section.

On program start-up, the displayed user interface consists of a menu bar, a status bar and four display areas.

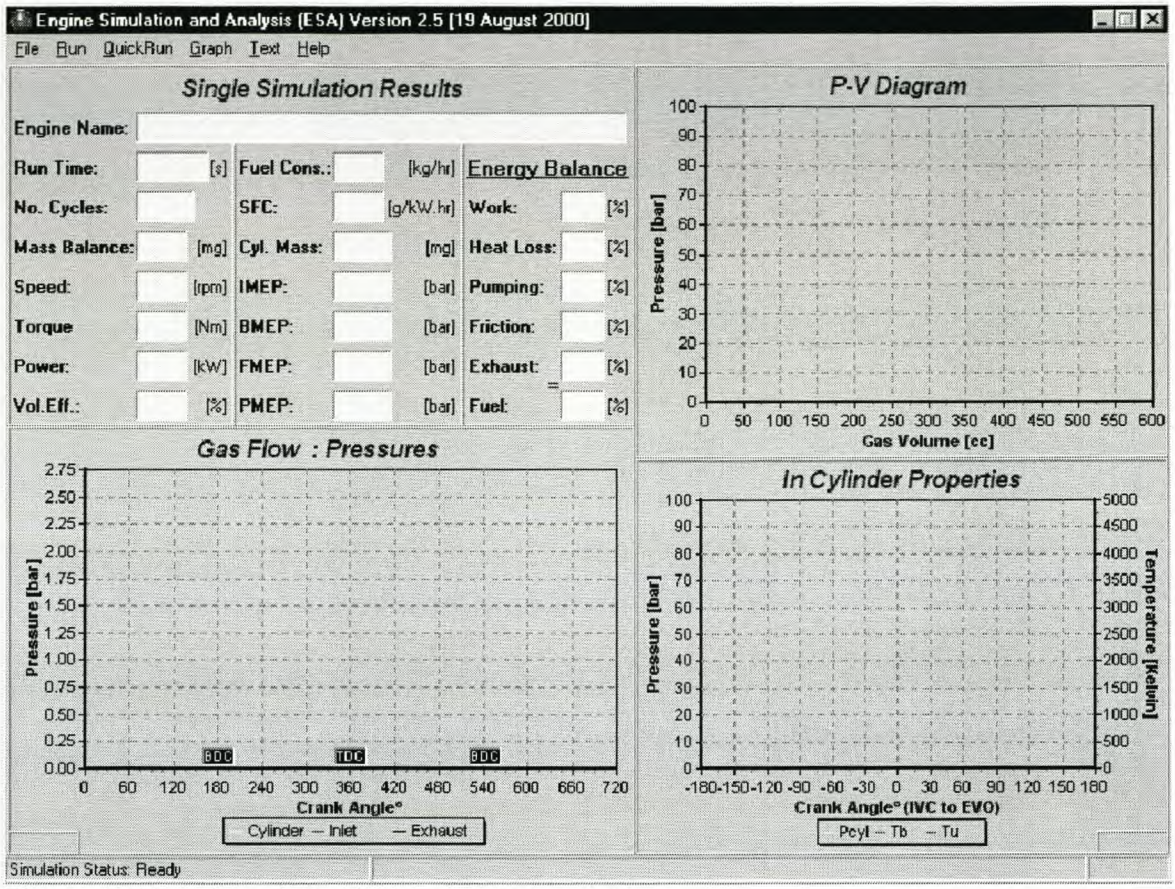

Figure 2: User interface during program start-up

In the top left corner is a multiple text box area where the program reports the results of a single simulation run. Some of the reporting is online while the program is running. Other information is only displayed, as it becomes available at the completion of the simulation.

In the top right corner is a graph that displays an online indicator PV-diagram, cylinder pressure vs. volume for one cylinder. This graph scales automatically unless the user performs a manual scaling as described later in this manual.

In the bottom right corner is a graph providing a trace of in-cylinder properties vs. crank angle. The properties displayed are cylinder pressure (P_{cyl}), mixture burnt temperature (T_b) and mixture unburned temperature (T_u).

In the bottom left corner is a graph that can display the following:

Cylinder conditions: pressure, total trapped mass, unburned mass and burnt mass vs. crank angle

Inlet valve conditions: pressure, velocity and mass transfer vs. crank angle

Exhaust valve conditions: pressure, velocity and mass transfer vs. crank angle.

The status bar display information regarding the files loaded or saved by the user as well as the simulation status including crank angle and simulation time elapsed.

The initial available menu items are the following (Figure 2):

File | Run | QuickRun | Graph | Text | Help.

Under the **File** menu, the user elects to **Load**, **Save** and **Edit** the geometrical and operational details of a desired simulation as well as **Exit** the program.

The **Run** menu is used to initialise or **Pause** and **Stop** the various simulation modes. Selecting the **Single Point Simulation** option initialises the simplest simulation mode. To run multiple point simulation runs, choose **Multi Point Simulation**. These options are executed after an engine file has been loaded.

The **QuickRun** menu is used to initialise the **Single Point Simulation** option by loading the default engine data file and configuration.

The **Graph** menu is used to alter the various parameters that are displayed on the graphs during and after completion of the simulation. Some of the options are only available after an engine file has been loaded. The options are changing **Run-Time Graph Options**, viewing a **Torque Curve**, **Valve Opening** and the **Energy Balance** during the last engine cycle.

The **Text** menu is used to view and save (default to *Lastcyc.text*) the results of a completed simulation. The text format is suitable for use in a spreadsheet e.g. Excel. This provides accurate data for all simulated parameters at each crank angle degree.

The **Help** menu provides access to this **User Manual** that serves as a help document and the **About** box, giving some detail on the software and its creators.

5. Creating an Engine Data File

This section describes the basic use of the program and creating an engine data file. For the purposes of this tutorial, the user will load the default engine file; modify a few operating parameters and then run a simple simulation.

On initialising the program, the user interface (Figure 1) becomes visible.

To load the engine data files, the user clicks **File, Load**. The *Open Engine Data File* dialog box is displayed (). The user can select the desired *.eng files using the standard windows dialog box. Select the file and then click **Open**.

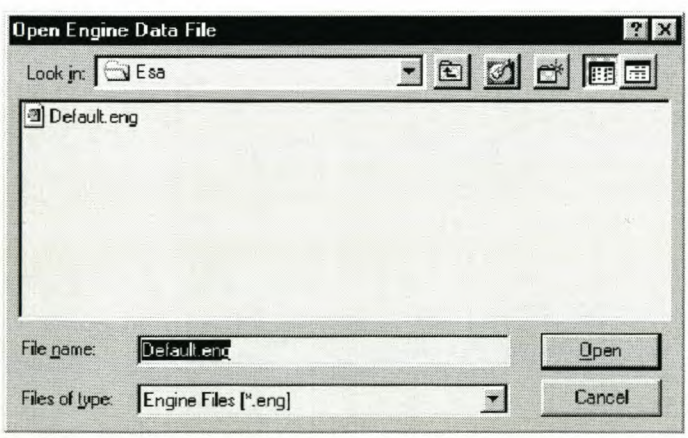

Figure 3: Load engine data file

The loaded filename is displayed in the lower status bar. To load the default engine file automatically, the user clicks **File, Load Default**.

To modify the engine model input data, click **File, Edit**. The *Edit Engine Data* dialog box will be displayed (Figure 2).

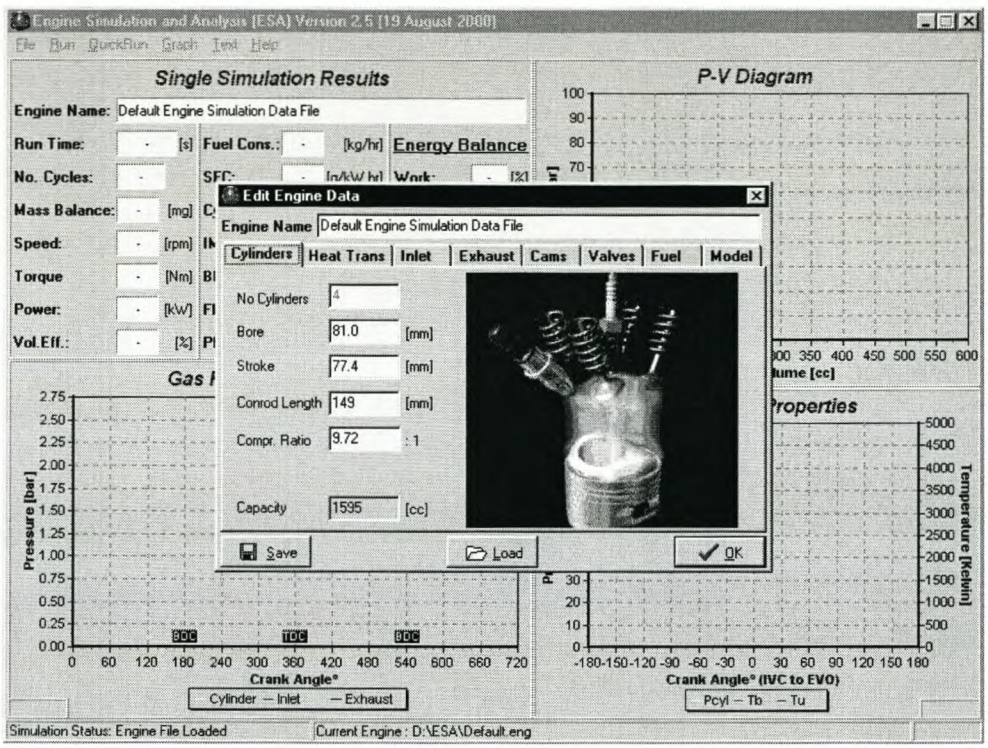

Figure 4: Edit engine data file

To modify any parameter, change the text or value in the edit boxes (Figure). **Cylinders** is the first edit tab to be displayed (Figure). The geometric information on the engine can be changed here:

The capacity of the engine is then calculated and displayed as in Figure .

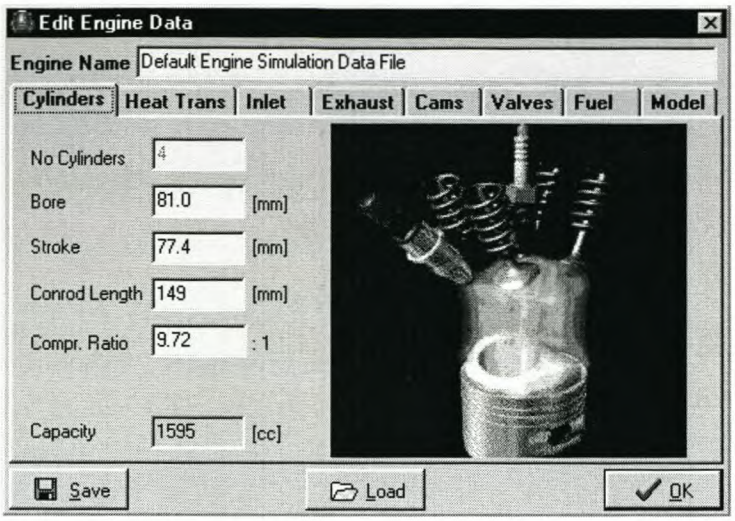

Figure 5: Cylinder data

Heat Trans (heat transfer) is the next edit tab (Figure 4). Here information on the heat transfer of the engine, burn angle and ignition timing of the engine can be changed. The surface temperatures of the head, piston, upper and lower liners are given as an input file to the program via a text file, *.cwt (Figure 5). Different input files are selected by clicking the *Browse* button. In this file surface temperatures at different engine speeds are given. The format of the text file is the same for all the other input files to the program. The value in the first text line sets the number of data lines in the text file. The second line has headings for all the data sets. The remaining lines, as specified by the value in the first text line, have all the necessary input data for the program.

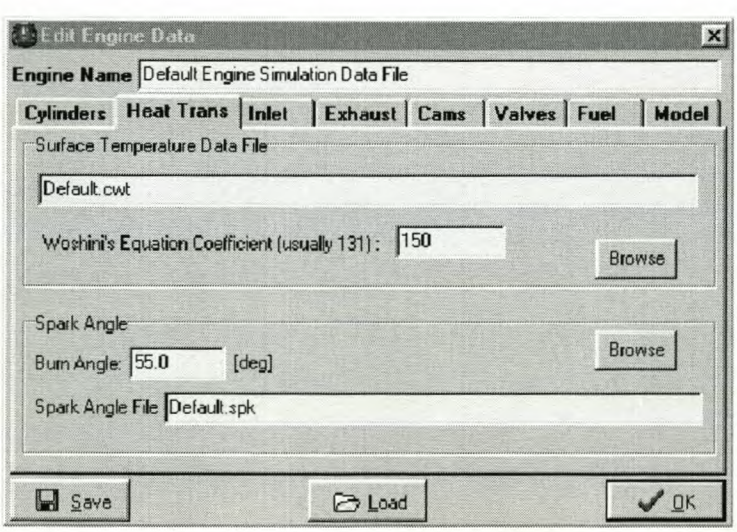

Figure 6: Heat transfer and ignition timing data

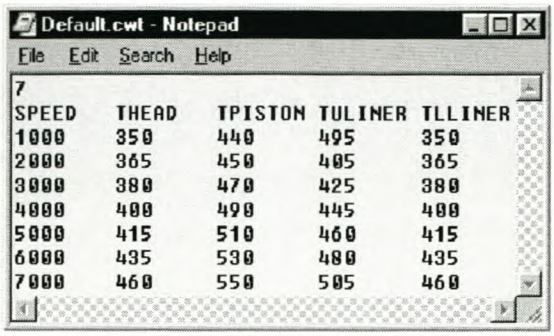

Figure 7: Temperature data for the head, piston and liners

The *Woshini's Equation Coefficient* [2] exists to fine-tune the heat transfer in the model. The model is not accurate enough to calculate the heat transfer exactly as in the physical engine. Because of limited information, the model needs to be fine-tuned to get the heat transfer equalling the right percentage loss of the total available energy of the engine. This percentage value can be obtained by doing physical engine tests or by assuming a value of 30 ± 5% [2].

The *Burn Angle* of the fuel also depends very much on the combustion chamber design of the engine. By doing a full combustion analysis on the engine, the burn angle can be obtained at each engine speed. If this information is not available, a good estimate is a value between 40° - 60° crank angle [2].

The information needed for the *Spark Angle File* (Figure 6) is usually only obtained after doing physical engine tests. If this is not possible, experience and other similar data from other engines are used to create such a file. The most beneficial timing (MBT) can also be estimated by doing variable ignition timings with the model at the same speed and with the same burn angle. The ignition timing that gives the maximum torque will then be used, until further engine data is available.

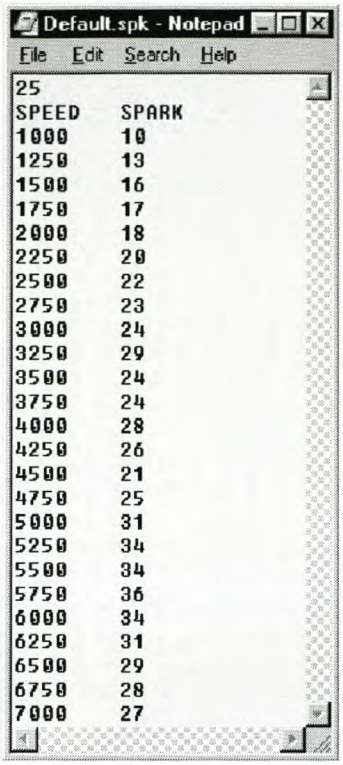

Figure 8: Ignition timing information

Inlet is the next edit tab (Figure 7). In the edit boxes of this tab, all the information on the inlet manifold is displayed. The first information needed is the geometrical detail on the inlet manifold. For this information the program uses an input file that is created by clicking on the *Edit* button. A new window is displayed that has length and area as input. This data is also displayed as a graph and saved as a text file, *.maf.

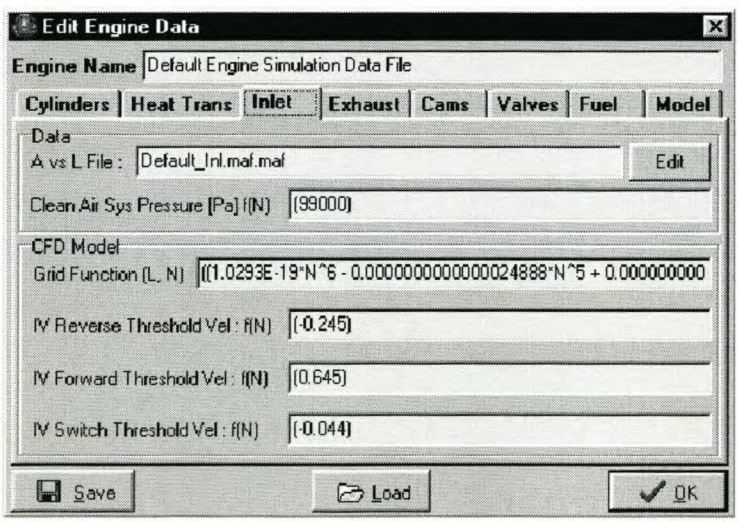

Figure 9: **Inlet manifold data**

The length of the manifold is taken from the entrance of the plenum (zero point) up to where the inlet valve ports end. The area along this length is then given in small length steps.

Sometimes it is necessary to simplify the area variation in the inlet port. Big area changes can be found in this region, which can lead to simulation instabilities. The simulation program is using a grid to solve the flow in the inlet. If the area change is very big, the grid might not be small enough to take it into account. The grid also changes with engine speed, meaning that sometimes this area change is taken into account and other times not. It is therefore better to keep area variation smooth, as illustrated in Figure 8.

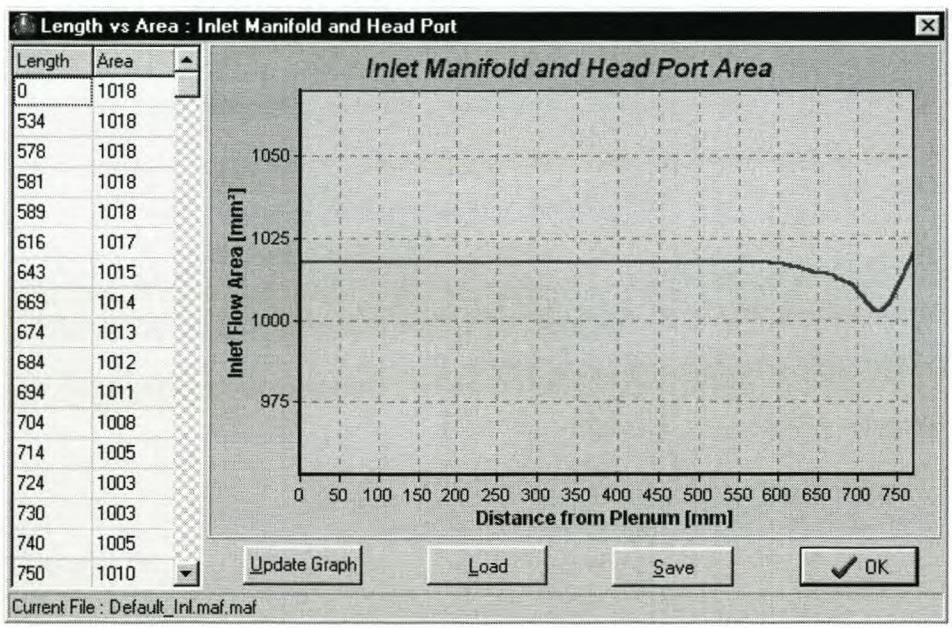

Figure 10: **Inlet manifold area vs. length**

The next information needed is the *Clean Air Sys Pressure*. This pressure is part of the boundary condition at the open end to the manifold plenum. In a well-designed inlet manifold this pressure is almost constant, but it will drop slightly as the engine speed increases. This data is usually obtained from engine tests. The pressure is given to the program as an equation, which is a function of engine speed for e.g. (E-10*N^3 - 1E-06*N^2 - 0.0009*N + 1014.4).

The information needed to ensure mathematical stability and smooth transition between forward and reverse flow is displayed in the last four edit boxes, as displayed in Figure 7. The first edit box, *Grid Function*, is the inlet grid size equation, which is a function of engine speed and inlet length. For each engine model this needs to be fine-tuned by first calculating the grid size using the CFL-stability criterion. The grid size is then tested and corrected by running simulations with a grid size just above and below the CFL calculated grid to correct for velocity changes.

Getting smooth transition between forward and reverse flow at the inlet valves can be very difficult. The pressures at the inlet valve and in the combustion chamber can sometimes be very close together; for example just before the inlet valve closes (described in Chapter 2). To help in the smoother transition between forward and reverse flow, a minimum velocity (trial-and-error based) at the valve is given before the flow will change from forward to reverse, or reverse to forward flow.

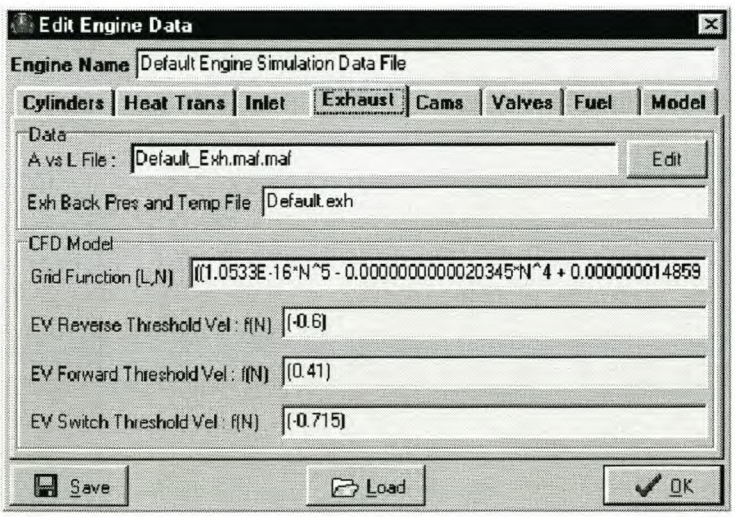

Figure 11: **Exhaust manifold data**

Exhaust is the next edit tab (Figure 9). In the edit boxes of this tab, all the information on the exhaust manifold and pipe is displayed. The first information needed is the geometrical detail on the exhaust manifold and pipe. For this information the program uses an input file that is created by clicking on the *Edit* button. A new window is displayed that has length and

area as input (similar to inlet Figure 8). This data is also displayed as a graph and saved as a text file, *.maf (Figure 10).

The length of the manifold and pipe is taken from the entrance of the exhaust valve ports (zero point) up to the first sudden expansion, usually a silencer box or catalyst.

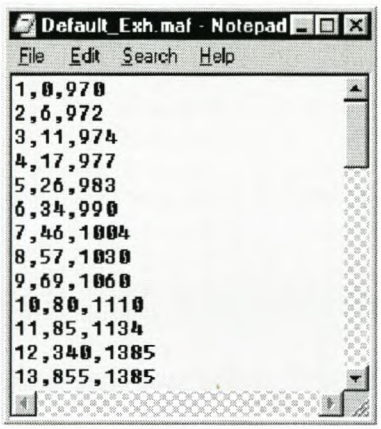

Figure 12: **Exhaust manifold area vs. length**

The next information the program will need is the exhaust back pressure and temperature boundary data. This information is given to the program as an input file, *.exh (Figure 11). The pressure and temperature data is given at each engine speed. This information can be obtained from engine tests or just using experience and other similar engine data. The back pressure of the exhaust system has a big influence on the gas flow through the engine and should therefore be obtained as early as possible in the design process of an engine or its manifolds.

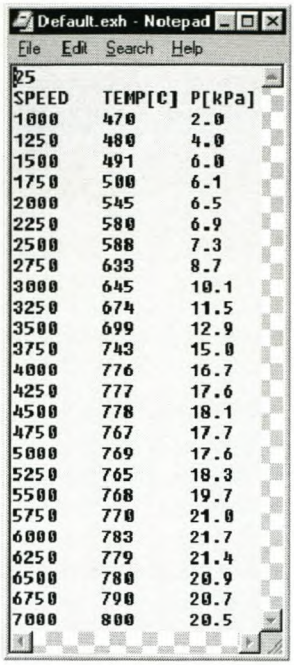

Figure 13: **Exhaust gas temperature and pressure**

The grid size information and velocities at the exhaust valve that will ensure smooth transition between forward and reverse flow, will not be discussed again for the exhaust. The same principles as discussed for the inlet valve, apply at the exhaust valve. It is a bit easier though, because of the larger pressure differences at the exhaust valve between the exhaust and the cylinder.

All the camshaft information can be entered in the **Cams** edit tab (Figure 12). The inlet and exhaust valve lift profiles are given to the program as an input file, *.cam. The camshaft model creates the data in this file. The model creates unit duration of zero to one and unit lift of zero to one. This makes it possible to fit the camshaft profile to any opening and closing angle or valve lift value.

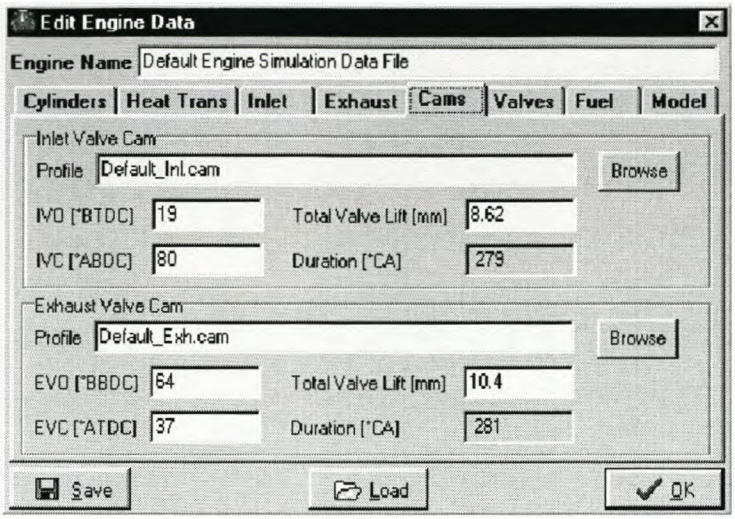

Figure 14: **Camshaft information**

The inlet and exhaust valve lift, opening and closing angles are all entered in this edit tab. The duration of each camshaft is then calculated from its opening and closing angles.

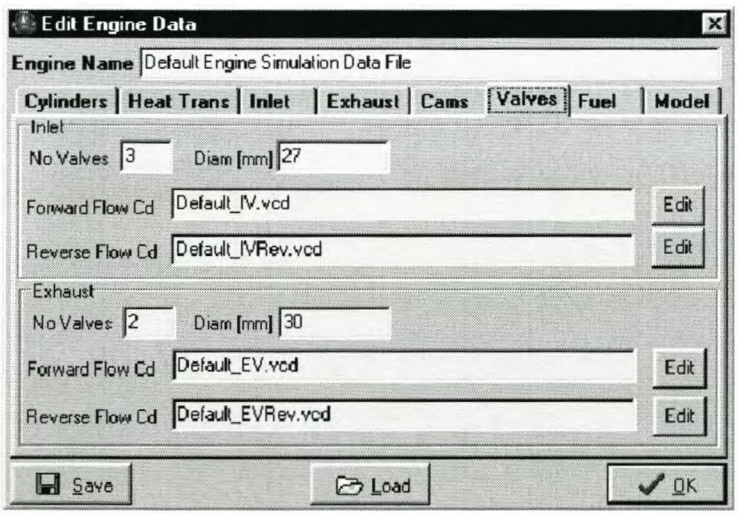

Figure 15: **Inlet and exhaust valve data**

Information on the valves of the engine is displayed in the **Valves** tab. In these edit boxes the following needs to be entered (Figure 13):

Number of inlet and exhaust valves for one cylinder

Diameter of a single inlet and exhaust valve

Input files containing the discharge coefficient (C_d) map data for each valve and for each flow direction, forward or reverse.

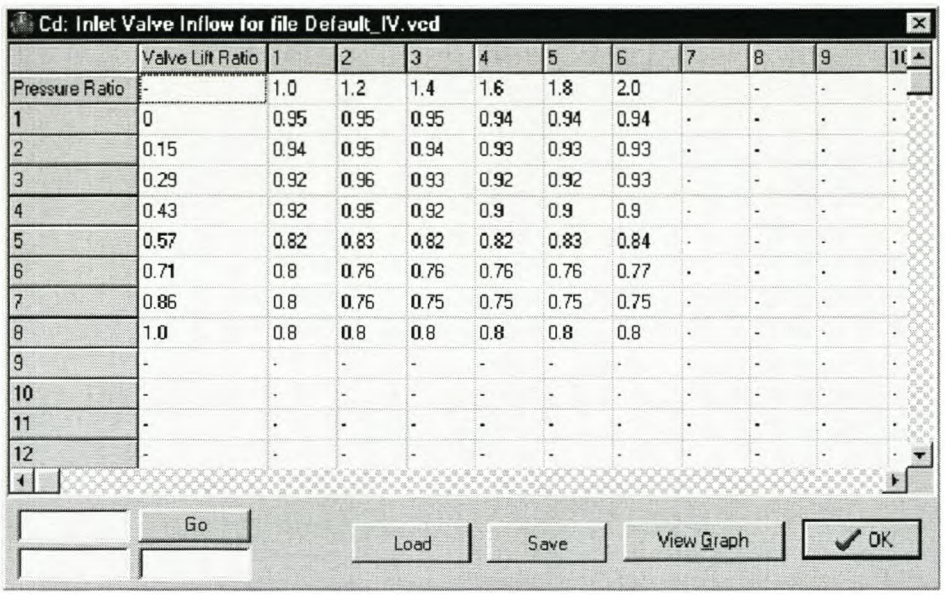

Pressure Ratio	Valve Lift Ratio	1	2	3	4	5	6	7	8	9	10
	-	1.0	1.2	1.4	1.6	1.8	2.0	-	-	-	-
1	0	0.95	0.95	0.95	0.94	0.94	0.94	-	-	-	-
2	0.15	0.94	0.95	0.94	0.93	0.93	0.93	-	-	-	-
3	0.29	0.92	0.96	0.93	0.92	0.92	0.93	-	-	-	-
4	0.43	0.92	0.95	0.92	0.9	0.9	0.9	-	-	-	-
5	0.57	0.82	0.83	0.82	0.82	0.83	0.84	-	-	-	-
6	0.71	0.8	0.76	0.76	0.76	0.76	0.77	-	-	-	-
7	0.86	0.8	0.76	0.75	0.75	0.75	0.75	-	-	-	-
8	1.0	0.8	0.8	0.8	0.8	0.8	0.8	-	-	-	-
9	-	-	-	-	-	-	-	-	-	-	-
10	-	-	-	-	-	-	-	-	-	-	-
11	-	-	-	-	-	-	-	-	-	-	-
12	-	-	-	-	-	-	-	-	-	-	-

Figure 16: **Discharge coefficient map**

Clicking *Edit* displays Figure 14, the C_d map data. The information is stored in a text file, *.vcd. The discharge coefficient is a function of the pressure ratio over the valve (row 1 in Figure 14) and the lift ratio (column 1 in Figure 14). These C_d values for valves are measured on a steady state flow bench as explained in Chapter 3 of this thesis. The C_d map can also be viewed as a 3-dimensional graph in Figure 15 (click *View Graph* button). These 3 dimensional maps are created for inlet and exhaust valves, and for forward and reverse flow.

The second last edit tab, **Fuel**, has data on the atmospheric conditions, oil and properties of the fuel (Figure 16). The atmospheric temperature and pressure must be entered in the top left corner. These values are important for the initial values in the manifolds. The viscosity of the oil is used to calculate engine friction.

The following fuel properties are needed:

Stoichiometric A/F Ratio is the amount of air units needed to burn one unit of fuel. Stoichiometric A/F Ratio is also known as the *Equivalence Ratio.*

Lambda is an indication of the amount of fuel or air left in the exhaust after combustion. In the model it is assumed that all the fuel and air were used for combustion. In a real engine it is quite common for an engine to run with excess fuel, lambda = 0.9, or it is said that the engine is running rich. An engine can also run lean with lambda > 1 and therefore with excess air.

Fuel Energy is a property of the fuel. Petrol usually has a value of 43 MJ/kg.

Fuel Temperature is usually the same as the atmospheric temperature, but can be different when running a physical engine.

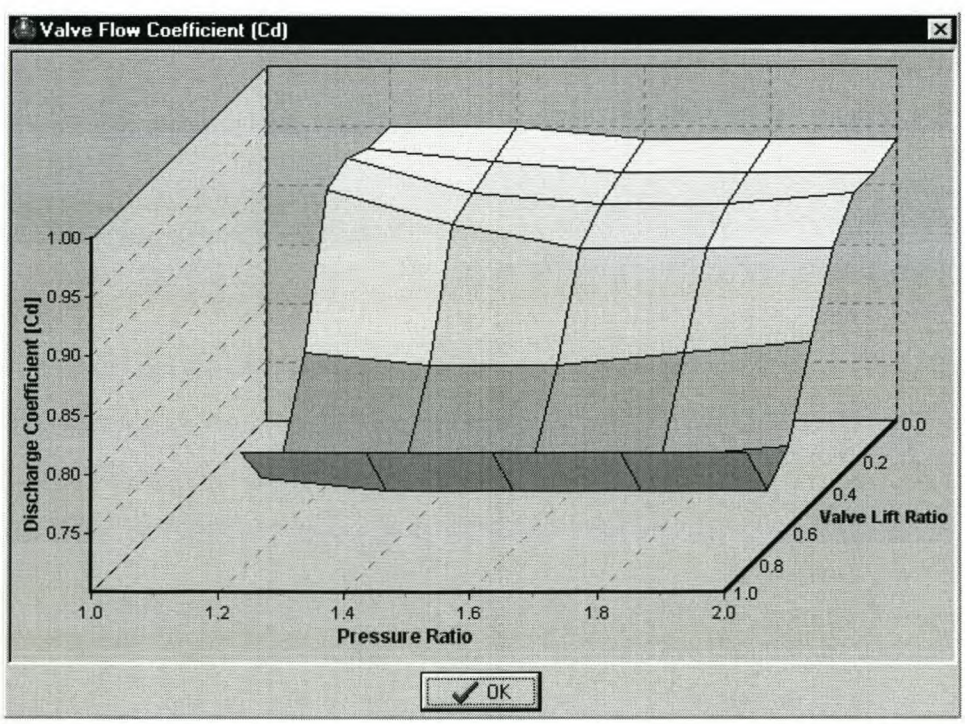

Figure 17: **Inlet valve C_d map graph**

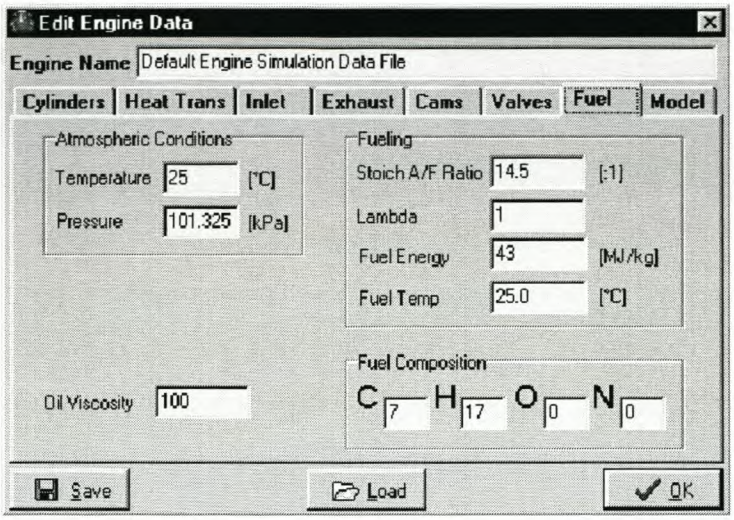

Figure 18: **Atmospheric, oil and fuel information**

At the moment the fuel composition is not used in the program. It is possible with the 2-zone combustion model though, to predict emissions and for this purpose the composition is necessary.

The last edit tab is called **Model** (Figure 17). Here the user can make changes to some of the general program options. The program is now only running with the 2-zone combustion model and the 1-zone model is therefore not available anymore. The integration method will default to the *Runga Kutte Felberg* method, because of the accuracy benefit, but it is also possible to run with the faster *Euler* integration method. These integration methods are only applicable to the combustion model. Manifold data can also be saved for each grid point at each crank angle degree. The performance data filename can also be changed.

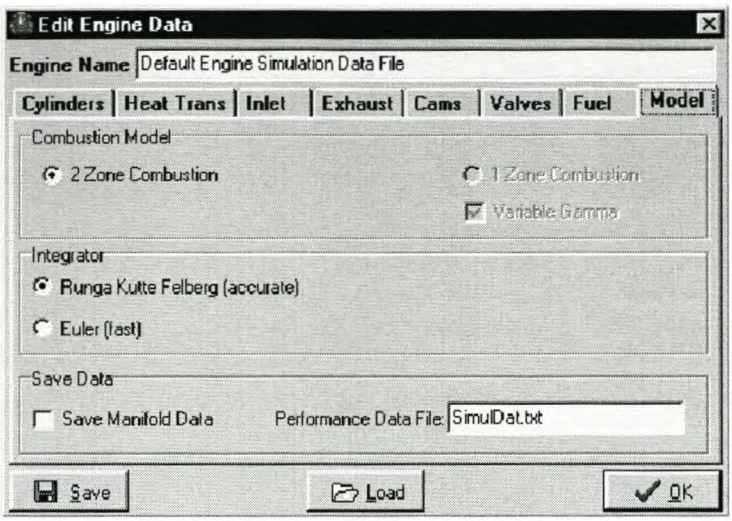

Figure 19: **General modelling information**

Clicking the *Save* button saves engine data files. Other engine files are loaded by clicking the *Load* button. Engine information can also be entered at the top of the *Edit Engine Data* box. Click the *OK* button to continue with the simulation.

6. Single Point Simulation

In this section it is explained how to run a single speed *Single Point Simulation*.

In the main menu, click **Run** and then **Single Point Simulation**. The user sees a small box appear on the display window (Figure 18). This small box gives the user the necessary information to run a single speed simulation. Enter the simulated engine speed as well as the number of iteration cycles (at least 5) and the maximum mass balance value. The program monitors the total iteration cycles and the mass balance values to check when to stop the simulation. Whichever criteria occur first, will stop the simulation. No more than 10 cycles are usually needed to get a reliable answer from the simulation.

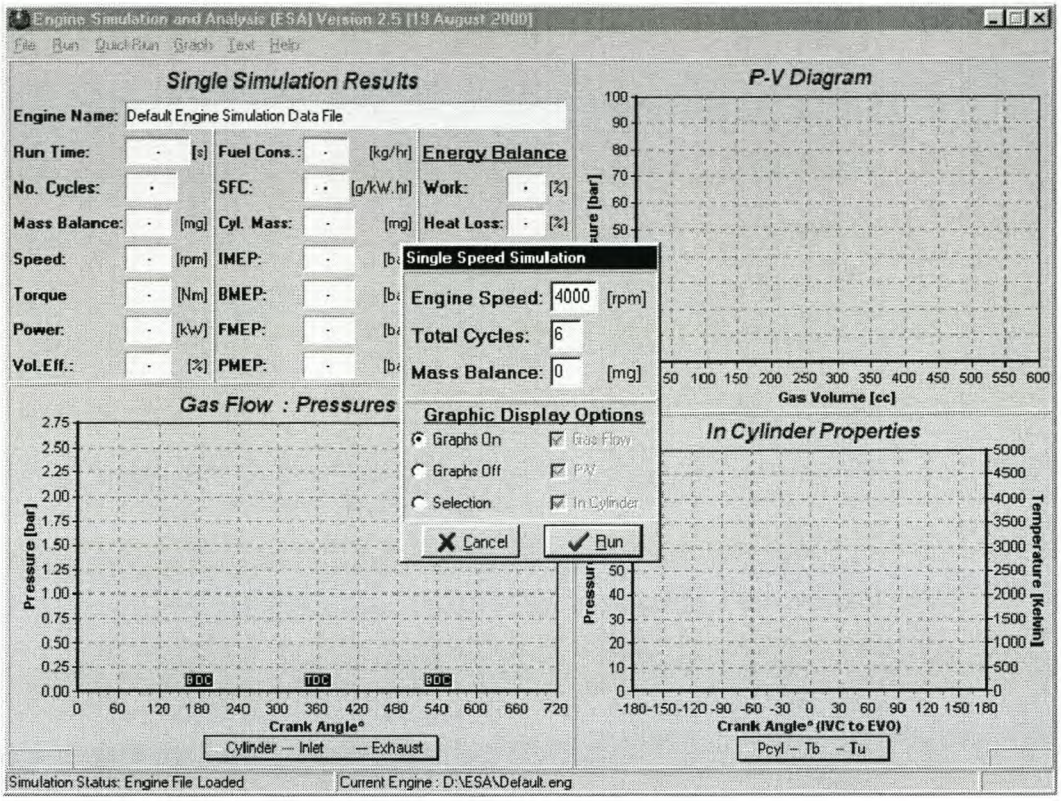

Figure 20: **Single speed simulation run**

During the runtime of the simulation the user have different options on what must be displayed on the three graphs of the main window. The user has three main options on what the graphs display during run-time (Figure 19).

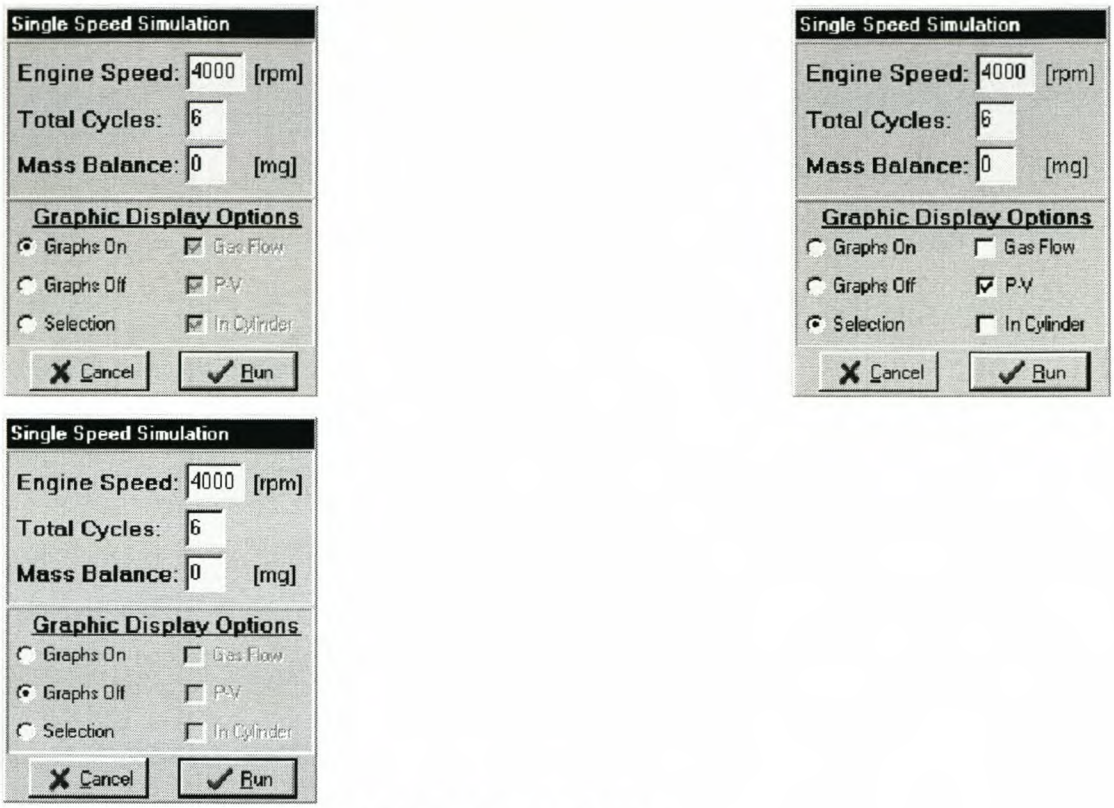

Figure 21: **Runtime graphic display options**

Checking the **Graphs On** option causes the simulation to show all the graphs displayed in the main window. Checking **Graphs Off** causes the simulation to show no online graphics. The **Graphs Off** simulations run considerably faster, because of the slow speeds of graphic cards compared to computer processors. The last graphic display option is **Selection**, where the user can specify which graphs to show.

Graphical options can also be changed while the simulation is running or at completion of the simulation. The user can access this option by either going to **Graph**, **Run-Time Graph Options** or by right clicking with the mouse on the display window and choosing **Options** (Figure 20), which displays Figure 21.

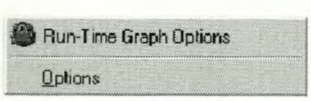

Figure 22: **Graph options**

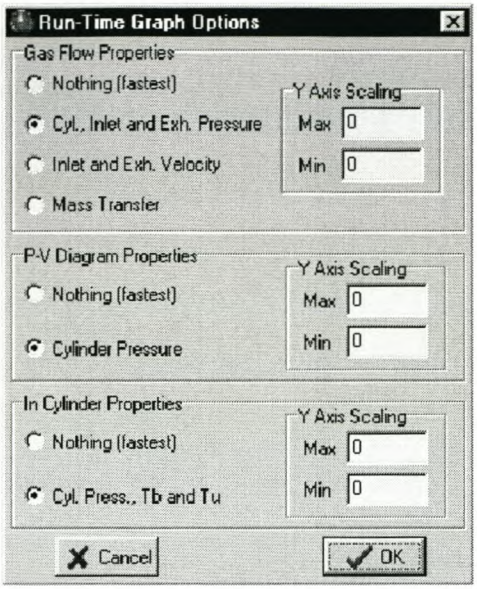

Figure 23: **Run-time graph options**

Using the edit boxes in Figure 21, the Y-axis scaling of the graphs can be changed. During the simulation the display window will look like Figure 22 (if the **Graphs On** option is taken). In the top left corner the *Run Time* will update online and the *No. Cycles* and *Mass Balance* will update after each cycle. The other display boxes will only update at the completion of the simulation.

At completion of the simulation, the results are displayed in the rest of the open edit boxes in the upper left corner. The three graphs will also update and display the final answer of the simulation, even if the **Graphs Off** option was selected during run-time .

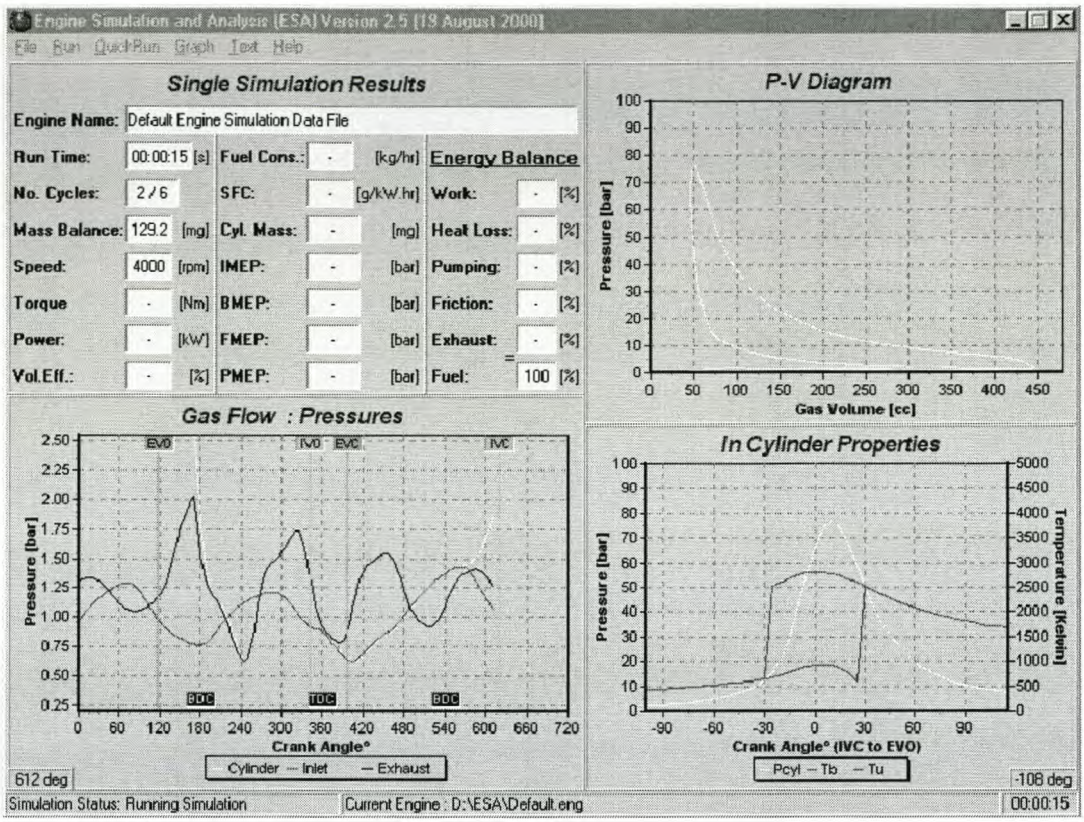

Figure 24: **Running simulation**

The display of the graph in the bottom left corner can be changed as discussed earlier. In Figure 21 the default view displays the pressure in the cylinder and at the inlet and exhaust valve. Figure 22 displays the velocity at the inlet and exhaust valve during exhaust blow-down, valve overlap and inlet induction. Figure 23 displays clearly the reverse flow at the exhaust valve and inlet valve. Figure 24 displays the mass transfer at the valves and the trapped mass in the cylinder. The graph also shows how the mass in the cylinder decreases (just after BDC, 540° CA) during reverse flow at the inlet valve. The graph also displays the change in mass from unburned mass to burnt mass. These three graphs can be viewed alternatively online during the simulation by using the **Run-Time Graph Options**.

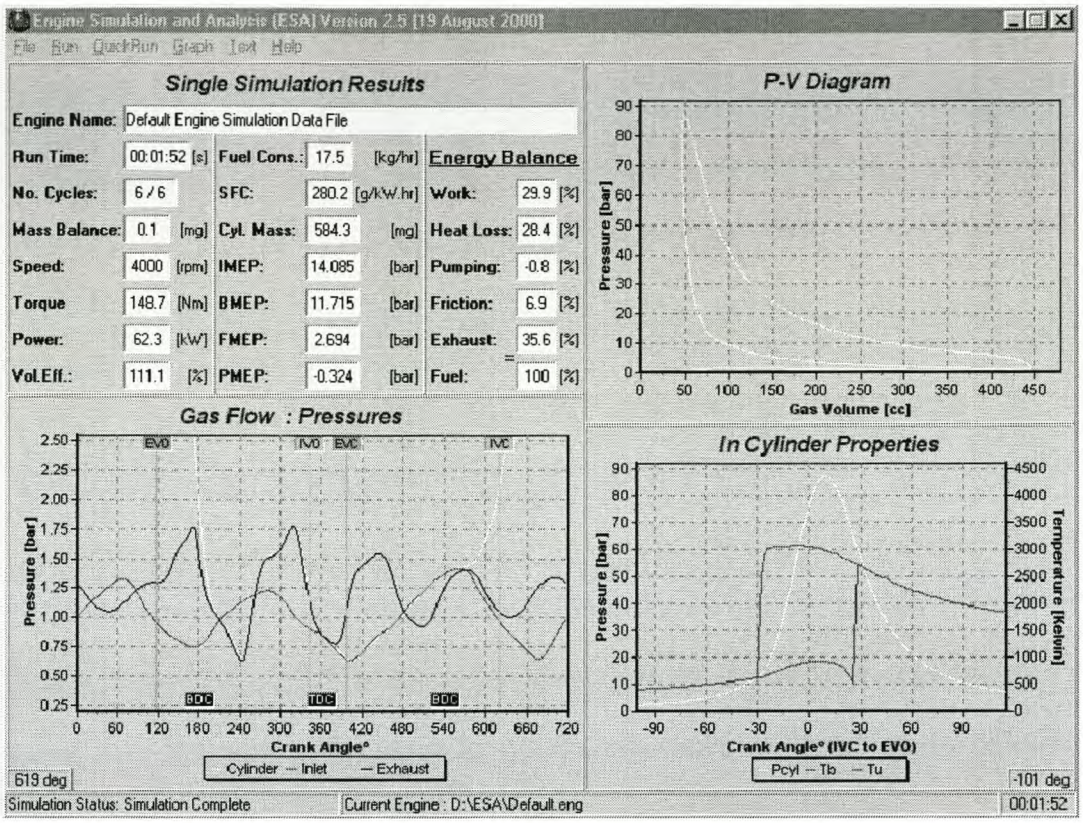

Figure 25: **Completed simulation**

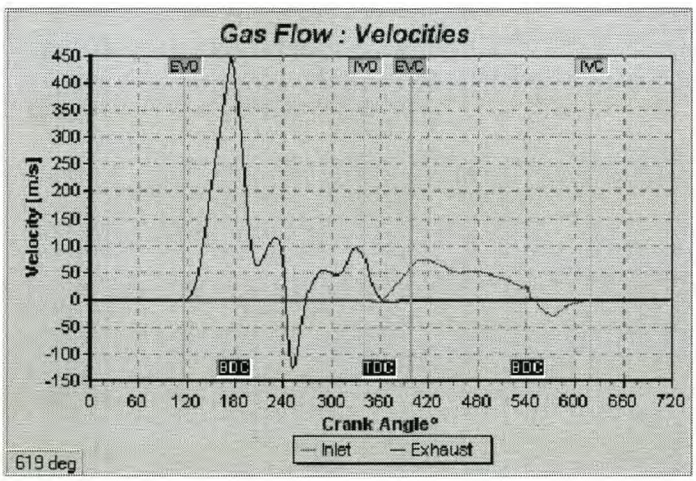

Figure 26: **Velocity at the inlet and exhaust valve**

The user can also zoom into the **PV-Diagram** in the top right corner (Figure 25) by clicking with the mouse on the graph and dragging a block, from left too right, around the desired view area. This enables the user to see for example the *Pumping Loop* of the engine (Figure 26). The original view can again be obtained by dragging a small block, from right too left, with the mouse.

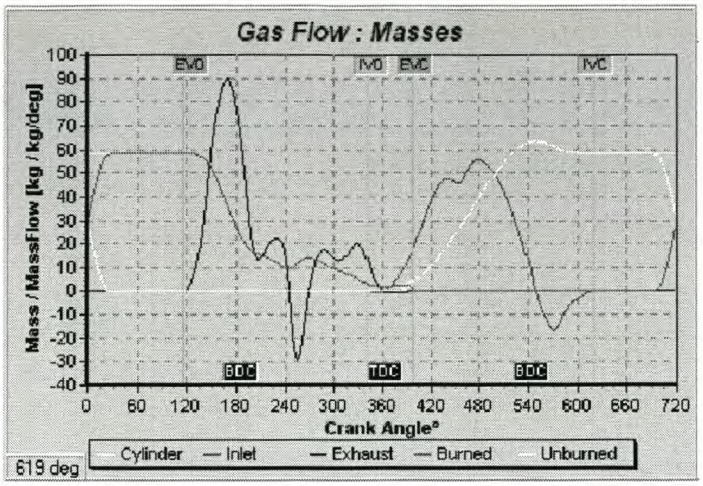

Figure 27: **Mass and mass flow**

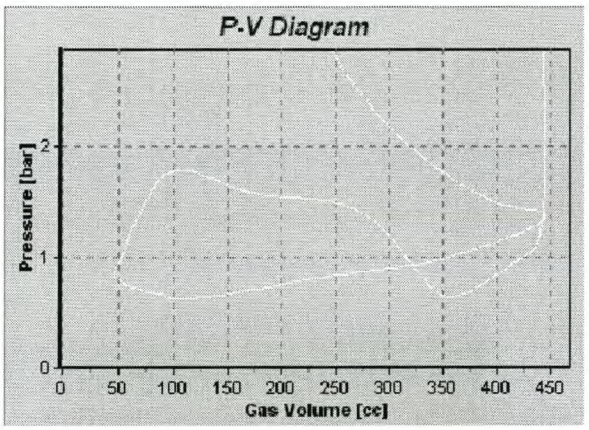

Figure 28: **Zoom into PV-diagram**

To view or save the results for each crank angle degree, click the **Text, PVT Trace** menu item. A table (Figure 27) is displayed with the state of each of the simulation variables for each 1° of crank angle. The full 720° (-360° to 360°) of the simulation (4-stroke) for the final cycle of the simulation is displayed. This data can be saved to a text file (default to *Lastcyc.txt*) using the **Save As** button and following the standard windows method of file saving. This saves a comma delimited text file (*.txt) with a user defined filename. This data can then be loaded into a spreadsheet program e.g. Excel, and the user can create graphs. It is important to note that this does not include manifold grid information. This information is available in separate text files.

Some of these results can also be displayed graphically using the **Graph** menu option. Below the **Run-Time Graph Options** menu item, three available graph types are listed:

Torque Curve displays the resulting torque, power and volumetric efficiency points. This graph is active when different speed points have been simulated with the **Multi Point Simulation**. More on this graph is shown in the next section on **Multi Point Simulation** runs.

Valve Opening displays the valve lift profile for the inlet and exhaust valve (Figure 28).

Energy Balance displays the heat loss, work done and pump work of the last simulation cycle (Figure 29).

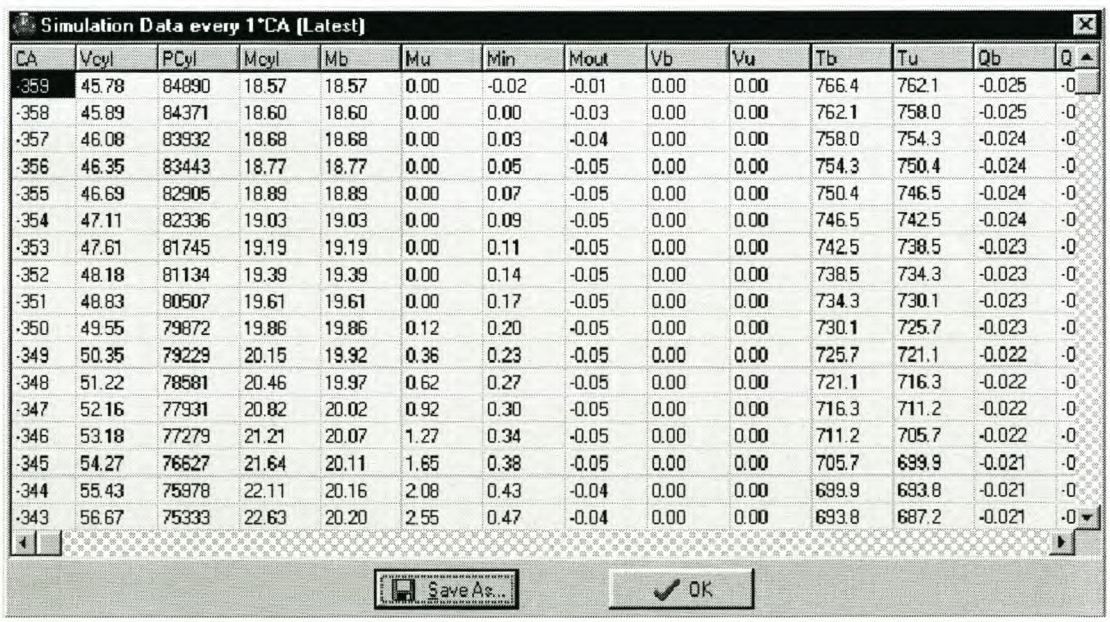

CA	Vcyl	PCyl	Mcyl	Mb	Mu	Min	Mout	Vb	Vu	Tb	Tu	Qb	Q
-359	45.78	84890	18.57	18.57	0.00	-0.02	-0.01	0.00	0.00	766.4	762.1	-0.025	-0
-358	45.89	84371	18.60	18.60	0.00	0.00	-0.03	0.00	0.00	762.1	758.0	-0.025	-0
-357	46.08	83932	18.68	18.68	0.00	0.03	-0.04	0.00	0.00	758.0	754.3	-0.024	-0
-356	46.35	83443	18.77	18.77	0.00	0.05	-0.05	0.00	0.00	754.3	750.4	-0.024	-0
-355	46.69	82905	18.89	18.89	0.00	0.07	-0.05	0.00	0.00	750.4	746.5	-0.024	-0
-354	47.11	82336	19.03	19.03	0.00	0.09	-0.05	0.00	0.00	746.5	742.5	-0.024	-0
-353	47.61	81745	19.19	19.19	0.00	0.11	-0.05	0.00	0.00	742.5	738.5	-0.023	-0
-352	48.18	81134	19.39	19.39	0.00	0.14	-0.05	0.00	0.00	738.5	734.3	-0.023	-0
-351	48.83	80507	19.61	19.61	0.00	0.17	-0.05	0.00	0.00	734.3	730.1	-0.023	-0
-350	49.55	79872	19.86	19.86	0.12	0.20	-0.05	0.00	0.00	730.1	725.7	-0.023	-0
-349	50.35	79229	20.15	19.92	0.36	0.23	-0.05	0.00	0.00	725.7	721.1	-0.022	-0
-348	51.22	78581	20.46	19.97	0.62	0.27	-0.05	0.00	0.00	721.1	716.3	-0.022	-0
-347	52.16	77931	20.82	20.02	0.92	0.30	-0.05	0.00	0.00	716.3	711.2	-0.022	-0
-346	53.18	77279	21.21	20.07	1.27	0.34	-0.05	0.00	0.00	711.2	705.7	-0.022	-0
-345	54.27	76627	21.64	20.11	1.65	0.38	-0.05	0.00	0.00	705.7	699.9	-0.021	-0
-344	55.43	75978	22.11	20.16	2.08	0.43	-0.04	0.00	0.00	699.9	693.8	-0.021	-0
-343	56.67	75333	22.63	20.20	2.55	0.47	-0.04	0.00	0.00	693.8	687.2	-0.021	-0

Figure 29: **Table with simulation results**

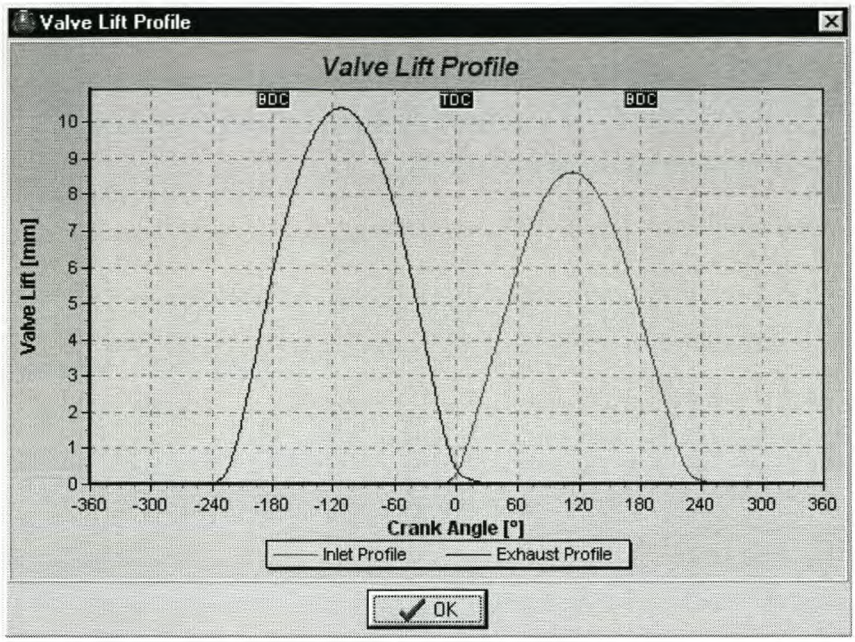

Figure 30: **Valve lift profile**

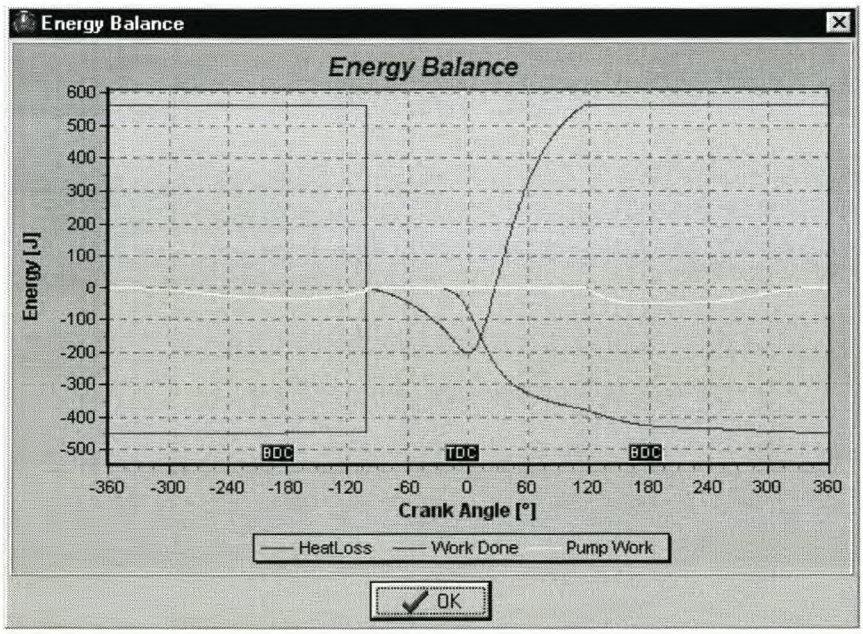

Figure 31: **Energy balance**

Single Point Simulation runs are very useful when the user is in the process of creating a reliable engine model. It gives the user a quick, but sufficient indication of engine performance and other characteristics to further fine-tune the engine model.

7. Multi Point Simulation

In this section it is described how to do a *Multi Point Simulation*. This type of simulation gives the user the opportunity to do for example a torque curve at different engine speeds, without running the engine speed points separately using the *Single Point Simulation* option.

In the main menu, click Run and then Multi Point Simulation. A user box appears on the display window (Figure 30). In the top left corner the engine file in use is displayed. In the table the following can be changed:

Speed can vary for a torque curve or stay constant when testing other engine parameters.

Iters is the amount of iterations or cycles to run for each simulation point.

IManfFile and *EManfFile* give the option to enter any *.maf text file for the inlet and exhaust manifold. This is used for running manifolds with different lengths and diameters.

ICamFile and *ECamFile* give the option to load any other camshaft lift profile by specifying a *.cam text file.

IVO, *IVC*, *EVO* and *EVC* can be changed to let the inlet and exhaust valve open or close at different crank angle degrees. It gives the user the opportunity to change the overlap between the inlet and exhaust valve as well as the duration of the inlet and exhaust valve.

IValveLift and *EValveLift* are used to change the maximum lift of the inlet and exhaust valve.

Spark°BTDC gives the user the opportunity to change the ignition timing of the engine at different engine speeds. It is therefore possible to run a torque curve at different engine speeds and with a specific set of ignition timings.

Burn Angle° gives the option to change the burn angle duration, in crank angle degrees, of the burning fuel.

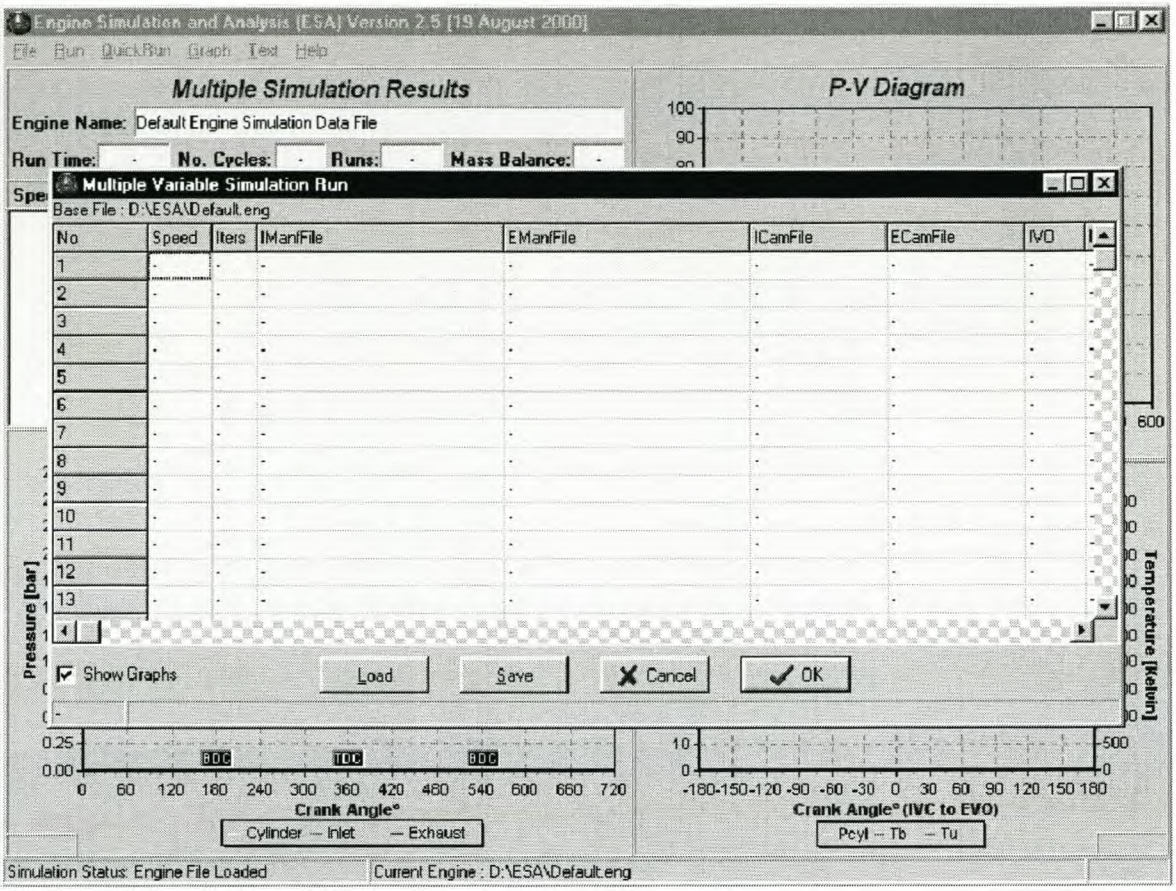

Figure 32: Multiple simulation runs

All this information can be stored, using the *Save* button, in a user defined text file *.msr. Saved text files can also be loaded by clicking the *Load* button.

The user now has the option to run the Multi Point Simulation. In Figure 30 a text file is displayed that was created to do a torque curve from a 1500 rpm to 6500 rpm in 250 rpm steps. The user also has the option to keep all the graphics on or to have it all off by making a selection in the bottom left corner. The simulation runs faster when the Show Graphs option is not selected.

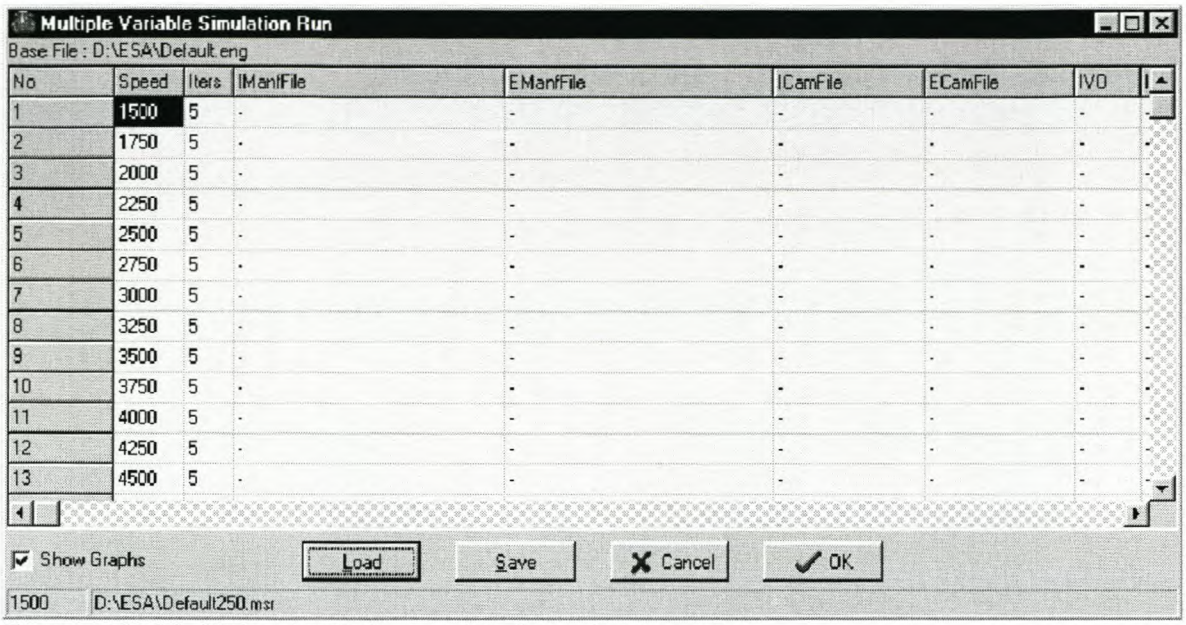

Figure 33: Multiple simulation setup for a torque curve

During run-time the user is able to see the following (Figure):

- Total run-time of the simulation.
- Number of cycles at the simulated point.
- Total number of simulated points and the current simulated point.
- Mass balance at the simulated point.

Performance results of the completed simulation points. The results that are displayed are only a few of the more important engine parameters. More extensive results are illustrated in the Text, PVT Trace menu table.

During the run-time of the program and at completion of the simulation, the same graph options, as for a single simulation point, are available. At the completion of the simulation, the displayed data is of the last cycle of the last simulation point. All other menu options as for a single simulation point are still available.

The user might be interested to see the torque curve graphically when running such a Multi Point Simulation. This graph is selected under the Run-Time Graph Options menu item, Torque Curve.

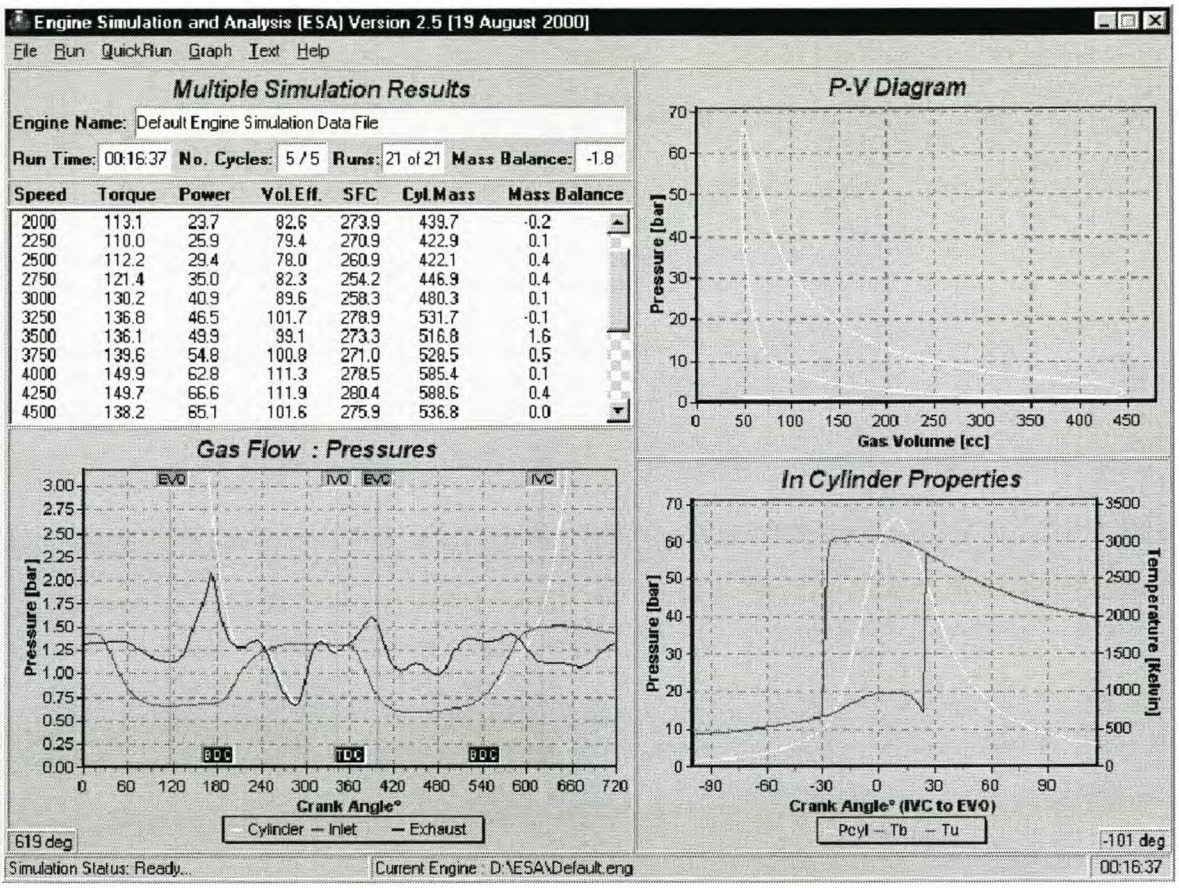

Figure 34: Completion of Multi Point Simulation

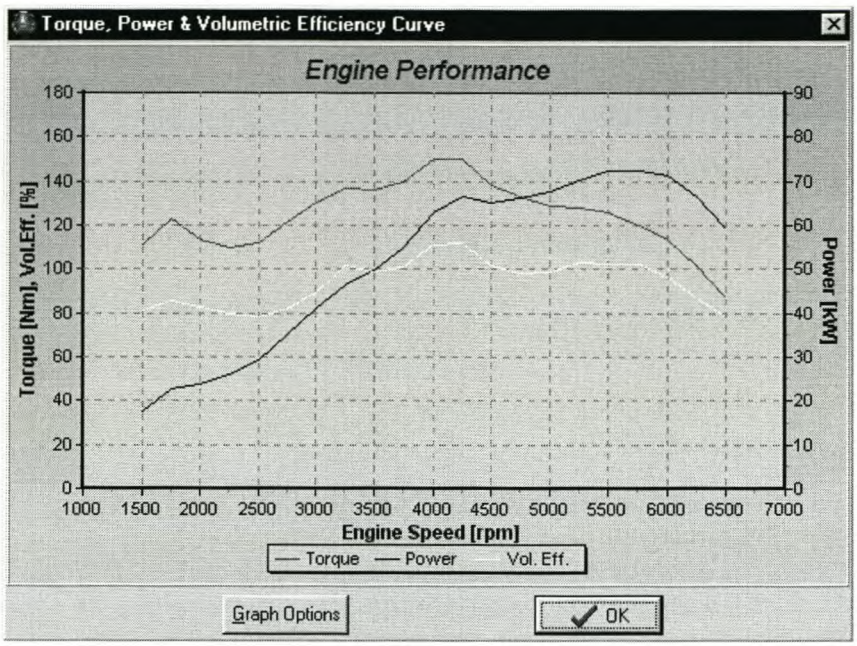

Figure 35: Torque, power and volumetric efficiency curve

Graph options for Figure 34 are available to the user by clicking the *Graph Options* button. Figure 35 then displays edit boxes to change the maximum and minimum values for the graph axes.

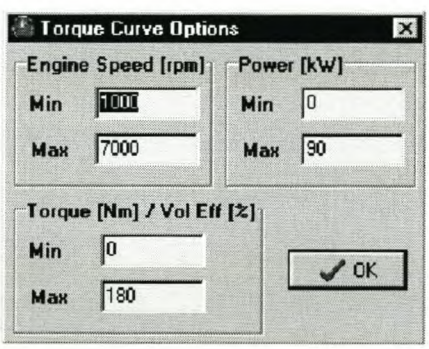

Figure 36: Torque graph options

The *Multi Point Simulation* option in the ESA program is one of the must powerful and convenient options. It allows the user to do up to 100 simulation points at a time and can therefore gather a substantial amount of data in a relative short space of time. An accurate engine data file will contribute to the accuracy of these results.

8. General Information

An online user manual is available by clicking the **Help**, **User Manual** menu item. More about this program and its creators are displayed in the **Help**, **About** menu item

1. Integrator

```
//~~~~~~~~~~~~~~~~~~~~~~~~~~~~~~~~~~~~~~~~~~~~~~~~~~~~~~~~~~~~~~~~~~~~~~~~~~~~~~~~//
// 5th Order Runga Kutta Fehlberg : Engine Simulation and Analysis (ESA)
//~~~~~~~~~~~~~~~~~~~~~~~~~~~~~~~~~~~~~~~~~~~~~~~~~~~~~~~~~~~~~~~~~~~~~~~~~~~~~~~~//

unit RKF5;

interface

uses classes;

const MaxN = 4; //can be anything

type
  yarray =array[1..MaxN] of Double;
  dxdyFunction = function (x : Double; y : yarray) : Double;


  TRKF = class
    NEqns : Integer;
    Integrator : Integer;
    x, dx : Double;
    y : yarray;
    fn : array [1..MaxN] of dxdyFunction;
    Procedure Integrate;
    Procedure IntegrateRKF;
    Procedure IntegrateEuler;
    Constructor Create;
    Destructor Destroy; Override;
  end; //TRKF

//~~~~~~~~~~~~~~~~~~~~~~~~~~~~~~~~~~~~~~~~~~~~~~~~~~~~~~~~~~~~~~~~~~~~~~~~~~~~~~~~//

implementation

Procedure TRKF.Integrate;
begin
 If Integrator = 0 then IntegrateRKF else IntegrateEuler;
end; //TRKF.Integrate

//~~~~~~~~~~~~~~~~~~~~~~~~~~~~~~~~~~~~~~~~~~~~~~~~~~~~~~~~~~~~~~~~~~~~~~~~~~~~~~~~//

procedure TRKF.IntegrateRKF;
var
 k : array [1..6] of yarray;
 ytemp : yarray;
 i, j : Integer;
begin
 for i := 1 to NEqns do
  k[1,i] := dx*fn[i](x, y);

 for i := 1 to NEqns do
   begin
     for j := 1 to NEqns do ytemp[j] := y[j] + k[1,j]/4;
     k[2,i] := dx*fn[i](x+dx/4, ytemp);
   end;

 for i := 1 to NEqns do
   begin
     for j := 1 to NEqns do ytemp[j] := y[j] + 3/32*k[1,j] + 9/32*k[2,j];
     k[3,i] := dx*fn[i](x+3/8*dx, ytemp);
   end;

 for i := 1 to NEqns do
   begin
     for j := 1 to NEqns do ytemp[j] := y[j] + 1932/2197*k[1,j]
                                            - 7200/2197*k[2,j]
                                            + 7296/2197*k[3,j];
     k[4,i] := dx*fn[i](x+12/13*dx, ytemp);
```

```
    end;

  for i := 1 to NEqns do
    begin
      for j := 1 to NEqns do ytemp[j] := y[j] + 439/216*k[1,j]
                                              - 8*k[2,j]
                                              + 3680/513*k[3,j]
                                              - 854/4104*k[4,j];
      k[5,i] := dx*fn[i](x+dx, ytemp);
    end;

  for i := 1 to NEqns do
    begin
      for j := 1 to NEqns do ytemp[j] := y[j] - 8/27*k[1,j] + 2*k[2,j]
                                  -3544/2565*k[3,j] + 1859/4104*k[4,j]
                                  -11/40*k[5,j];
      k[6,i] := dx*fn[i](x+dx/2, ytemp);
    end;

  for i := 1 to NEqns do
     y[i] := y[i] + (16/135*k[1,i] + 6656/12825*k[3,i] + 28561/56430*k[4,i]
                   - 9/50*k[5,i] + 2/55*k[6,i]);
end; //TRKF.IntegrateRKF

//~~~~~~~~~~~~~~~~~~~~~~~~~~~~~~~~~~~~~~~~~~~~~~~~~~~~~~~~~~~~~~~~~~~~~~~~~~~~//

procedure TRKF.IntegrateEuler; //this here for A quick Alternative
var
 k : array [1..6] of yarray;
 ytemp : yarray;
 i, j : Integer;
begin
 for i := 1 to NEqns do
  ytemp[i] := y[i] + dx*fn[i](x,y);
 y := ytemp;
end; //TRKF.IntegrateEuler

//~~~~~~~~~~~~~~~~~~~~~~~~~~~~~~~~~~~~~~~~~~~~~~~~~~~~~~~~~~~~~~~~~~~~~~~~~~~~//

Constructor TRKF.Create;
var
 i : Integer;
begin
 inherited Create;
 for i := 1 to MaxN do y[i] := 0;
 x := 0;
 dx := 0;
end; //TRKF.Create

//~~~~~~~~~~~~~~~~~~~~~~~~~~~~~~~~~~~~~~~~~~~~~~~~~~~~~~~~~~~~~~~~~~~~~~~~~~~~//

Destructor TRKF.Destroy;
begin
  Inherited Destroy;
end; //TRKF.Destroy

//~~~~~~~~~~~~~~~~~~~~~~~~~~~~~~~~~~~~~~~~~~~~~~~~~~~~~~~~~~~~~~~~~~~~~~~~~~~~//
end.
```

2. Main Code Cycle

```
procedure TEngine2z.Run;
var
 err : integer;
begin
  x := CA * Pi / 180;
  state := GetState(CA);

  if (state <> oldstate) and (NoZones = 1) then
   begin // State Initialization 1z
    OldState := State;
    if state = Compression then
      begin
        WWork := 0;   PWork := 0;
        WorkDone := 0;  HeatLoss := 0;
```

```
      FEnergy := 0;
      PMax := 0;     TMax := 0;
      UIMax := 0;    UEMax := 0;
      NewAirMass := TotalMInIV;
      TotalMInIv := 0; TotalMOutEV := 0;
      Cyl.Fuel.M := (1/Cyl.Fuel.Lambda) * NewAirMAss / (Cyl.Fuel.AFRatio+1);
      fn[1] := Zero;
      fn[2] := dpdtheta1z;
      fn[3] := Zero;
      fn[4] := Zero;
      PMax := 0;
      TMax := 0;
     end; //Compression Initialization
 end; //State Changes (1z)

if (state <> oldstate) and (NoZones = 2) then
 begin
  OldState := State;
  if Init2z = FALSE then
   begin
    Init2z := TRUE;
    Cyl.mu := cyl.mgas;
    Cyl.mb := 0;
   end; //2z Initialised
  Case State of
   Compression :
    begin
     fn[1] := Zero;
     fn[2] := dpdthetaUB;
     fn[3] := Zero;
     fn[4] := dTudThetaUB;
     Cyl.burnt.eqbm1.frozen := FALSE;
     WWork := 0;
     Pwork := 0;
     Heatloss := 0;
     PMax := 0;
     TMax := 0;
      FEnergy := 0;
     PMax := 0;     TMax := 0;
     UIMax := 0;    UEMax := 0;
     NewAirMass := TotalMinIV;
     TotalMInIv := 0; TotalMOutEV := 0;
     Cyl.Fuel.M := (1/Cyl.Fuel.Lambda) * NewAirMAss / (Cyl.Fuel.AFRatio+1);
    end;
   Combustion :
    begin
     fn[1] := dVbdThetaB;
     fn[2] := dPdThetaB;
     fn[3] := dTbdThetaB;
     fn[4] := dTudThetaB;
     y[3] := initialTb (Cyl.Pgas, Cyl.Tu);
    end;
   Expansion :
    begin
     fn[1] := Zero;
     fn[2] := dpdThetaBd;
     fn[3] := dTbdThetaBd;
     fn[4] := Zero;
     Cyl.burnt.eqbm1.frozen := FALSE;
     Cyl.mb := Cyl.mgas;
     Cyl.mu := 0;
     Cyl.Vb := cyl.Vgas;
     Cyl.Vu := 0;
    end;
   Exhaust : TotalMoutEV := 0;
   Overlap :
    begin
     Cyl.Burnt.eqbm1.Frozen := TRUE;
     fn[1] := Zero;
     fn[2] := dPdTheta1z;
     fn[3] := Zero;
     fn[4] := Zero;
   {  fn[1] := dVbdThetaGE;
     fn[2] := dPdThetaGE;
     fn[3] := dTbdThetaGE;
     fn[4] := dTudThetaGE;}
     MbOutInlet := 0;
```

```
      MuOutExhaust := 0;
     end; //Overlap Initialization
    Intake :
     begin
      Cyl.Tu := (Cyl.Mb*Cyl.Tb + Cyl.Mu*Plenum.tu)/Cyl.Mgas;
      Cyl.mu := Cyl.mgas;
      Cyl.Vb := 0;
      Cyl.Vu := Cyl.Vgas;

      fn[1] := Zero;
      fn[2] := dPdThetaUB;
      fn[3] := Zero;
      fn[4] := dTudThetaUB;

      {with Cyl do IncylEGR := mb/mgas;
      Cyl.Unburnt.changeParam (99,99,99,99,forcedEGR+IncylEGR,99);}
      Cyl.mb := 0;
     end; // Intake Initialization
  end; //Case
 end; // State Changes (2z)

 if (NoZones = 2) and (State = Combustion) then
  begin
   if Cyl.mb = 0 then
    begin
     fn[1] := Zero;
     fn[2] := dpdthetaUB;
     fn[3] := Zero;
     fn[4] := dTudThetaUB;
    end
   else
    begin
     fn[1] := dVbdThetaB;
     fn[2] := dPdThetaB;
     fn[3] := dTbdThetaB;
     fn[4] := dTudThetaB;
    end;
  end; //Combustion mass check

 Integrate;

 case state of
  combustion :
     Cyl.UpdateB (x, VCyl(x), DVCyldTheta(x), y[1], y[2], y[3], y[4]);
  Intake, Compression :
     Cyl.UpdateUB (VCyl(x), DVCyldTheta(x), y[1], y[2], y[4]);
  Expansion, Exhaust :
     Cyl.UpdateBD (VCyl(x), DVCyldTheta(x), y[1], y[2], y[3]);
  Overlap :
     Cyl.UpdateGE (VCyl(x), DVCyldTheta(x), y[1], y[2], y[3], y[4]);
 end; //case state

 If (NoZones = 1) then
  begin
   Cyl.mb := Cyl.mgas;
   Cyl.mu := Cyl.mgas;
   Cyl.Tb := Cyl.Pgas*Cyl.Vgas/Cyl.Rgas/Cyl.mgas;
   if Cyl.Tb < 273.15 then Cyl.Tb := 273.15;
   Cyl.Tu := Cyl.Tb;
   y[3] := Cyl.Tb;
   y[4] := Cyl.Tu;
  end; //if 1 zone

 Emmissions := Cyl.Burnt.Eqbm1.x;

//masses
 Manifold.Main_Prog(SaveManfData, NCycles,(x*180/pi)+360,tStep,Nrpm,
              dCA, Cyl.Pgas, Cyl.Tgas, IPt,EPt,VCyl(x),Cyl.mgas,
              Atm.Pgas, Atm.Tgas, Manifold.IV.FlowArea(CA),
              Manifold.EV.FlowArea(CA),
              MIn,MOut,dPMass, PInlet,PExhaust,UInlet,UExhaust);

Plenum.UpdateUB(0, DVCyldTheta(x), 0, PInlet, Manifold.InletT);

//Pressure Correction 1z
 if (NoZones = 1) or (state = overlap) then
  begin
```

```
   Cyl.Pgas := Cyl.Pgas + dPMass;
   y[2] := Cyl.Pgas;
  end;

//Mass Calculation
 Cyl.mgas := Cyl.mgas +Min -Mout;
 if Cyl.mgas < 0 then raise EEngineError.Create('Negative engine Gas Mass.');

if (NoZones = 1) then
 begin
  TotalMInIV := TotalMInIV + MIn;
  TotalMOutEV := TotalMOutEV + Mout;
 end
else
 begin
// 2 Zone masses , mass flow check
 case State of
  Exhaust :
   begin
    Cyl.mb := Cyl.mb - Mout;
    Cyl.dmoutdTheta := Mout/dx;
    TotalMOutEV := TotalMOutEV + Mout;
   end;
  Intake :
   begin
    Cyl.mu := Cyl.mu + Min;
    Cyl.dmindtheta := -Min/dx;
    TotalMInIV := TotalMInIV + MIn;
   end;
  Overlap :
   begin
    if (Mout > 0) and (Cyl.mb > 0) then //burnt gas out exhaust
     begin
       Cyl.Mb := Cyl.mb - mout;
       TotalMOutEV := TotalMOutEV + MOut;
     end;
    if (Mout > 0) and (Cyl.mb = 0) then //unburned gas out exhaust
     begin
      Cyl.Mu := Cyl.mu - mout;
      MuOutExhaust := MuOutExhaust + Mout;
     end;
    if (Mout < 0) and (MuOutExhaust = 0) then  //burnt gas in exhaust
     begin
      Cyl.Mb := Cyl.mb - mout;     //mout is negative - reversion
      TotalMOutEV := TotalMOutEV + MOut;
     end;
    if (Mout < 0) and (MuOutExhaust > 0) then  //unburned gas in exhaust
     begin
      Cyl.Mu := Cyl.mu - mout;     //mout is negative - reversion
      MuOutExhaust := MuOutExhaust + Mout;
     end;

    //correction if burnt portion <0 during previous calcs
    if Cyl.mb < 0 then
     begin
      Cyl.mu := Cyl.mu + Cyl.mb;
      MuOutExhaust := MuOutExhaust-Cyl.mb;
      Cyl.mb := 0;
     end;
    if MuOutExhaust < 0 then
     begin
      Cyl.mb := Cyl.mb - MuOutExhaust;
      MuOutExhaust := 0;
     end;

    if (Min > 0) and (MbOutInlet = 0) then  //unburned in Inlet
    begin
     Cyl.mu := Cyl.mu + min;
     TotalMInIV := TotalMInIV + MIn;
    end;
    if (Min > 0) and (MbOutInlet > 0) then   //burnt in inlet
     begin
      Cyl.mb := Cyl.mb + min;
      MbOutInlet := MbOutInlet - Min;
     end;
    If (Min < 0) and (Cyl.mu > 0) then  // unburned out inlet
     begin
```

```
      Cyl.mu := Cyl.mu + min;
      TotalMInIV := TotalMInIV + MIn;
     end;
    If (Min < 0) and (Cyl.mu = 0) then  // burnt out inlet
     begin
      Cyl.mb := Cyl.mb + min;
      MbOutInlet := MbOutInlet - Min;
     end;

    //correction if mu fell below zero during previous calcs
    If Cyl.mu < 0 then
     begin
      Cyl.mb := Cyl.mb + Cyl.Mu;
      MbOutInlet := MbOutInlet-Cyl.mu;
      Cyl.mu := 0;
     end;
    If MbOutInlet < 0 then
     begin
      Cyl.mu := Cyl.mu - MbOutInlet;
      MbOutInlet := 0;
     end;

   Cyl.Tu := Cyl.Pgas*Cyl.Vgas/Cyl.Rgas/Cyl.mgas;
   y[3] := cyl.Tu;
   y[4] := cyl.Tu;
  end;
end; //case state
end;  //if NOT 1z

// Calculate Work
Case State of
 Combustion, Compression, Expansion : WWork := WWork + dx*dwdTheta(x,y);
 Overlap, Intake, Exhaust :  PWork := PWork - dx*dwdTheta(x,y);
end; //Case

//??#### 2Z Fuel Energy
FEnergy := FEnergy + Cyl.Fuel.M*Cyl.Fuel.Q*Cyl.dxdTheta(CA)*dx;

if Cyl.Pgas > PMax then PMax := Cyl.Pgas;
if Cyl.Tgas > TMax then TMax := Cyl.Tgas;

Qb := dQbdtheta(x,Y)*dx;
Qu := dQudTheta(x,y)*dx;
HeatLoss := HeatLoss + Qb + Qu;
```

(Page intentionally blank)

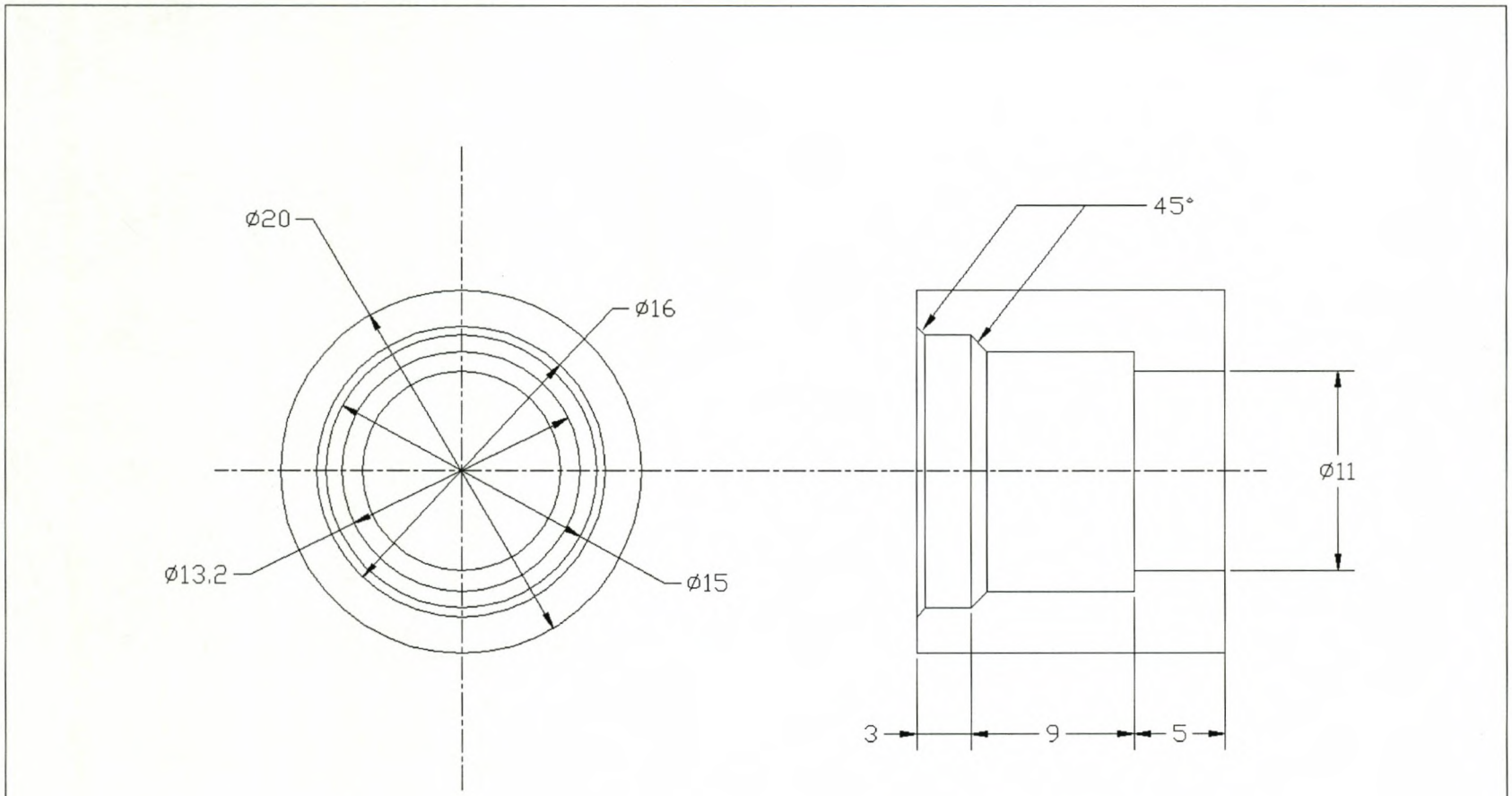

NOTES:
MAKE TO FIT INJECTOR AS SUPPLIED
MATERIAL MILD STEEL

TITLE: NISSAN NA20 INLET MANIFOLD : INJECTOR HOUSINGS	Unless otherwise stated, all Projections are Third Angle, all Linear dimensions are in millimeters and all Angular dimensions in decimal degrees. IF IN DOOUBT – PLEASE ASK		Dwg No: PNTNAMNF SCALE: DRAWN P WILLIAMS DATE : 03/05/98	Original Dwg Print Size A1

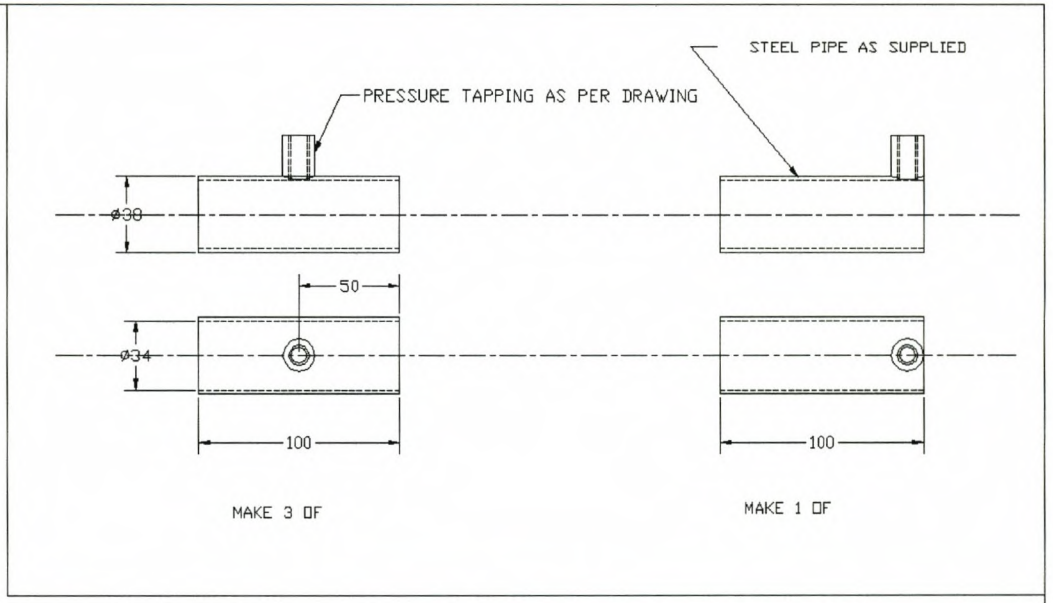

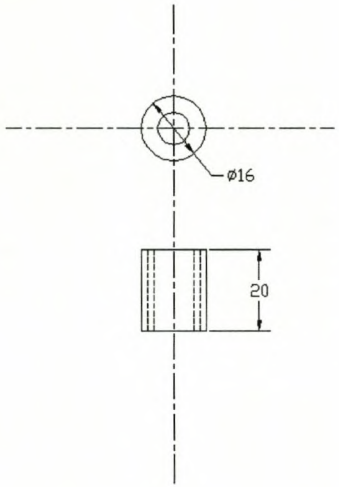

FITTING FOR 2200V1 PRESSURE PROBE

INTERNAL DIMENSIONS AS SUPPLIED DRAWING

MAKE 7 OF MILD STEEL

TITLE: NISSAN NA20 INLET MANIFOLD : INJECTOR HOUSINGS	Unless otherwise stated, all Projections are Third Angle, all Linear dimensions are in millimeters and all Angular dimensions in decimal degrees. IF IN DOOUBT – PLEASE ASK		Dwg No: PNTNAMNF SCALE: DRAWN P WILLIAMS DATE : 03/05/98 Original Dwg Print Size A1

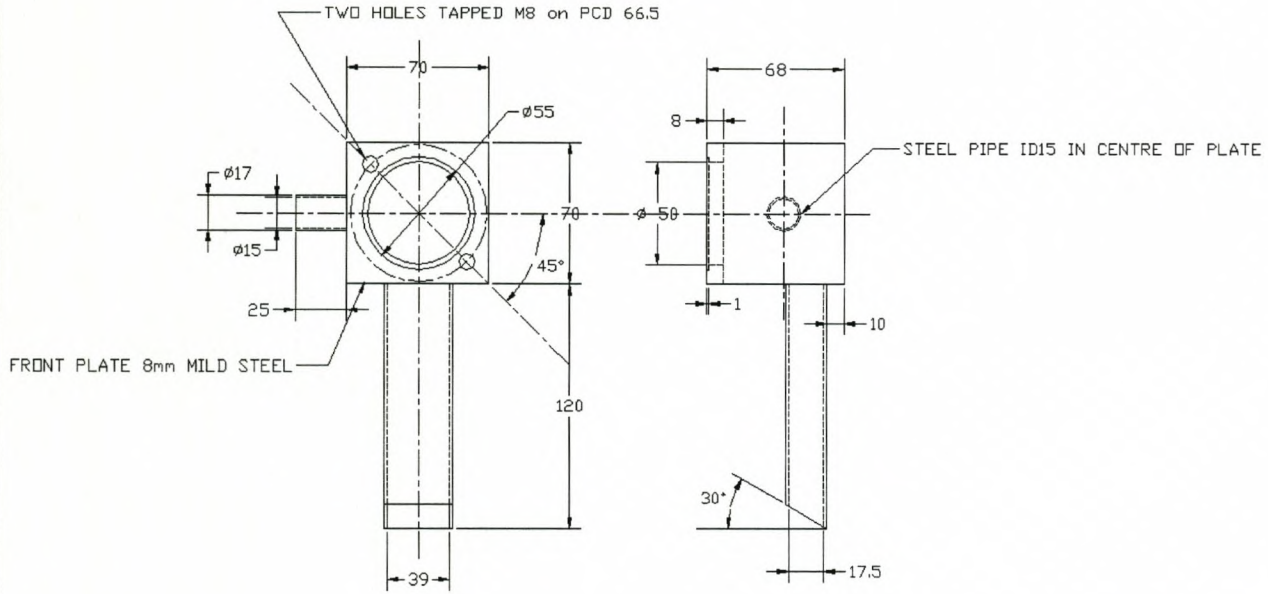

NOTES:
ALL JOINTS WELDED UNLESS OTHERWISE SPECIFIED
TO FIT THERMOSTAT AND HOUSING AS SUPPLIED
1.5mm STAINLESS PLATE EXCEPT WHERE INDICATED

TITLE NISSAN NA20 INLET MANIFOLD THERMOSTAT HOUSING	Unless otherwise stated, all Projections are Third Angle, all Linear dimensions are in millimeters and all Angular dimensions in decimal degrees. IF IN DOOUBT – PLEASE ASK		Dwg No: PNTNAMNF SCALE: DRAWN P WILLIAMS DATE : 03/05/98	Original Dwg Print Size A1

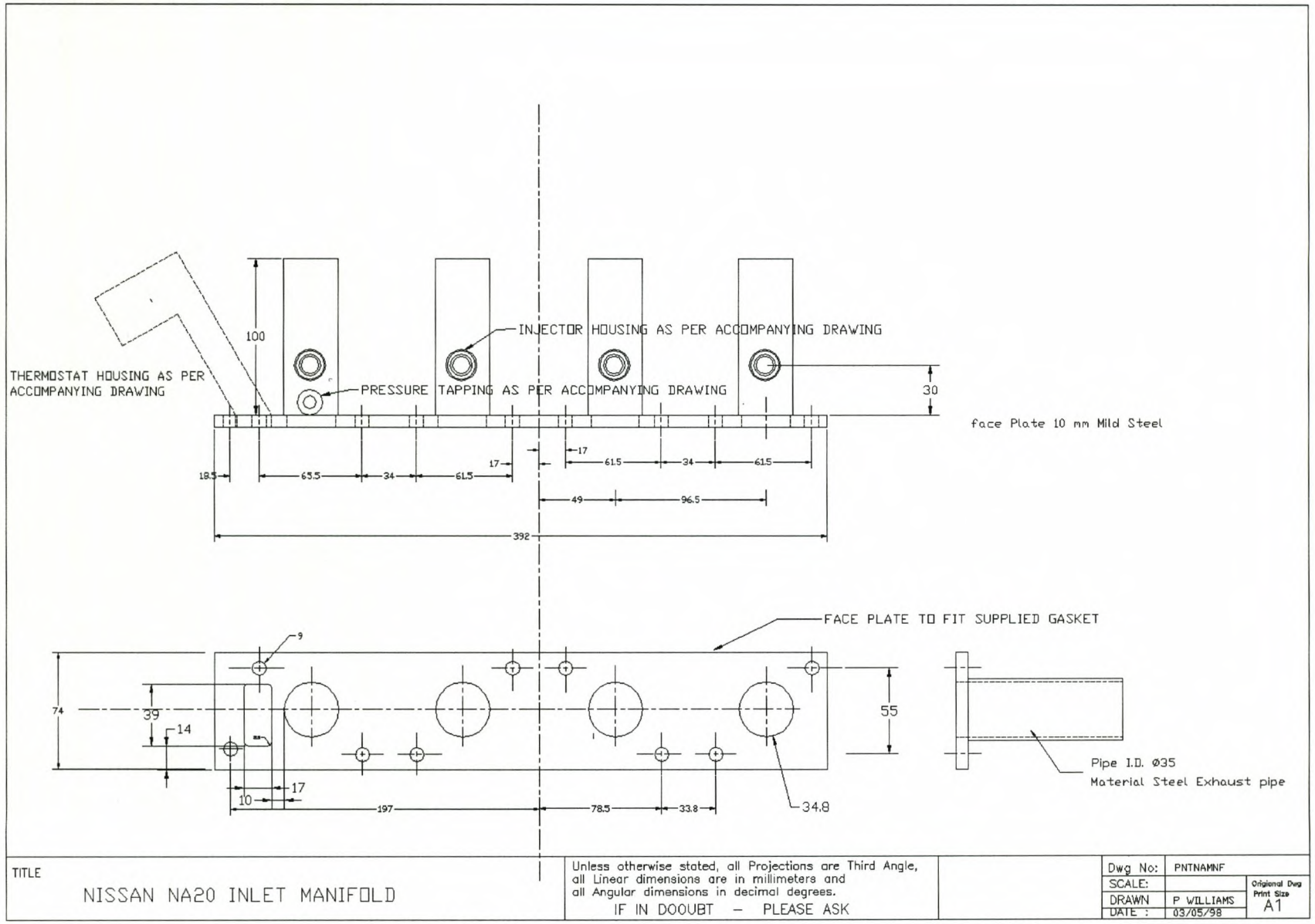
THERMOSTAT HOUSING AS PER ACCOMPANYING DRAWING
100
INJECTOR HOUSING AS PER ACCOMPANYING DRAWING
PRESSURE TAPPING AS PER ACCOMPANYING DRAWING
30
face Plate 10 mm Mild Steel
18.5
65.5
34
61.5
17
17
61.5
34
61.5
49
96.5
392
FACE PLATE TO FIT SUPPLIED GASKET
9
74
39
14
55
17
10
197
78.5
33.8
34.8
Pipe I.D. Ø35
Material Steel Exhaust pipe
TITLE
NISSAN NA20 INLET MANIFOLD
Unless otherwise stated, all Projections are Third Angle, all Linear dimensions are in millimeters and all Angular dimensions in decimal degrees.
IF IN DOOUBT – PLEASE ASK
Dwg No: PNTNAMNF
SCALE:
DRAWN P WILLIAMS
DATE : 03/05/98
Original Dwg Print Size A1

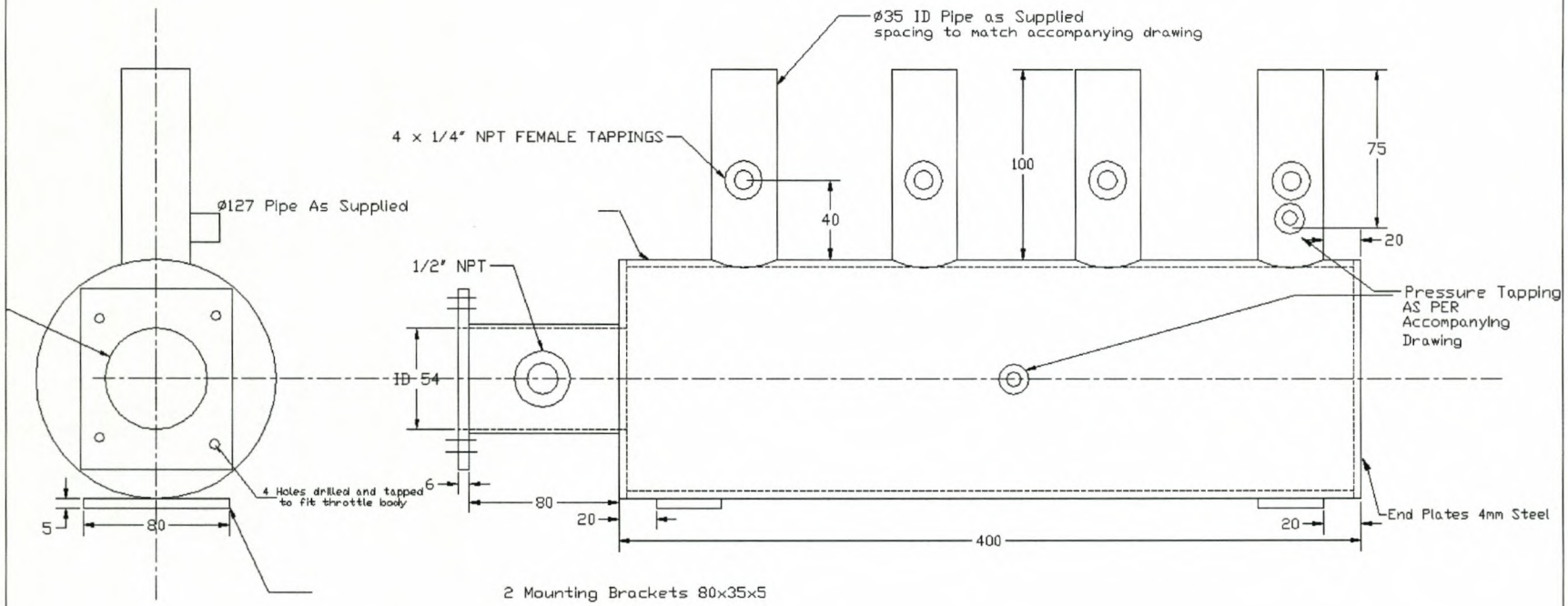

NOTES:

ALL JOINTS WELDED UNLESS OTHERWISE SPECIFIED

PLENUM PIPE AND Ø 35 PIPES SUPPLIED

THROTTLE BODY HOLES DRILLED AND TAPPED TO FIT AS SUPPLIED

TITLE: NISSAN NA20 INLET MANIFOLD PLENUM	Unless otherwise stated, all Projections are Third Angle, all Linear dimensions are in millimeters and all Angular dimensions in decimal degrees. IF IN DOOUBT – PLEASE ASK		Dwg No: PNTNAMNF SCALE: DRAWN P WILLIAMS DATE : 03/05/98 Original Dwg Print Size A1

(Page intentionally blank)

1. Introduction

ESACam is a supplementary program to the ESA Engine Simulation and Analysis package. The program performs a simple geometrical and dynamic analysis of the motion of an automotive poppet valve train resulting from an input cam profile. The result is a table of valve lift vs. cam angle that can be used as an input to the ESA program.

ESACam is a Microsoft Windows application written in Delphi V for the IBM PC. The program can be run under Windows 95, 98, NT4, Me and 2000.

2. Interface Overview

The primary interface of the program is shown in the figure below.

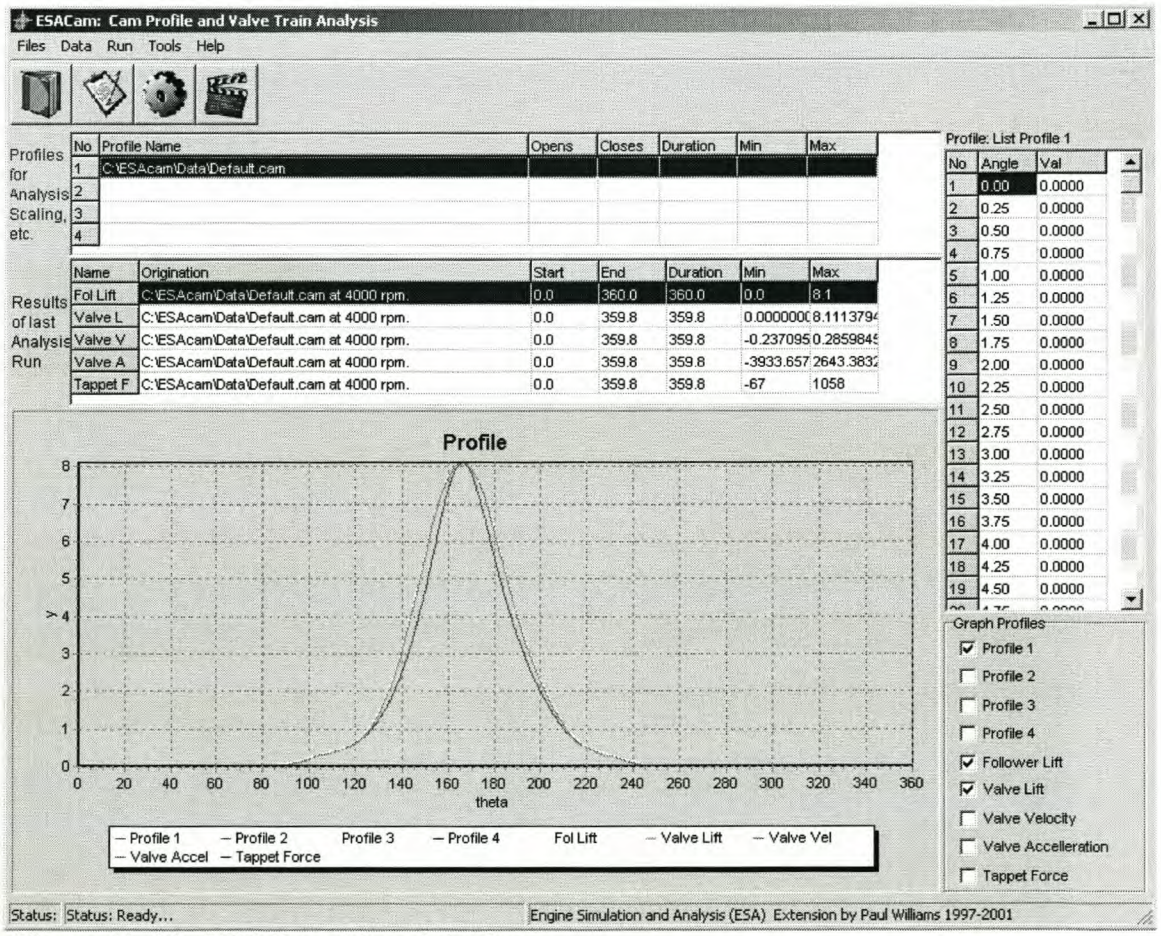

Figure F. 11. ESACam User Interface.

The interface consists of 4 main sections of the program window, a toolbar, a menu and a status bar. The sections are:

1. The cam profile list. This has 5 entries into which different input cam profiles can be loaded. The user can select different entries for analysis. Details of the profile are also shown.

2. The results list. This shows details of the last analysis. Follower lift and force and valve lift, velocities and acceleration are detailed here.

3. The profile table shows the tabulated data of the currently selected profile.

4. The graph region shows plots of the various input profiles and results vs. Cam angle.

The menu consists of various commands for loading, editing and saving cam and valve train data, as well as starting the various analyses.

The toolbar consists of 4 buttons for quick access to the primary program functions. Clicking on the first button activates the dialog windows for loading a cam profile and valve train data. The second button allows editing of the valve train data. The third starts the analysis and the last button closes the program.

3. Cam Data

Cam data can be loaded into the program using the menu(Data->Profile->Load) or using the toolbar. This data must be present in a text file with a .cam extension. The data consists of cam angle and cam eccentricity values arranged with one data set per line. The values must be tab delimited and run from 0 deg to 360 deg. A spacing of 0.25 cam degrees is preferred for accuracy. No empty lines should be present in the file. If data to be loaded is correct, the data will appear in the profile table.

4. Valve Train Data

Valve train data can be loaded, edited and saved using the Valve Train Settings Dialog. This can be activated from the Menu (Data->Valve Train-> Edit) or by the second button on the toolbar. The dialog is shown below.

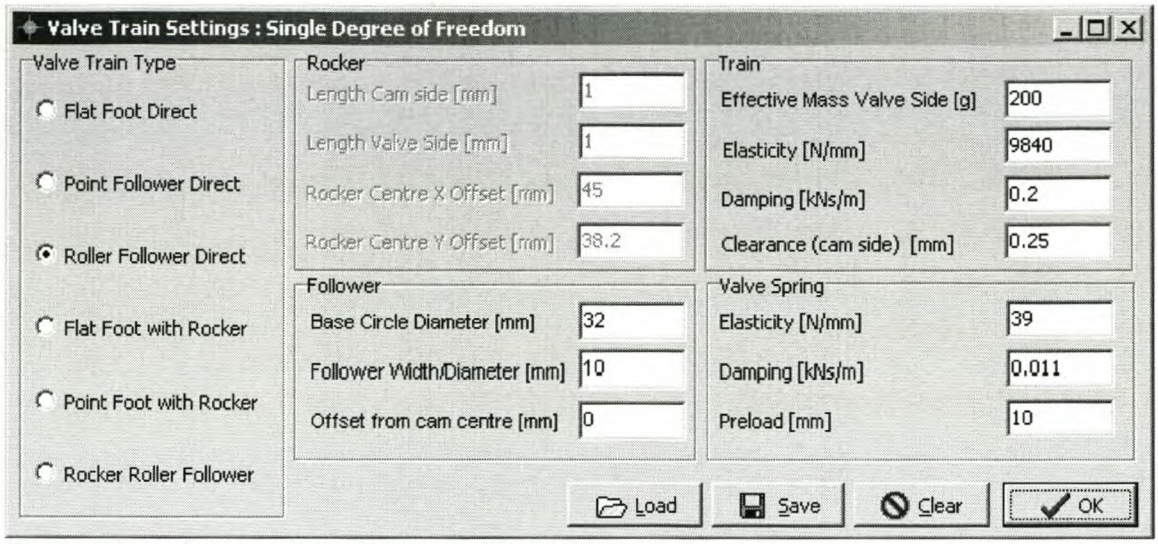

Figure F.12. Valve Train Settings Dialog.

The following settings and data must be entered:

1. Valve Train Type: The valve train type can be selected from the list.

2. Rocker Data: If a valve train type with a rocker is selected, the rocker data must be entered. This consists of the lengths of the two arms of the rocker, as well as the distance from the cam centre axis to the axis of rotation of the rocker.

3. Follower Data: The cam profile base circle diameter as well as the follower width (or diameter for a roller follower) must be entered. If the axis of motion of the follower does not cross the centreline of the cam, this offset must also be entered.

4. Valve Train Data: This consists of the effective mass, elasticity and damping of the valve train. The user must ensure that these values are based on lumped effective values on the valve side of the follower system. One third of the valve spring mass must also be included in the lumped mass. If there is any clearance in the system that must be taken up by the cam profile before valve train motion commences, this must be given under “clearance”.

5. Valve Spring Data: The valve spring rate and damping data, including any pre-loading of the spring must be given.

The data can be entered, loaded and saved to files of the user's choice from the dialog.

5. A Quick Tutorial

This quick tutorial serves to demonstrate the basic task of loading a cam profile and valve train data, running a simulation and saving the resulting valve profile:

1. Click on the "Load Files" toolbar button. A dialog appears requesting a cam profile. Click on the "Default.cam" file and click OK. A second dialog appears requesting valve train data. Click on the "Default.vts" file and click OK. The data should appear on the main interface and the graph of the profile should be drawn. Your screen should look identical to the following figure:

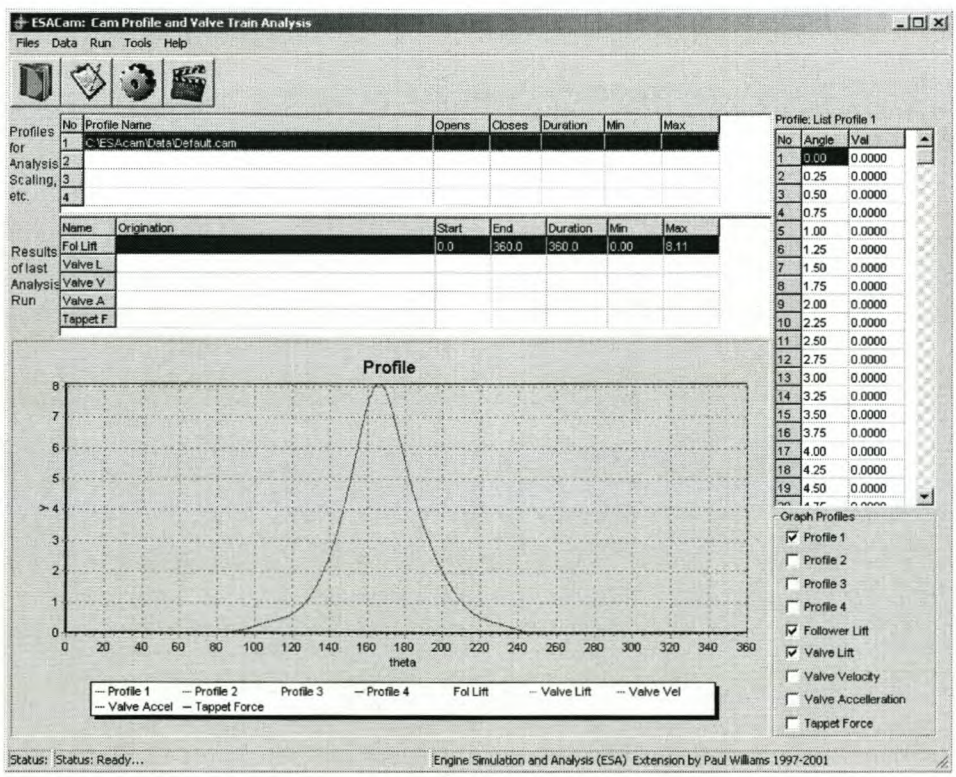

Figure F.13. Display after loading default data.

2. The valve train data can now be edited by clicking the second toolbar button. Refer to section 4 for more details.

3. Click on the Run analysis button. The Analysis Settings dialog appears. Here the user must enter the engine speed at which the analysis must take place, as well as the coefficients for the numerical analysis.

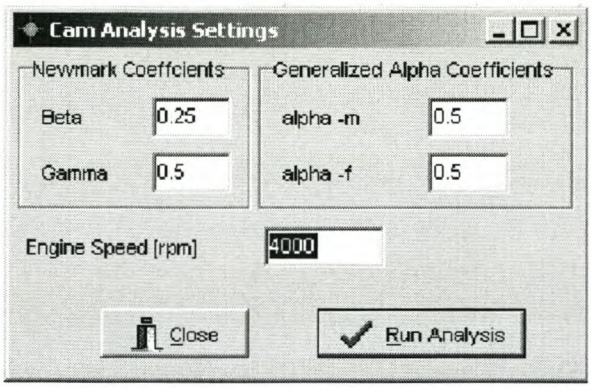

Figure F.14. Analysis Settings Dialog.

4. Click Run Analysis. Another dialog appears showing the progress of the analysis. When the analysis is complete, the result data will be displayed as in figure F.1.

5. To save the resulting valve lift profile – select this profile from the results table. Click again on it using the right mouse button and select save. The program will request a filename and the data will then be saved in the same format as the cam profile. This must be scaled to a unit profile (see later section) for use in the ESACam program.

6. Click Exit to close the program.

6. Additional Functions

The program has the following additional functions:

1. Cam profile viewing: Choose Tools->Profile->XY View for a view of the cam profile on the base circle.

2. Profile Scaling. Select a profile and click Tools->Profile->Scale. This allows you to scale a profile into unit form. This unit profile can be loaded into ESA, which then scales it to the correct angles and maximum lift.

3. Profile Searching: Click Tools->Profile->Find Point to find the exact profile lift (eccentricity) at a given cam angle.

4. Profile Smoothing: Click Tools->Profile->Smooth to initiate the built in profile smoother. This will convert your measured data into profile data ready for analysis.

APPENDIX E: DERIVATION BY BELL (1998) OF THE TWO-ZONE HEAT RELEASE FORMULAS GIVEN *BY KRIEGER AND BORMAN, 1966*

This derivation by Bell(1998) is included here as his work has not yet been published. The differences between symbols used in this study, and those used by Bell should be noted.

The following is a derivation of the equations presented by Kreiger and Borman [i] for a two-zone, mass transfer based combustion analysis model suitable for spark-ignition engine analyses.

Consider the schematic of an engine cylinder while combustion is occurring in an infinitely thin flame separating the burned zone from the unburned zone, as in Figure E-1.

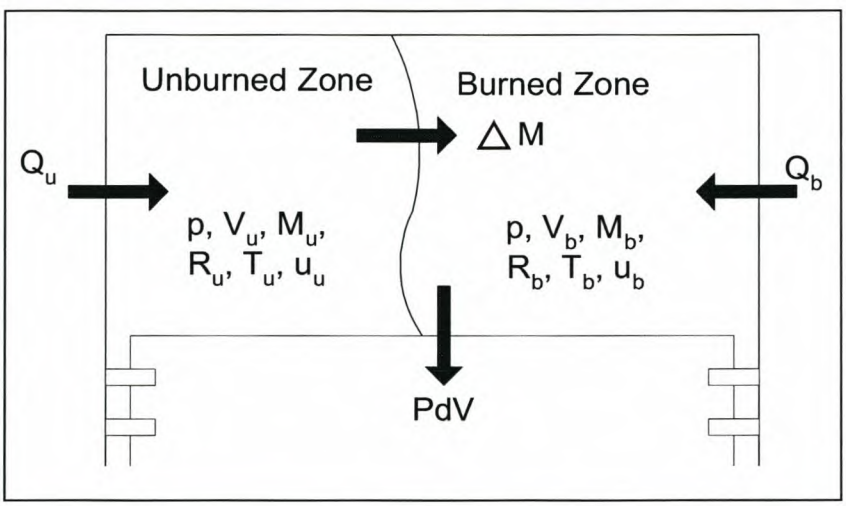

Figure E-1 Schematic of the two-zone, mass transfer based combustion analysis model.

Assumptions:

1. Pressure, p, in the burned and unburned zones is equal
2. The individual zones are in thermal equilibrium (there are no temperature gradients within the zones), this assumption leads to a "fully mixed model"
3. There is no heat transfer between the burned and unburned zones
4. No chemical reactions take place in the unburned zone (zone is said to be frozen)

   i.e. $\frac{\partial x}{\partial \mathrm{T}} = \frac{\partial x}{\partial \mathrm{p}} = 0 \Rightarrow \frac{\partial M}{\partial \mathrm{T}} = \frac{\partial R}{\partial \mathrm{T}} = \frac{\partial M}{\partial \mathrm{p}} = \frac{\partial R}{\partial \mathrm{p}} = \frac{\partial u}{\partial \mathrm{p}} = 0$ ..... Eqn E-1

5. The flame has zero volume or mass

   i.e. the total cylinder volume and mass is taken up by the burned and unburned volumes

and masses only

$\therefore V = V_u + V_b$ and $m = m_u + m_b$ ..... Eqn E-2

6. From Eqn E-2 we can write

$m_{u1} - \Delta m = m_{u2}$ and $m_{b1} + \Delta m = m_{b2}$ which leads to $-\dot{m}_u = \dot{m}_b$ ..... Eqn E-3

The ideal gas law states

$pV = mRT$ ..... Eqn E-4

from which we can write

$$p = \frac{m_b R_b T_b}{V_b} = \frac{m_u R_u T_u}{V_u} \quad \text{..... Eqn E-5}$$

Differentiating Eqn E-4 gives

$pdV + Vdp = mRdT + mTdR + RTdm$ ..... Eqn E-6

Dividing by pV gives

$$\frac{dV}{V} + \frac{dp}{p} = \frac{mR}{pV}dT + \frac{mT}{pV}dR + \frac{RT}{pV}dm \quad \text{..... Eqn E-7}$$

Using Eqn E-4 gives

$$\frac{dV}{V} + \frac{dp}{p} = \frac{dT}{T} + \frac{dR}{R} + \frac{dm}{m} \quad \text{..... Eqn E-8}$$

Writing in reduced notation and applying to unburned and burned zones gives

$$\frac{\dot{p}}{p} = \frac{\dot{m}_b}{m_b} + \frac{\dot{R}_b}{R_b} + \frac{\dot{T}_b}{T_b} - \frac{\dot{V}_b}{V_b} = \frac{\dot{m}_u}{m_u} + \frac{\dot{R}_u}{R_u} + \frac{\dot{T}_u}{T_u} - \frac{\dot{V}_u}{V_u} \quad \text{..... Eqn E-9}$$

Writing the energy equation for the unburned zone gives

$$m_{u2}u_{u2} = m_{u1}u_{u1} - \Delta m h_u + Q_u - \int_1^2 pdV_u \quad \text{..... Eqn E-10}$$

$$m_{u2}u_{u2} - m_{u1}u_{u1} = -\Delta m h_u + Q_u - \int_1^2 pdV_u \quad \text{..... Eqn E-11}$$

writing in differential form

$$\dot{m_u u_u} = \dot{m}_u h_u + \dot{Q}_u - pdV_u \quad \text{..... Eqn E-12}$$

$$\dot{m}_u u_u + m_u \dot{u}_u = \dot{m}_u h_u + \dot{Q}_u - p\dot{V}_u \quad \text{..... Eqn E-13}$$

Similarly, writing the energy equation for the burned zone gives

$$m_{b2}u_{b2} = m_{b1}u_{b1} + \Delta m h_u + Q_b - \int_1^2 pdV_b \quad \text{..... Eqn E-14}$$

$$m_{b2}u_{b2} - m_{b1}u_{b1} = \Delta m h_u + Q_b - \int_1^2 pdV_b \quad \text{..... Eqn E-15}$$

writing in differential form

$$\dot{\overline{m_b u_b}} = \dot{m}_b h_u + \dot{Q}_b - pdV_b \quad \text{Eqn E-16}$$

$$\dot{m}_b u_b + m_b \dot{u}_b = \dot{m}_b h_u + \dot{Q}_b - p\dot{V}_b \quad \text{Eqn E-17}$$

Solving for $\dot{T}_u$:

From Eqn E-13 we can write

$$\dot{m}_u\left(u_u - h_u\right) + m_u\left(\frac{\partial u_u}{\partial \mathrm{T}_u}\dot{T}_u + \frac{\partial u_u}{\partial \mathrm{p}}\dot{p}\right) = \dot{Q}_u - p\dot{V}_u \quad \text{Eqn E-18}$$

but from Eqn E-1 this simplifies to

$$\dot{m}_u\left(u_u - h_u\right) + m_u\frac{\partial u_u}{\partial \mathrm{T}_u}\dot{T}_u = \dot{Q}_u - p\dot{V}_u \quad \text{Eqn E-19}$$

From the definition of enthalpy [ii] $h = u + RT \Rightarrow u - h = -RT$ Eqn E-20

$$-\dot{m}_u R_u T_u + m_u\frac{\partial u_u}{\partial \mathrm{T}_u}\dot{T}_u = \dot{Q}_u - p\dot{V}_u \quad \text{Eqn E-21}$$

$$\dot{m}_u R_u T_u - m_u\frac{\partial u_u}{\partial \mathrm{T}_u}\dot{T}_u = p\dot{V}_u - \dot{Q}_u \quad \text{Eqn E-22}$$

$$\dot{m}_u = m_u\frac{\partial u_u}{\partial \mathrm{T}_u}\frac{\dot{T}_u}{R_u T_u} + \frac{p\dot{V}_u}{R_u T_u} - \frac{\dot{Q}_u}{R_u T_u} \quad \text{Eqn E-23}$$

dividing by m_u

$$\frac{\dot{m}_u}{m_u} = \frac{\partial u_u}{\partial \mathrm{T}_u}\frac{\dot{T}_u}{R_u T_u} + \frac{p\dot{V}_u}{m_u R_u T_u} - \frac{\dot{Q}_u}{m_u R_u T_u} \quad \text{Eqn E-24}$$

From Eqn E-9 and Eqn E-1

$$\frac{\dot{p}}{p} = \frac{\dot{m}_u}{m_u} + \frac{\dot{T}_u}{T_u} - \frac{\dot{V}_u}{V_u} \quad \text{Eqn E-25}$$

Substituting Eqn E-24 into Eqn E-25

$$\frac{\dot{p}}{p} = \frac{\partial u_u}{\partial \mathrm{T}_u}\frac{\dot{T}_u}{R_u T_u} + \frac{p\dot{V}_u}{m_u R_u T_u} - \frac{\dot{Q}_u}{m_u R_u T_u} + \frac{\dot{T}_u}{T_u} - \frac{\dot{V}_u}{V_u} \quad \text{Eqn E-26}$$

$$\frac{\dot{T}_u}{T_u}\left(1 + \frac{\partial u_u}{\partial \mathrm{T}_u}\frac{\dot{T}_u}{R_u}\right) = \frac{\dot{p}}{p} - \frac{p\dot{V}_u}{m_u R_u T_u} + \frac{\dot{Q}_u}{m_u R_u T_u} + \frac{\dot{V}_u}{V_u} \quad \text{Eqn E-27}$$

However

$$\frac{\dot{V}_u}{V_u} - \frac{p\dot{V}_u}{m_u R_u T_u} = \frac{\dot{V}_u}{V_u}\left(1 - \frac{pV_u}{m_u R_u T_u}\right) = 0 \quad \text{Eqn E-28}$$

Therefore Eqn E-27 becomes

$$\frac{\dot{T}_u}{T_u}\left(1+\frac{\partial u_u}{\partial \mathrm{T}_u}\frac{\dot{T}_u}{R_u}\right)=\frac{\dot{p}}{p}+\frac{\dot{Q}_u}{m_u R_u T_u} \quad \text{Eqn E-29}$$

$$\dot{T}_u\left(1+\frac{\partial u_u}{\partial \mathrm{T}_u}\frac{\dot{T}_u}{R_u}\right)=T_u\frac{\dot{p}}{p}+\frac{\dot{Q}_u}{m_u R_u} \quad \text{Eqn E-30}$$

$$\dot{T}_u=\left(\frac{T_u\dfrac{\dot{p}}{p}+\dfrac{\dot{Q}_u}{m_u R_u}}{1+\dfrac{\partial u_u}{\partial \mathrm{T}_u}\dfrac{\dot{T}_u}{R_u}}\right) \quad \text{Eqn E-31}$$

Solving for $\dot{m}_b$:

From Eqn E-17

$$\dot{m}_b\left(u_b-h_u\right)+m_b\left(\frac{\partial u_b}{\partial \mathrm{T}_b}\dot{T}_b+\frac{\partial u_b}{\partial \mathrm{p}}\dot{p}\right)=\dot{Q}_b-p\dot{V}_b \quad \text{Eqn E-32}$$

$$\dot{m}_b\left(u_b-\left(u_u+R_u T_u\right)\right)=\dot{Q}_b-p\dot{V}_b-m_b\left(\frac{\partial u_b}{\partial \mathrm{T}_b}\dot{T}_b+\frac{\partial u_b}{\partial \mathrm{p}}\dot{p}\right) \quad \text{Eqn E-33}$$

$$\dot{m}_b\left(\left(u_b-u_u\right)-R_u T_u\right)=\dot{Q}_b-p\dot{V}_b-\frac{\partial u_b}{\partial \mathrm{T}_b}\dot{T}_b m_b-\frac{\partial u_b}{\partial \mathrm{p}}\dot{p}m_b \quad \text{Eqn E-34}$$

From Eqn E-9

$$\frac{\dot{p}}{p}=\frac{\dot{m}_b}{m_b}+\frac{\dot{R}_b}{R_b}+\frac{\dot{T}_b}{T_b}-\frac{\dot{V}_b}{V_b} \quad \text{Eqn E-9}$$

However if the assumption that $\dfrac{\partial u_b}{\partial \mathrm{T}_b}=\dfrac{\partial u_b}{\partial p}=0$ is made (this is supported by numerical investigation according to the authors), then $\dot{R}_b=0$ and therefore

$$\dot{T}_b=T_b\left(\frac{\dot{p}}{p}-\frac{\dot{m}_b}{m_b}+\frac{\dot{V}_b}{V_b}\right) \quad \text{Eqn 7-35}$$

Substituting Eqn E-35 into Eqn E-34 gives

$$\dot{m}_b\left(\left(u_b-u_u\right)-R_u T_u\right)=\dot{Q}_b-p\dot{V}_b-\frac{\partial u_b}{\partial \mathrm{T}_b}T_b m_b\left(\frac{\dot{p}}{p}-\frac{\dot{m}_b}{m_b}+\frac{\dot{V}_b}{V_b}\right)-\frac{\partial u_b}{\partial \mathrm{p}}\dot{p}m_b \quad \text{Eqn E-36}$$

$$\dot{m}_b\left((u_b-u_u)-R_uT_u-\frac{\partial u_b}{\partial \mathrm{T}_b}T_b\right)=\dot{Q}_b-p\dot{V}_b$$
$$-\frac{\partial u_b}{\partial \mathrm{T}_b}T_bm_b\left(\frac{\dot{p}}{p}+\frac{\dot{V}_b}{V_b}\right)-\frac{\partial u_b}{\partial \mathrm{p}}\dot{p}\,m_b \quad \text{..... Eqn E-37}$$

$$\dot{m}_b\left((u_b-u_u)-R_uT_u-\frac{\partial u_b}{\partial \mathrm{T}_b}T_b\right)=\dot{Q}_b-p\dot{V}_b\left(1+\frac{\partial u_b}{\partial \mathrm{T}_b}\frac{T_bm_b}{V_bp}\right)$$
$$-\dot{p}\left(\frac{\partial u_b}{\partial \mathrm{T}_b}\frac{T_bm_b}{p}+\frac{\partial u_b}{\partial \mathrm{p}}m_b\right) \quad \text{..... Eqn E-38}$$

$$\dot{m}_b\left((u_b-u_u)-R_uT_u-\frac{\partial u_b}{\partial \mathrm{T}_b}T_b\right)=\dot{Q}_b-p\dot{V}_b\left(1+\frac{\partial u_b}{\partial \mathrm{T}_b}\frac{1}{R_b}\right)$$
$$-V_b\dot{p}\left(\frac{\partial u_b}{\partial \mathrm{T}_b}\frac{1}{R_b}+\frac{\partial u_b}{\partial \mathrm{p}}\frac{m_b}{V_b}\right) \quad \text{..... Eqn E-39}$$

From Eqn E-2 $V=V_b+V_u$ we get

$$\dot{V}=\dot{V}_b+\dot{V}_u \quad \text{..... Eqn E-40}$$

Substituting Eqn E-40 into Eqn E-39

$$\dot{m}_b\left((u_b-u_u)-R_uT_u-\frac{\partial u_b}{\partial \mathrm{T}_b}T_b\right)=\dot{Q}_b-p\left(\dot{V}-\dot{V}_u\right)\left(1+\frac{\partial u_b}{\partial \mathrm{T}_b}\frac{1}{R_b}\right)$$
$$-(V-V_u)\dot{p}\left(\frac{\partial u_b}{\partial \mathrm{T}_b}\frac{1}{R_b}+\frac{\partial u_b}{\partial \mathrm{p}}\frac{m_b}{V_b}\right) \quad \text{..... Eqn E-41}$$

$$\dot{m}_b\left((u_b-u_u)-R_uT_u-\frac{\partial u_b}{\partial \mathrm{T}_b}T_b\right)=\dot{Q}_b-\left(p\dot{V}-p\dot{V}_u\right)\left(1+\frac{\partial u_b}{\partial \mathrm{T}_b}\frac{1}{R_b}\right)$$
$$-\dot{p}V\left(\frac{\partial u_b}{\partial \mathrm{T}_b}\frac{1}{R_b}+\frac{\partial u_b}{\partial \mathrm{p}}\frac{m_b}{V_b}\right)+\dot{p}V_u\left(\frac{\partial u_b}{\partial \mathrm{T}_b}\frac{1}{R_b}+\frac{\partial u_b}{\partial \mathrm{p}}\frac{m_b}{V_b}\right) \quad \text{..... Eqn E-42}$$

From Eqn E-25 we can write

$$\dot{V}_u=V_u\left(\frac{\dot{m}_u}{m_u}+\frac{\dot{T}_u}{T_u}-\frac{\dot{p}}{p}\right) \quad \text{..... Eqn E-43}$$

Substituting Eqn E-43-into Eqn E-42

$$\dot{m}_b\left((u_b-u_u)-R_uT_u-\frac{\partial u_b}{\partial \mathrm{T}_b}T_b\right)=\dot{Q}_b-$$

$$\left(p\dot{V}-pV_u\left(\frac{\dot{m}_u}{m_u}+\frac{\dot{T}_u}{T_u}-\frac{\dot{p}}{p}\right)\right)\left(1+\frac{\partial u_b}{\partial \mathrm{T}_b}\frac{1}{R_b}\right) \qquad \text{..... Eqn E-44}$$

$$-\dot{p}V\left(\frac{\partial u_b}{\partial \mathrm{T}_b}\frac{1}{R_b}+\frac{\partial u_b}{\partial \mathrm{p}}\frac{m_b}{V_b}\right)+\dot{p}V_u\left(\frac{\partial u_b}{\partial \mathrm{T}_b}\frac{1}{R_b}+\frac{\partial u_b}{\partial \mathrm{p}}\frac{m_b}{V_b}\right)$$

$$\dot{m}_b\left((u_b-u_u)-R_uT_u-\frac{\partial u_b}{\partial \mathrm{T}_b}T_b\right)=\dot{Q}_b-\left(p\dot{V}-m_uR_u\dot{T}_u\right)\left(1+\frac{\partial u_b}{\partial \mathrm{T}_b}\frac{1}{R_b}\right)$$

$$+\frac{pV_u\dot{m}_u}{m_u}\left(1+\frac{\partial u_b}{\partial \mathrm{T}_b}\frac{1}{R_b}\right)-V_u\dot{p}\left(1+\frac{\partial u_b}{\partial \mathrm{T}_b}\frac{1}{R_b}\right) \qquad \text{..... Eqn E-45}$$

$$-\dot{p}V\left(\frac{\partial u_b}{\partial \mathrm{T}_b}\frac{1}{R_b}+\frac{\partial u_b}{\partial \mathrm{p}}\frac{m_b}{V_b}\right)+\dot{p}V_u\left(\frac{\partial u_b}{\partial \mathrm{T}_b}\frac{1}{R_b}+\frac{\partial u_b}{\partial \mathrm{p}}\frac{m_b}{V_b}\right)$$

Substituting Eqn E-3 into Eqn E-45

$$\dot{m}_b\left((u_b-u_u)-R_uT_u-\frac{\partial u_b}{\partial \mathrm{T}_b}T_b+R_uT_u\left(1+\frac{\partial u_b}{\partial \mathrm{T}_b}\frac{1}{R_b}\right)\right)=\dot{Q}_b$$

$$+\left(m_uR_u\dot{T}_u-p\dot{V}\right)\left(1+\frac{\partial u_b}{\partial \mathrm{T}_b}\frac{1}{R_b}\right)$$

$$+V_u\dot{p}\left(-1-\frac{\partial u_b}{\partial \mathrm{T}_b}\frac{1}{R_b}+\frac{\partial u_b}{\partial \mathrm{T}_b}\frac{1}{R_b}+\frac{\partial u_b}{\partial \mathrm{p}}\frac{m_b}{V_b}\right) \qquad \text{..... Eqn E-46}$$

$$-\dot{p}V\left(\frac{\partial u_b}{\partial \mathrm{T}_b}\frac{1}{R_b}+\frac{\partial u_b}{\partial \mathrm{p}}\frac{m_b}{V_b}\right)$$

$$\dot{m}_b\left((u_b-u_u)+\left(\frac{R_uT_u}{R_b}-T_b\right)\frac{\partial u_b}{\partial \mathrm{T}_b}\right)=\dot{Q}_b+\left(m_uR_u\dot{T}_u-p\dot{V}\right)\left(1+\frac{\partial u_b}{\partial \mathrm{T}_b}\frac{1}{R_b}\right)$$

$$+V_u\dot{p}\left(\frac{\partial u_b}{\partial \mathrm{p}}\frac{m_b}{V_b}-1\right)-\dot{p}V\left(\frac{\partial u_b}{\partial \mathrm{T}_b}\frac{1}{R_b}+\frac{\partial u_b}{\partial \mathrm{p}}\frac{m_b}{V_b}\right) \qquad \text{..... Eqn E-47}$$

Substituting a rearranged Eqn E-2, $V_u=V-V_b$ into Eqn E-47

$$\dot{m}_b\left((u_b-u_u)+\left(\frac{R_uT_u}{R_b}-T_b\right)\frac{\partial u_b}{\partial \mathrm{T}_b}\right)=\dot{Q}_b+\left(m_uR_u\dot{T}_u-p\dot{V}\right)\left(1+\frac{\partial u_b}{\partial \mathrm{T}_b}\frac{1}{R_b}\right)$$

$$+\dot{p}(V-V_b)\left(\frac{\partial u_b}{\partial \mathrm{p}}\frac{m_b}{V_b}-1\right)-\dot{p}V\left(\frac{\partial u_b}{\partial \mathrm{T}_b}\frac{1}{R_b}+\frac{\partial u_b}{\partial \mathrm{p}}\frac{m_b}{V_b}\right) \qquad \text{..... Eqn E-48}$$

$$\dot{m}_b\left(\left(u_b-u_u\right)+\left(\frac{R_uT_u}{R_b}-T_b\right)\frac{\partial u_b}{\partial \mathrm{T}_b}\right)=\dot{Q}_b+\left(m_uR_u\dot{T}_u-p\dot{V}\right)\left(1+\frac{\partial u_b}{\partial \mathrm{T}_b}\frac{1}{R_b}\right)$$
$$+\dot{p}V\left(\frac{\partial u_b}{\partial \mathrm{p}}\frac{m_b}{V_b}-1\right)-\dot{p}V_b\frac{\partial u_b}{\partial \mathrm{p}}\frac{m_b}{V_b}+\dot{p}V_b \quad \text{.....Eqn E-49}$$
$$-\dot{p}V\left(\frac{\partial u_b}{\partial \mathrm{T}_b}\frac{1}{R_b}+\frac{\partial u_b}{\partial \mathrm{p}}\frac{m_b}{V_b}\right)$$

$$\dot{m}_b\left(\left(u_b-u_u\right)+\left(\frac{R_uT_u}{R_b}-T_b\right)\frac{\partial u_b}{\partial \mathrm{T}_b}\right)=\dot{Q}_b+\left(m_uR_u\dot{T}_u-p\dot{V}\right)\left(1+\frac{\partial u_b}{\partial \mathrm{T}_b}\frac{1}{R_b}\right) \quad \text{.....Eqn E-50}$$
$$-\dot{p}\left(\frac{\partial u_b}{\partial \mathrm{p}}m_b+V_b\right)-\dot{p}V\left(\frac{\partial u_b}{\partial \mathrm{T}_b}\frac{1}{R_b}+\frac{\partial u_b}{\partial \mathrm{p}}\frac{m_b}{V_b}-\frac{\partial u_b}{\partial \mathrm{p}}\frac{m_b}{V_b}+1\right)$$

$$\dot{m}_b\left(\left(u_b-u_u\right)+\left(\frac{R_uT_u}{R_b}-T_b\right)\frac{\partial u_b}{\partial \mathrm{T}_b}\right)=\dot{Q}_b+\left(m_uR_u\dot{T}_u-p\dot{V}\right)\left(1+\frac{\partial u_b}{\partial \mathrm{T}_b}\frac{1}{R_b}\right) \quad \text{.....Eqn E-51}$$
$$-\dot{p}V\left(\frac{\partial u_b}{\partial \mathrm{T}_b}\frac{1}{R_b}+1+\frac{\partial u_b}{\partial \mathrm{p}}\frac{m_b}{V}-\frac{V_b}{V}\right)$$

From Eqn E-2, $V=V_u+V_b$ we can write

$$1=\frac{V_u}{V}+\frac{V_b}{V} \quad \text{.....Eqn E-52}$$

Substituting Eqn E-52 into Eqn E-51

$$\dot{m}_b\left(\left(u_b-u_u\right)+\left(\frac{R_uT_u}{R_b}-T_b\right)\frac{\partial u_b}{\partial \mathrm{T}_b}\right)=\dot{Q}_b+\left(m_uR_u\dot{T}_u-p\dot{V}\right)\left(1+\frac{\partial u_b}{\partial \mathrm{T}_b}\frac{1}{R_b}\right) \quad \text{.....Eqn E-53}$$
$$-\dot{p}V\left(\frac{\partial u_b}{\partial \mathrm{T}_b}\frac{1}{R_b}+\frac{\partial u_b}{\partial \mathrm{p}}\frac{m_b}{V}+\frac{V_u}{V}\right)$$

$$\dot{m}_b=\frac{\dot{Q}_b+\left(m_uR_u\dot{T}_u-p\dot{V}\right)\left(1+\frac{\partial u_b}{\partial \mathrm{T}_b}\frac{1}{R_b}\right)-\dot{p}V\left(\frac{\partial u_b}{\partial \mathrm{T}_b}\frac{1}{R_b}+\frac{\partial u_b}{\partial \mathrm{p}}\frac{m_b}{V}+\frac{V_u}{V}\right)}{\left(u_b-u_u\right)+\left(\frac{R_uT_u}{R_b}-T_b\right)\frac{\partial u_b}{\partial \mathrm{T}_b}} \quad \text{.....Eqn E-54}$$

Solving for $\dot{V}_b$:

Substituting Eqn E-3, $-\dot{m}_u=\dot{m}_b$ into Eqn E-43 gives

$$\dot{V}_u=V_u\left(\frac{-\dot{m}_b}{m_u}+\frac{\dot{T}_u}{T_u}-\frac{\dot{p}}{p}\right) \quad \text{.....Eqn E-55}$$

From Eqn E-40, $\dot{V}=\dot{V}_b+\dot{V}_u$ we can write

$$\dot{V} - \dot{V}_b = V_u \left(\frac{-\dot{m}_b}{m_u} + \frac{\dot{T}_u}{T_u} - \frac{\dot{p}}{p} \right) \quad \text{Eqn E-56}$$

$$\dot{V}_b = V_u \left(\frac{\dot{m}_b}{m_u} - \frac{\dot{T}_u}{T_u} + \frac{\dot{p}}{p} \right) + \dot{V} \quad \text{Eqn E-57}$$

The authors did not give an equation for the calculation of the burned gas temperature but one was derived using a similar methodology as above.

Again, starting with the energy equation for the burned gas Eqn E-17 and rearranging

$$\dot{m}_b u_b + m_b \left(\frac{\partial u_b}{\partial T_b} \dot{T}_b + \frac{\partial u_b}{\partial p} \dot{p} \right) = \dot{m}_b h_u + \dot{Q}_b - p\dot{V}_b \quad \text{Eqn E-58}$$

$$m_b \left(\frac{\partial u_b}{\partial T_b} \dot{T}_b + \frac{\partial u_b}{\partial p} \dot{p} \right) = \dot{m}_b \left(h_u - u_b \right) + \dot{Q}_b - p\dot{V}_b \quad \text{Eqn E-59}$$

$$m_b \frac{\partial u_b}{\partial T_b} \dot{T}_b = \dot{m}_b \left(h_u - u_b \right) + \dot{Q}_b - p\dot{V}_b - m_b \frac{\partial u_b}{\partial p} \dot{p} \quad \text{Eqn E-60}$$

$$\dot{T}_b = \frac{\dot{m}_b \left(h_u - u_b \right) + \dot{Q}_b - p\dot{V}_b - m_b \dfrac{\partial u_b}{\partial p} \dot{p}}{m_b \dfrac{\partial u_b}{\partial T_b}} \quad \text{Eqn E-61}$$

---

i Krieger, R. B. and Borman, G. L., "The Computation of Apparent Heat Release for Internal Combustion Engines," ASME paper 66-WA/DGP-4, 1966.

ii Howell, J. R. and Buckius, R. O., *Fundamentals of Engineering Thermodynamics.* McGraw Hill, New York, 1987.